STUDY OF STRUCTURAL, OPTICAL AND ELECTRICAL PROPERTIES OF $Zn_{1-X}Mn_XO$ THIN FILMS DEPOSITED BY SPRAY PYROLYSIS TECHNIQUE

BY

MD. KHORSHED ALAM
ROLL NO. 1009143001F
SESSION: OCTOBER, 2009
MASTER OF PHILOSOPHY

DEPARTMENT OF PHYSICS
BANGLADESH UNIVERSITY OF ENGINEERING AND TECHNOLOGY
DHAKA-1000, BANGLADESH.
12 May, 2012

STUDY OF STRUCTURAL, OPTICAL AND ELECTRICAL PROPERTIES OF $Zn_{1-X}Mn_XO$ THIN FILMS DEPOSITED BY SPRAY PYROLYSIS TECHNIQUE

BY

MD. KHORSHED ALAM

A dissertation submitted in partial fulfillment of the requirement for the degree of M.Phil. in the department of Physics, Bangladesh University of Engineering and Technology, Dhaka-1000

DEPARTMENT OF PHYSICS
BANGLADESH UNIVERSITY OF ENGINEERING AND TECHNOLOGY
DHAKA-1000, BANGLADESH.
12 May, 2012

CANDIDATE'S DECLARATION

It is hereby declared that this thesis or any part of it has not been submitted elsewhere for the award of any degree or diploma.

Signature of the candidate

MD. KHORSHED ALAM
ROLL NO. 1009143001F
SESSION: OCTOBER, 2009

BANGLADESH UNIVERSITY OF ENGINEERING AND TECHNOLOGY
DHAKA
DEPARTMENT OF PHYSICS

Certification of Thesis

The thesis titled "***STUDY OF STRUCTURAL, OPTICAL AND ELECTRICAL PROPERTIES OF*** $Zn_{1-X}Mn_XO$ ***THIN FILMS DEPOSITED BY SPRAY PYROLYSIS TECHNIQUE***", submitted by **MD. KHORSHED ALAM**, Roll No: 1009143001F, Registration No: 1009143001, Session: October/2009, has been accepted as satisfactory in partial fulfillment of the requirement for the degree of **MASTER OF PHILOSOPHY (M. Phil.) in Physics** on **12 May, 2012.**

BOARD OF EXAMINERS

1.
-- Chairman
Dr. Jiban Podder (Supervisor)
Professor
Department of Physics, BUET, Dhaka

2.
-- Member (Ex-Officio)
HEAD
Department of Physics, BUET, Dhaka

3.
-- Member
Dr. Md. Abu Hashan Bhuiyan
Professor, Department of Physics, BUET, Dhaka

4.
-- Member
Dr. Md. Mostak Hossain
Professor, Department of Physics, BUET, Dhaka

5.
-- Member (External)
Dr. M. Khalilur Rahman Khan
Professor, Department of Physics
University of Rajshahi, Rajshahi.

Dedicated

To

My Parents

CONTENTS

	Page No.
CANDIDATE DECLARATION	**iii**
DEDICATION	**v**
CONTENTS	**vi**
APENDIX	**xii**
ACKNOLEDGEMENT	**xvi**
ABSTRACT	**xviii**
CHAPTER-I: GENERAL INTRODUCTION	**1-19**
1.1 Introduction	2
1.2 Historical development of thin films	3
1.3 Thin film formation steps	4
1.4 Characteristics of thin films	5
1.5 Applications of thin film	5
1.6 Diluted Magnetic Semiconductor	6
1.6.1 Alloy of II–VI semiconductors with magnetic materials	7
1.6.2 Importance of DMS	8
1.7 Spintronics	9
1.8 Spintronics devices	10
1.8.1 Spin FET	10
1.8.2 Spin LED	11

1.9 Properties of Zinc Oxide 12

1.10 Properties of Manganese 14

1.11 Review of the previous works 14

1.12 Motivation of the present work 16

References 18

CHAPTER-II: THIN FILM DEPOSITIN TECHNOLOGY 20-33

2.1 Introduction 21

2.2 Classification of the thin film deposition techniques 21

2.2.1 Chemical deposition 22

2.2.2 Physical deposition 23

2.2.3 Thermal or vacuum evaporation 23

2.2.4 Dipping and withdrawing 24

2.2.5 Chemical vapor deposition (CVD) 25

2.2.6 Sputtering 25

2.2.7 Epitaxial growth 26

2.2.8 Molecular beam epitaxy (MBE) 27

2.2.9 Electroplating 28

2.2.10 Sol gel method 29

2.2.11 Pulsed laser deposition 29

2.2.12 Thermal oxidation technique 30

2.2.13 Spray pyrolysis (SP) 31

References 33

CHAPTER-III: THEORETICAL STUDY 34-63

PART A: FORMATION OF THIN FILM

3.1 Introduction 35

3.2 Different stages of thin film formation 36

3.2.1 Condensation 36

3.2.2 Nucleation 37

3.2.3 Growth 38

3.2.3.1 The island stage 38

3.2.3.2 The coalescence stage 39

3.2.3.3 The channel stage 39

3.2.3.4 The continuous film stage 40

PART B: METHODS OF THIN FILM THICKNESS MEASUREMENT

3.3 Introduction 41

3.3.1 Gravimetric method 41

3.3.2 Interference fringe method 42

3.3.3 Newton's ring method 43

PART C: STUDY OF STRUCTURAL AND OPTICAL PROPERTIES OF THIN FILM

3.4 X-ray diffraction 45

3.4.1 The powder method 46

3.4.2 Calculations of lattice parameters 47

3.4.3 Calculations of crystallite size 47

3.5 Optical properties of thin films 48

3.6 Absorption coefficient 48

3.7 Optical bandgap 49

3.7.1 Direct bandgap of semiconductor 50

3.7.2 Indirect band gap of semiconductor 51

3.8 Refractive index, extinction coefficient and phase angle determination 52

3.9 Optical conductivity 54

PART D: STUDY OF ELECTRICAL PROPERTIES OF THIN FILM

3.10 Introduction 55

3.10.1 Resistivity and conductivity measurement 56

3.10.2 Methods to determine the resistivity 56

3.10.2 (i) Direct method 56

3.10.2 (ii) Two-probe method 57

3.10.2 (iii) Four-probe technique 57

3.10.2 (iv) Van-der Pauw method 57

3.12 Hall effect 59

3.12 The Hall constant and carrier concentration 60

References 63

CHPTER-IV: EXPERIMENTAL DETAILS 64-74

PART A: FILM PREPARATION

4.1 Introduction 65

4.2 Experimental equipments for spray pyrolysis technique 65

4.2.1 Preparation of mask 65

4.2.2 Heater 66

4.2.3 The design of reactor 66

4.2.4 The fume chamber 67

4.2.5 The air compressor 68

4.2.6 Nozzle 68

4.3 Substrate and substrate cleaning 68

4.4 Working solution 69

4.5 Sample deposition 69

4.6 Deposition rate and thickness control 70

PART B: EXPERIMENTAL MEASUREMENT

4.7 Measurement of film thickness 71

4.8 Structural study by XRD analysis 71

4.9 Measurement of absorbance and transmittance 71

4.10 Measurement of absorption coefficient and optical bandgap 71

4.11 Attachment of conducting wire with films 72

4.12 Measurement of resistivity, conductivity and activation energy 72

References 74

CHAPTER-V: RESULTS AND DISCUSSION 75-98

5.1 Thickness Measurement 76

5.2 Surface morphology of $Zn_{1-x}Mn_xO$ 76

5.3 Compositional studies 80

5.4 Structural study by XRD analysis 83

5.5 Optical properties 85

5.5.1 Transmittance and absorbance 85

5.5.2 Optical bandgap 87

5.5.3 Refractive index and optical conductivity 90

5.6 Electrical properties 92

5.6.1 Variation of resistivity with temperature 92

5.6.2 Variation of conductivity with temperature 93

5.6.3 Estimation of activation energy 94

5.7 Measurement of Hall Effect 96

References 98

CHAPTER-VI: CONCLUSIONS AND SUGGESTIONSFOR FUTURE WORK 99-102

6.1 Conclusion 100

6.2 Suggestions for Future Work 102

APENDIX

List of figures **Page No.**

Fig.1.1: Thin-film formation steps. 4

Fig.1.2: The different types of semiconductor 7

Fig.1.3: Scheme of the Datta-Das spin field-effect transistor (SFET) 11

Fig.1.4: A schematic spin LED 12

Fig.1.5: Wurtzite Structure of Zinc Oxide Crystal 13

Fig. 2.1: Classification of the most common thin film deposition techniques. 22

Fig. 2.2: Electron beam evaporation method. 24

Fig. 2.3: Schematic diagram of chemical vapor deposition process. 25

Fig. 2.4: Schematic diagram of sputtering process. 26

Fig. 2.5: Schematic diagram of epitaxial growth layer. 27

Fig. 2.6: Schematic diagram of molecular beam epitaxy method. 28

Fig. 2.7: Schematic diagram of electroplating process. 28

Fig. 2.8: Schematic diagram of pulsed laser deposition process. 30

Fig. 2.9: Schematic diagram of thermal oxidation process. 30

Fig. 2.10: Schematic diagram of spray pyrolysis technique. 31

Fig.3.1: Different stages of film growth. 40

Fig.3.2: Interferometer arrangements for producing Fizeau fringes of equal thickness. 43

Fig.3.3: Schematic diagram for measurement of thickness by Newton's ring method. 44

Fig.3.4: Photon energies much larger than the forbidden gap are required to give transition of electrons from the valance band to conduction band. 51

Fig.3.5: A film bounded by air and glass. 53

Fig. 3.6: Circuit arrangements to determine electrical resistivity. 58

Fig.3.7: The forces acting on a current carrier in a conductor placed in a magnetic field leading to the observable Hall field E_H. 61

Fig.4.1: Mask used for the thin film preparation. 66

Fig.4.2: Schematic diagram of spray pyrolysis technique. 67

Fig. 4.3: Diagram of film with lead attachment 72

Fig. 4.4: Schematic diagram for the measurement of film resistivity. 1, 2, 3 and 4 are meter terminals and A, B, C and D are the film terminals. 73

Fig.5.1a: SEM image of (10000X magnification) ZnO thin film for (a) x=0.00 77

Fig.5.1b: SEM image of (10000X magnification) $Zn_{1-x}Mn_xO$ thin film for (b) x=0.02 77

Fig.5.1c: SEM image of (10000X magnification) $Zn_{1-x}Mn_xO$ thin film for (c) x=0.04 78

Fig.5.1d: SEM image of (10000X magnification) $Zn_{1-x}Mn_xO$ thin film for (d) x=0.06 78

Fig.5.1e: SEM image of (10000X magnification) $Zn_{1-x}Mn_xO$ thin film for (e) x=0.10 79

Fig.5.1f: SEM image of (10000X magnification) $Zn_{1-x}Mn_xO$ thin film for (f) x=0.20 79

Fig 5.2a: EDX spectrum of as-deposited ZnO thin film. 80

Fig 5.2b: EDX spectrum of $Zn_{1-x}Mn_xO$ thin film for x=0.04. 81

Fig 5.2c: EDX spectrum of $Zn_{1-x}Mn_xO$ thin film for x=0.06. 81

Fig.5.2d: EDX spectrum of $Zn_{1-x}Mn_xO$ thin film for x=0.10. 82

Fig 5.3: X-ray patterns of as-deposited $Zn_{1-x}Mn_xO$ thin films 84

Fig.5.4: Variation of transmittance as a function of wavelength for $Zn_{1-x}Mn_xO$ films for different concentrations. 86

Fig.5.5: Variation of absorbance as a function of wavelength for $Zn_{1-x}Mn_xO$ film86 for different concentrations. 86

Fig. 5.6: Variation of $(\alpha h\nu)^2$ with hν for x=0.00, 0.02, 0.04 of $Zn_{1-x}Mn_xO$ 87

Fig. 5.7: Variation of $(\alpha h\nu)^2$ with hν for x=0.06, 0.10, 0.15, 0.20 of $Zn_{1-x}Mn_xO$ 88

Fig. 5.8: Variation of band gap of $Zn_{1-x}Mn_xO$ films for different doping concentrations. 89

Fig.5.9: Variation of refractive index as a function of wavelength of $Zn_{1-x}Mn_xO$ films for different Mn concentrations. 90

Fig.5.10: Variation of optical conductivity as a function of wavelength of $Zn_{1-x}Mn_xO$ films for different concentrations. 91

Fig.5.11: Variation of resistivity with temperature of $Zn_{1-x}Mn_xO$ films for different concentrations. 92

Fig.5.12: Variation of conductivity with temperature of $Zn_{1-x}Mn_xO$ films for different concentrations. 93

Fig.5.13: Variation of ln σ with 1/T of $Zn_{1-x}Mn_xO$ films for different concentrations. 94

Fig.5.14: Variation of activation energy of $Zn_{1-x}Mn_xO$ films for different Mn concentrations. 95

Fig. 5.15: Variation of Hall constant R_H with Mn concentration for Mn-doped ZnO thin films at room temperature. 96

Fig. 5.15: Variation of carrier concentration n with Mn concentration for Mn-doped ZnO thin films at room temperature. 97

List of Table

Table-1.1: Applications of thin film. 6

Table- 1.2: Physical Properties of ZnO 13

Table-1.3: Physical properties of Manganese 14

Table-5.1: Elemental analysis data for $Zn_{1-x}Mn_xO$ thin films. 82

Table-5.2: Crystallite size of as-deposited $Zn_{1-x}Mn_xO$ thin films. 85

Table-5.3**:** Variation of bandgap with doping concentration of $Zn_{1-x}Mn_xO$ thin films. 88

Table-5.4: Variation of activation energy for $Zn_{1-x}Mn_xO$ thin films. 95

Table-5.5: Values of Hall co-efficient, R_H and carrier concentration n for different Mn concentration at room temperature. 97

ACKNOWLEDGEMENTS

First of all I express very much gratefulness to the Almighty Allah, who gives me the strength and energy to fulfill this research work.

I would like to express my profound gratitude to my supervisor **Dr. Jiban Podder,** Professor, Department of Physics, Bangladesh University of Engineering & Technology, Dhaka, for the continuous support and for being always open to discussions. I am grateful to him for his constant guidance, valuable discussions, active help, untold patience and important suggestions during the course of this work.

I am deeply indebted to my respected teacher **Prof**. **Dr. Md. Mostak Hossain**, Head, Department of Physics, Bangladesh University of Engineering & Technology, Dhaka, for providing necessary facilities to carry out this research work and valuable suggestion regarding my thesis.

I wish to express my gratefulness to **Prof. Dr. Md. Abu Hashan Bhuiyan** for his constructive criticism, stimulating encouragement and various help. I also would like to express my thanks to all of my teachers of the department of Physics, BUET specially: **Prof. Dr. Md. Feroz Alam Khan, Prof. A. K. M. Akther Hossain, Dr. Md. Forhad Mina, and Md. Khorshed Alam** for their kind help and valuable suggestions.

I would like to give my special thanks to **Dr. D. K. Saha,** Chief Scientific Officer and **Mr. Md. Al-Mamun,** of Materials Science Division, AEC, Dhaka, for help in taking the SEM and EDX data.

I am grateful to **Dr. Md. Abdul Gafur**, Senior Engineer, BCSIR Laboratories for **UV-VIS.**

I am very much grateful to **Professor Dr. Md. Khalilur Rahman Khan** and his student **Alop, Polash,** Department of Physics , University of Rajshahi for his kind help during the study of electrical property.

I am also thankful to Department of Physics & Engineering Physics, **University of Saskatchewan, Canada**, for giving permission for XRD measurements on my samples.

I would like to thank **Sanjoy Chandra Das, Ms. Mahajabin Taskin, Dr. Ferdousi Akter, Dr. Ms. Farhana Khanam, Md. Kamal Uddin Azad, Ms. Tamjida Rahman Luna, Mohammed Arifur Rahman, Mr. Anis Munshi,** for there sincere help to this work.

Finally, I express my heartfelt gratitude to my parents and other family members for their constant support and encouragement during this research work.

I thank the authority of **Bangladesh University of Engineering & Technology** and **Ministry of Science and Technology, The People's Republic of Bangladesh** for providing financial support and **"NSICT Fellowship"** to this thesis work.

Abstract

Undoped and manganese doped zinc oxide thin films were prepared on glass substrate at 300 °C temperature using spray pyrolysis technique. Structural, optical, and electrical properties of the films have been investigated. The surface morphology of the films were taken by a scanning electron microscope (SEM). From the micrograph it is seen that more or less smooth surface and a large variety of crystal growth, such as circular disk, nano-ropes, nano-wires structure were randomly distributed around the nucleation centre. Compositional study of the samples was taken by energy dispersive X-ray (EDX). EDX result reveals that as-deposited $Zn_{1-x}Mn_xO$ films are very nearly-stoichiometric. The structure of as-deposited samples was investigated by X-ray diffraction experiment. XRD patterns show as-deposited $Zn_{1-x}Mn_xO$ thin films are crystalline in nature. Diffraction peaks revealed that the presence of hexagonal wurtzite structure without any secondary phase. Lattice constant were calculated a = 3.23 Å and c = 5.17Å. The observed grain sizes are found in the range of 9 nm to 18 nm. From the optical studies it is observed that the transmittance of the $Zn_{1-x}Mn_xO$ films are highly transparent near about 80% in VIS region. Optical band gap was calculated from the optical measurement. Band gap tuning was found with different Mn concentration. The bandgap energy is observed to vary from 3.10 eV to 3.24 eV at different doping concentrations. The optical band gap decreases when the Mn concentration increases from 0 to 4% and then increases upto 10% . For 15% Mn doped ZnO film, the band gap then shows a decrease upto 20%. The electrical measurements of the $Zn_{1-x}Mn_xO$ films have been investigated from room temperature to 440 K. Resistivity decreases with increase of temperature in all cases of the samples. It was also found that resistivity decreases with doping concentration. The activation energy was estimated from the slopes of $\ln\sigma$ verses $1/T$ graph and its value is found from 0.44 eV to 0.66 eV. The Hall effect measurement was done at room temperature by Vander pauw's method. Measurement shows that Mn-doped ZnO thin films have negative Hall co-efficient, R_H and this indicates the n-type behavior of ZnO:Mn at room temperature. The carrier concentration was found to be of the order of 10^{18} cm^{-3}.

CHAPTER -I
GENERAL INTRODUCTION

CHAPTER -I
GENERAL INTRODUCTION

1.1 Introduction

The contribution of thin film technology makes the present world a global village. Research in the physical properties of matter has progressed so much during the last hundred years that today physics is divided into a large number of groups of special branches, which are often very different from each other, thin film technology is important special branch of physics in which the characteristics of different semiconductor, magnetic semiconductor and insulators are investigated in the from of thin film.

The word “Thin” gives a relative measurement of any dimension but not to any absolute value and “Film” means a coating of layer. The term thin as it applies to thin films is quite ambiguous. It is used to define a layer of thickness, which is comparable with the mean free path of the conduction electrons. Its value differs from material to material. In practice, this branch deals with films having thickness between the tenths of a nanometer and a few micrometers. When a thin layer of solid material is formed on a solid substrate and if the layer thickness becomes comparable in magnitude with mean free path of the conduction electrons of solid material then this layer is termed as thin film. The properties of thin films are quite different from their bulk value. The phonon rise in thin film researches is no doubt due to their expensive applications in the diverse field of electronics, spintronics, optics, space science, aircrafts, defense and other industries. These investigations have led to numerous inventions in the forms of active devices and passive components, piezo-electric device, reflection and amplification, sensors element, magnetic memories, spin feet, spin lead, data storage device and other spintronics devices.

Deposition of thin films is achieved by one or more phase transformations and the study of the thermodynamics and kinetics of these transformations reveal the formation of thin films. Thin films exhibits different electrical, optical, mechanical,

structural, and magnetic properties than their corresponding bulk bodies. These different characteristics of thin films from bulk materials are very important in thin film applications and hence these properties must be studied before application.

1.2 Historical development of thin films

According to Chopra, thin solid films were probably first obtained by electrolysis in 1838 [1]. In the recorded literature Faraday obtained metal films in 1851 [2] by means of chemical reaction and by glow discharge sputtering respectively. The possibility of depositing thin metal films in a vacuum by Joule heating of platinum wires was discovered in 1887 by Nahrwold [3] and a year later adopted by Kundt [4] for the purpose of measuring refractive index of metal films. Edison and others (1883) while experiencing with carbon filament lamp probably first discovered free evaporation and condensation of thin films in vacuum. In the following decades, evaporated thin films remained in the domain of academic interest until the development of vacuum equipment had progressed for enough to permit large-scale applications and control of films properties. During the last 40 years, evaporated films have found industrial usage for an increasing number of purposes. Examples are antireflection coatings, front surface mirrors, interface filters, sunglasses, decorative coatings on plastics and textiles in the manufacture of cathode ray tubes and most recently in the integrated circuits and in modern technology spintronics and data storage device are the most widely used applications of thin solid films. The properties of thin films are rather different from balk material; theoretical explanations regarding the properties of thin film were required vigorously. Thomson [5] first proposed the “size-effect” theory to explain the high electrical resistivity of thin film specimen as compared with that of bulk material. For a spherical Fermi-surface and a free electron model, the “size-effect” theory was explained by Fuchs [6] and later explained by Sondheimer [7] to include the galvanometric effect. For metal films Mayadas and Shatzkes [8] have proposed conduction taking into consideration of grain boundary scattering along with other scattering mechanism. After world war the thin film technology developed rapidly when vacuum evaporated metal and dielectric films were used in optics and the development of diffusion pump made it possible. Since then a new branch of optical

technology has emerged which is based on optical interference system. The most modern development in the field of thin film physics is that of the optoelectronic devices. Photovoltaic, photoconductive, and solid state layer devices are now under consideration of the experimental physics of this respect. Now-a-day extensive studies on different properties of thin films proceeded along different lines throughout the world. Recently an event greater application known as thin film Spintronics has emerged in the field of data storage and consequently of rapid development occurred in computer industry throughout the world.

1.3 Thin film formation steps

All thin-film formation contain the four sequential steps shown in Fig. 1.1. A source of film material is provided, the material is transported to the substrate, deposition takes place, sometimes the film is subsequently annealed, and finally it is analyzed to evaluate the process. The results of the analysis are then used to adjust the conditions of the other steps for film property modification.

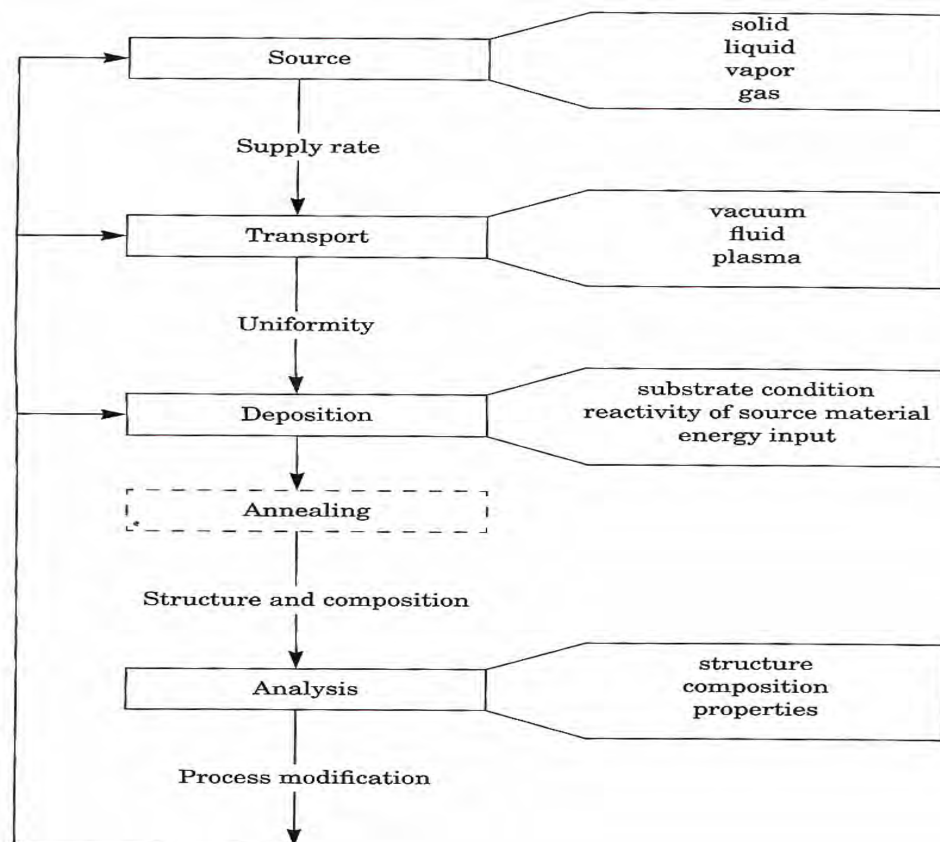

Fig.1.1: Thin-film formation steps.

1.4 Characteristics of thin films

Thin films are something different from their bulk material in structural, electrical and optical properties. The properties of thin film changes appreciably when it is cooled to a very low temperature or heated at a higher temperature (above room temperature). The study of the changes in the properties of thin film with temperature provides a great deal of information about the properties of thin films. In general the physical properties of thin film are determined by a number of factors, such as

- **The nature of substrate:** This may be non-crystalline solids, e.g. glass of vitreous silica or crystalline material such as cleavage plates of rock-salts or mica.
- **Substrate temperature during deposition:** At low temperature poly-crystalline films with high densities of structural imperfections are formed on both vitreous and crystalline substrates, but at high temperature oriented single-crystal films are formed on crystalline substrates.
- **Deposition conditions:** The properties of thin films depend on the deposition conditions, such as source temperature, pressure, deposition angle, substrate temperature etc.
- **The annealing temperature:** The relative value of the minimum annealing temperature i.e. heating the film to a higher temperature and cooling it back to room temperature after deposition.
- **Annealing cycle:** Annealing cycle, however, also plays an important role for the surface mobility of the atoms at the temperature of the substrate during deposition.

1.5 Applications of thin film

Thin films are deposited onto glass substrate to achieve properties unattainable or not easily attainable in the substrates alone. These properties are classified into six basic categories and classification and applications within each category are shown in Table-1.1.

Table-1.1: Applications of thin film.

Categories of thin film by properties	Typical applications
Optical	Reflective/antireflective coatings, interference filters, Decoration (color, luster), memory discs (CDs), waveguides and static-free coatings etc.
Electrical	Insulation, conduction, semiconductor devices, piezoelectric drivers, transparent electrodes in flat panel displays, electrochromic devices, transparent semiconducting device and photovoltaic cells etc.
Magnetic	Memory discs. Spin- Fet, Spin -Led, MRAM, data storage.
Chemical	Barriers to diffusion or alloying, protection against oxidation or corrosion, gas/liquid sensors etc.
Mechanical	Tribological (wear-resistant) coatings, hardness, adhesion, micro-mechanics.
Thermal	Barrier layers, heat sink.

1.6 Diluted Magnetic Semiconductor (DMS)

Diluted magnetic semiconductors (DMSs), are semiconductors in which a fraction of the host Cations can be substitutionally replaced by magnetic ions, combining the two interesting properties: semiconducting and magnetic. Such a compound Fig.(B) is an alloy between a non-magnetic semiconductor Fig.(C) and a magnetic element Fig.(A). Transition metals (TMs) that have partially filled d states (Mn, Fe, Co, and Ni), have been used as magnetic atoms in DMS. The partially d states contain unpaired electrons, in terms of this spin, which are responsible for them to exhibit magnetic behavior.

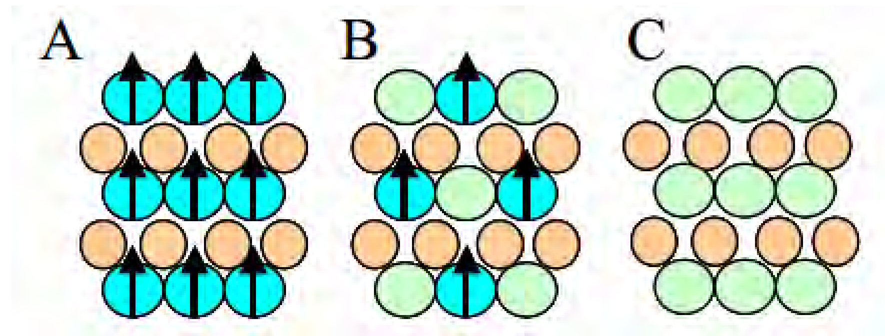

Fig.1.2: The different types of semiconductor : (A) a magnetic semiconductor, (B) a DMS and (C) a non-magnetic semiconductor.

1.6.1 Alloy of II–VI semiconductors with magnetic materials:

Most of the semiconductor materials are diamagnetic by nature and therefore can not take active part in the operation of the magneto electronic devices. In order to enable them to be useful for such devices a recent effort has been made to develop diluted magnetic semiconductors (DMS) in which small quantity of magnetic ion is introduced into normal semiconductors. The first known such DMS are II–VI semi- conductors diluted with magnetic ions like Mn, Fe, Co, Ni, etc. Most of these DMS exhibit very high electron and hole mobility and thus useful for high speed electronic devices. Diluted magnetic semiconductors (DMS) are compound of alloy semiconductors containing a large fraction of magnetic ions (Mn^{+2}, Cr^{+2}, Fe^{+2}, Co^{+2}) and are studied mainly on II–VI based materials such as CdTe and ZnO etc. This is because such +2 magnetic ions are easily incorporated into the host II–VI crystals by replacing group II cations. Although this phenomenon makes these DMS relatively easy to prepare in bulk form as well as thin epitaxial layers, II– VI based DMS are difficult to dope to create *p*- and *n*-type, which makes the material less attractive for applications. The magnetic interaction in II–VI DMSs is dominated by the anti-ferromagnetic exchange among the Mn spins, which results in the paramagnetic, antiferromagnetic, or spins glass behaviour of the material. It was not possible until very recently to make a II–VI DMS ferromagnetic at low temperature.

Recently, the II–VI compound semiconductor ZnO have attracted revival attention since it was found that high quality epitaxial thin film display excitonic ultraviolet laser action at room temperature . Furthermore, the thermal equilibrium solubility of magnetic materials (such as Mn) is larger than 10 mol %. Therefore, the amount of injected spin and carriers into the film can be very large.

1.6.2 Importance of DMS

Magnetic and semiconductor materials, respectively, have been extensively investigated and demonstrate significant results and application in scientific and industrial categories in the past years. The spin property of electrons has been successful utilized to achieve useful magnetic devices, such as magnetic sensors, magnetoresistance (MR) read-heads and magneto-optical recording elements. On the other hand, the semiconductor industry has used another property, change of electrons to fabricate a plenty of electronic devices, like integrated circuits (ICs), transistor, laser and light emitting diode (LED) Devices and has significantly promoted the development of computer and communication. With the development of semiconductor materials, advanced devices have the improving properties of high integrated density, high signal processing speed and good reliability. The operation principle of ICs is related to the control of carriers with the application of electric field, based on the charge property of carriers. In order to explore higher performance, the size of semiconductor devices has to be decreased to submicro or nano-size. The effect of exchange interaction of carriers can become a more predominant factor influencing the properties of devices. Therefore the use of both charge and spin properties may explore advanced spin dependant electronic (spintronics) devices [8]. In this spin of electron that carries the information can be used as an added degree of freedom in novel electronic devices. Scientists have proposed the small type of many spintronics devices, such as the magnetoresistive random access memory (MRAM), spin field effect transistor (spin-FET), spin light emitting diode (spin-LED), optical isolator and quantum computer. Therefore, the integration of magnetism and electronics to explore advanced spintronic devices is a very important research and application topic.

One of the most important issues in spintronics is how to effectively inject the spin into semiconductor materials. The next step is to control spin transport in the semiconductor and further to detect these spin. These issues will greatly influence the performance of spintronic devices. So it is very important to understand the basic mechanism underlying for the spin injection, transport and detection. For the topic of spin injection searching a high spin polarized material to enhance the efficiency of spin injection is very important. But the difference of physical properties between metal (or half-metals) and semiconductor limits the efficiency of spin injection. An alternative choice is the use of DMS. For years, scientists have devoted to search materials with both ferromagnetic and semiconducting materials, ie, ferromagnetic semiconductor which can be directly utilized in the process of semiconductor devices. The ferromagnetic semiconductor can facilitate a source of spin polarized carriers. Thus the development of functional ferromagnetic semiconductors is a key to the development of spintronics that will certainly be the devices utilized in the future.

1.7 Spintronics

The two most important successful technologies today in the world have been Si integrated circuit (ICs) and the data storage industry. Both continue to advance at a rapid pace. In the case of the integrated circuit obey to the Moore law that predicts number of the transistor of a chip doubled about every year. On the other hand the data storage industry has a great and significant advance in the elaboration of different devices for this end. For example, magnetic hard disk drive technology, a typical desk-top computer drive today has a 500GB, whereas in 2000 this capacity was approximately 80 GB.

All integrated circuit operate controlling the flow of the carrier of charge in this case (electron and hole) through the semiconductor when we applied an electric field. This is the dominant parameter in this type of devices. For the case of magnetic data storage, the dominant parameter is the spin of the electron where this characteristic can be considerd as the fundamental origin of the magnetic moment.

A new field of the electronics opens the possibility for the study and understands of the properties a new material that tries combining these two promise characteristic (charge and spin). This branch of the electronic is know like, semiconductor *''spin transfer electronics''* (spintronics). Spintronics, or spin electronics, consist in the study of actives control and manipulation of spin degrees of freedom in solid state system. On this base several group of investigator in the world is trying looking for material which combining both properties, to create an amazing new generation of electronic devices.

This characteristic open the possibility of developing spintronics devices that could be much smaller, with consume less electricity and be more powerful for certain types of computations than is possible with electron-charge based system. The scientific community hope to understand the behavior of electron spin in these kind of material, in order to provide something foundations new about solid state physics that will lead to a new generation of electronic devices based on the flow of spin in addition of the flow of charge.

1.8 Spintronics devices

1.8.1 Spin FET:

The most important goal in many spintronics devices is to maximize the spin detection sensitivity to the point that it detects on the spin itself, but changes in the spin states. In 1990 Datta and Das [9] proposed a design for a spin-polarized field-effect transistor, or spin FET, maybe was the first idea of a spintronic device. Figures 1.3a and 1.3b, illustrate the scheme of the structure of the usual FET, with a drain, a source, a narrow channel, and a gate for controlling the current. The gate allows the current to flow (ON) or does not (OFF). In the Datta-Das SFET the source and the drain are ferromagnets acting as injector and detector of the electron spin, the drain injects electrons with spins parallel to the transport direction. The electrons are transported ballistically through the channel. When they arrive at the drain, their spin is detected. The electron can enter the drain (ON) if its pin points in the same direction as of the spin in the drain, if not it is scattered away (OFF). The role of the gate is generating an effective magnetic field in the direction of show in the picture. This

effective magnetic field causes the electron spins to process. By modifying the voltage, one can cause the precession to lead to either parallel or antiparallel electron spin at the drain, effectively controlling the current.

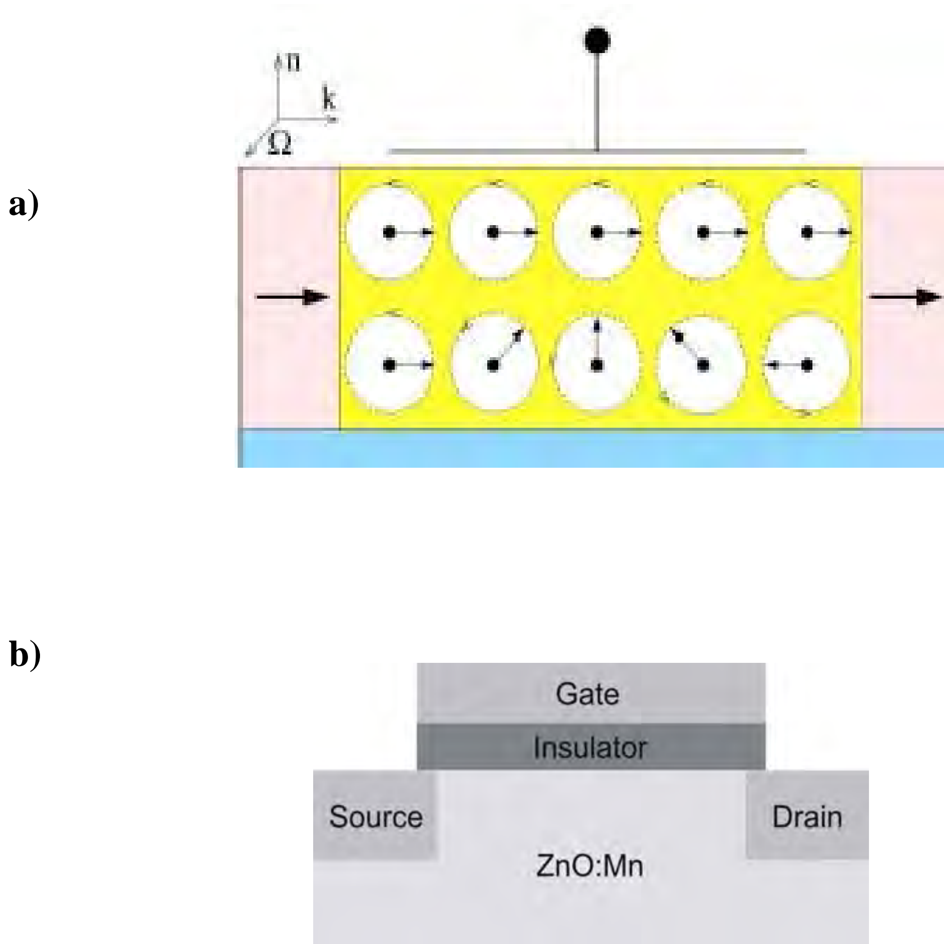

Fig.1.3: Scheme of the Datta-Das spin field-effect transistor (SFET)

1.8.2 Spin LED:

Efficient spin injection from the ferromagnetic metal and dilute magnetic semiconductor into semiconductor is the fundamental requirement of the semiconductor-based spintronics device. Spin-LED is used to measure the spin injection efficiency into materials. In a spin LED circularly polarized light is emitted after the recombination of spin- polarized carriers that are electrically injected into semiconductor structure.

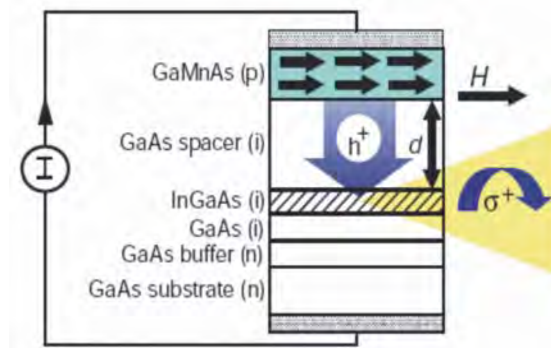

Fig.1.4: A schematic spin LED

Such a device should allow us to modulate the polarization of the light emitted by the spin LED by application of an external magnetic field in figure. The most straightforward approach to achieve this goal would be to implant Mn into the top contact p-GaN layer of the standard GaN/InGaN LED.

In conclusion today everyone already has a spintronics device on their desktop, as all modern computers use the spin valve in order to read and write data on their hard drive. It was followed immediately by the discovery of Tunneling Magnetoresistance (TMR) leading to the magnetic tunnel junction that has been utilized for the next generation computer memory known as Magnetic Random Access Memory (MRAM), another spintronics device for computers. Therefore, the initial driving force for spintronics has been the improvement of computer technology.

1.9 Properties of Zinc Oxide

In materials science, Zinc oxide (ZnO) is often called II-VI semiconductor because Zn and Oxygen belong to 2nd and 6th group of the periodic table respectively. ZnO has a unique semiconducting, photoconducting, piezoelectric and optical properties. This combination of properties makes zinc oxide attractive for use in opto-electronic, electronic and sensor devices. Zinc Oxide is an inorganic compound which usually appears as a white powder. Physical properties are detailed in Table 1.2.

ZnO crystallizes in three forms hexagonal Wurtzite, zincblende and cubic rock salt. The predominant form is hexagonal Wurtzite since this structure is the most stable at room temperature and pressure. Zinc oxide crystals exhibit several typical surface

orientations. The most important surfaces are the basal plane, the prism plane, and the pyramidal plane crystal faces.

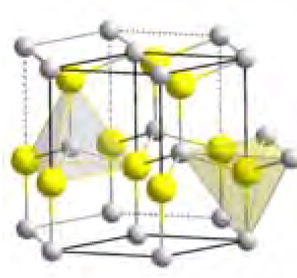

Fig.1.5: Wurtzite Structure of Zinc Oxide Crystal

The hexagonal form has two interpenetrating sub lattices of Zn^{2+} and O^{2-} which make up the alternating basal planes. The zinc to oxygen coordination number is four with the cations surrounded by four anions in the corners of a tetrahedron and vice versa. The tetrahedral arrangement of atoms in the Wurtzite structure results is a non-centrosymmetric structure which gives rise to a dipole moment. This characteristic of zinc oxide Wurtzite is believed to be what gives rise to some of its unique properties such as piezoelectricity. The hexagonal lattice constants are a = 3.25 Å and c = 5.2 Å. The ratio c/a is about 1.60 which is close to the ideal value for a hexagonal cell i.e., c/a = 1.633. Zinc ions are located on alternate basal planes to the oxygen ions. To achieve transparency and good conductivity the preferred crystal growth is in the (002) plane where atomic density is highest.

Table: 1.2 Physical Properties of ZnO	
Molecular formula	ZnO
Appearance	White solid
Molar mass	81.408g/mol
Density	5.606 g/cm^3
Ionic radius	Zn^{2+} (0.74 Å)
Melting point	1975°C

Boiling point	2360°C
Band gap	3.4 eV (direct)
Refractive index	2.008
Exciton binding energy	60 MeV
Crystal Structure	Hexagonal wurtzite
Lattice constant	a=3.246Å & c=5.207Å
Semiconductor type	n-type

1.10 Properties of Manganese

Manganese is a transitional metal which is d-block molecule. It has some extra ordinary properties like various oxidation number, its forms color compound, exhibit par magnetism and a good catalyst also. Manganese is an inorganic compound which usually appears as a solid material. Physical properties are detailed in Table 3.

Table: 1.3 Physical properties of Manganese	
Molecular symbol	Mn
Physical state	Solid
Atomic weight	54.938 g/mole
Density	7.21 g·cm^{-3}
Ionic radius	Mn^{2+} (0.80 Å)
Melting point	1246 °C
Boiling point	2061 °C
Crystal structure	body-centered cubic
Electron configuration	$1s^2 2s^2 2p^6 3s^2 3p^6 3d^5 4s^2$
Oxidation state	+2, +3, +4, +6, +7
Type of metal	Transition metal
Magnetic ordering	paramagnetic

1.11 Review of the previous work

Mn doped ZnO is an important component of spintronics and other optoelectronic devices. Recently, diluted magnetic semiconductors have attracted much attention

because of their possible application in spintronics based devices. Many researchers have investigated by various preparation techniques to fabricate thin film for high performance spintronic device.

In 2006 O D Jayakumar *et al.* [10] studied that 2 and 5 at.% Mn-doped ZnO nanocrystalline particles by a co-precipitation method. X-ray diffraction data revealed that Mn-doped ZnO crystallizes in the monophasic wurtzite structure and the unit cell volume increases with increasing Mn concentration. A well resolved EPR spectrum of 5% Mn-doped ZnO samples annealed at 875–1275 K confirmed that Mn was substitutionally incorporated into the ZnO lattice as Mn^{2+}. Finally the observed room temperature ferromagnetism in Mn-doped ZnO can be attributed to the substitutional incorporation of Mn at Zn-sites rather than due to the formation of any metastable secondary phases.

In 2007 Ruh Ullah *et al.* [11] studied that Doping of ZnO with manganese (Mn2+) was intended to create tail states within the band gap of ZnO. Photocatalysts prepared with these techniques, which were characterized with transmission electron microscopy (TEM), infrared spectroscopy (FTIR), photo-co-relation spectroscopy (PCS) and UV–vis-spectroscopy showed significant difference in the optical absorption of Mn-doped ZnO. It was found that manganese-doped ZnO ($ZnO:Mn^{2+}$) much faster than undoped ZnO upon its exposure to the visible light. The experiment demonstrated that the photo-degradation efficiency of $ZnO:Mn^{2+}$ was significantly higher than that of undoped ZnO.

In 2009 Munisamy Subramanian *et al.* [12] studied that Undoped and Manganese doped zinc oxide thin films were prepared on Si substrate using spray pyrolysis technique.Nanorods having random distribution were observed on the ZnO films by scanning electron microscopy. Grazing angle X-ray diffraction and Raman spectroscopy confirmed successful growth of the wurtzite structure $Zn_{1-x}Mn_xO$ films without any secondary phase. From Raman spectra, the lattice defect was found to increase with increasing Mn concentration. Optical gap energy determined by the optical reflectance measurement showed a maximum at Mn concentration 10 mol %.

It was also found that the strain parameter increases up to 10 mol% and then decreases at 15 mol %. These tendencies seem to be related to the coexistence of Mn^{3+} and Mn^{4+} (Mn^{3+}/Mn^{4+}) ions along with the Mn^{2+} ions in the $Zn_{1-x}Mn_xO$ films.

In 2009 Gao Li *et al.* [13] reported that the radio frequency magnetron sputtering is used to fabricate ZnO and Mn-doped ZnO thin films on glass substrates at 500 ±C. The Mn-doped ZnO thin films present wurtzite structure of ZnO and have a smoother surface, better conductivity. The oxygen in the Mn-doped ZnO thin films increases with increasing Mn doping concentration. The photoluminescence spectra of ZnO and Mn-doped ZnO thin films have a similar ultraviolet emission. The yellow green emissions of 4 wt.% and 10 wt.% Mn-doped thin films are quenched, whereas the bellow green emission occurs because of abundant oxygen vacancies in the Mn-doped ZnO thin films after 20 wt.% Mn doping. Compared with pure ZnO thin films, the bandgap of the Mn-doped ZnO thin films increases with increasing Mn content.

In 2010 A. R. Abd Rashid *et al.* [14] studied that Undoped and Mn doped ZnO films with different doping concentration were synthesized by sol gel method using a spin coating technique. The quantity of Mn in the sol was varied from x = 0, 0.02and 0.04 with annealing temperature of 700 ºC. The samples were characterized using AFM to investigate the surface morphology and nanostructures. The XRD analysis shows the crystalline structure and orientation of the films. He found that hexagonal wurtzite structure and improved crystalline quality by increasing the Mn doping. Meanwhile, the optical properties were characterized using UV-Vis where the transmittance and band gap decreases upon increment of Mn concentration.

1.12 Motivation of the present work

ZnO is a II-VI semiconductor with a wide band gap of about 3.4 eV. The stable crystal structure of ZnO is wurtzite in which each atom of ZnO is surrounded by four atoms of oxygen in tetrahedral coordination. It is interesting from the viewpoint of forming a transparent ferromagnetic material due to the wide band gap. Combined with the high conductivity that can be achieved by doping, this leads to application in

surface acoustic wave devices and transparent conducting electrodes. Finally ZnO is also a strong piezoelectric [15] materials, in which the piezoelectric properties can be change the characteristics of potential energy barriers at interface, and can be exploited in the metal oxide host. Thus transition metals doped ZnO has the potential to be a highly multifunctional material with coexisting magnetic semiconducting, electromechanical and optical properties.

In addition to the high applications in ZnO material in corporating (TM) ions substitutionally in II-VI ZnO should be less difficult than incorporating them in other semiconductor hosts, since the value of Zn^{+2} can be readily adopt by many 3d transition metal ions. Thus favors substitutions of the transition metal ion at the cation site and helps in achieving higher dopant concentration. It also means that in perfectly stoichiometric sample, substitutional TM introduces a magnetic moment without contributing carriers. To understand the origin of room temperature DMS is very important for spintronics application. Therefore, Mn doped Zn system has been systematically investigated. In the present work we decided to prepare Mn doped ZnO thin films by spray pyrolysis method and to study their various physical properties and to compare the results with those obtained by others. The following will be performed.

1. To study the effect of doping on the electrical conductivity and optical properties of the film.
2. Investigation of temperature dependence resistivity.
3. To study the crystal structure of the film.
4. To study the absorption coefficient with energy and to determine optical band gap.
5. Calculations of refractive index and optical conductivity.
6. To study the doping concentration dependence of activation energy.
7. To study the morphology of the surface of the films by SEM.

References

[1] Chopra, K. L.,“Thin Film Phenomena” McGraw-Hill Book Company-New York. (1969).

[2] Faraday, M., "Experimental Relations of Gold (and Other Metals) to Light," Philosophical Transaction of the Royal society of London, 147, 145-181(1857).

[3] Nahrwold, R., Wied. Ann., “Thin metal films in a vacuum” Physik ,31, 467 (1887).

[4] Kundt,A., Ann. “Hand book of Deposition Technologes for films and coatings”, Physik, 31 ,473 (1888).

[5] Thomson, J. J., “The Materials science of thin film”, Mathematical Proceedings of the Cambridge Philosophical society, 11 .120 (1901).

[6] Matsukura, F., Ohno, H., Shen, A. and Sugawara,Y., “Wide Energy Bandgap Electronic Devices”, Physical. Review, 57. 2037 (1998)

[7] Granqvist,C. G., “Solar Energy Materials and Solar Cells”, Thin Solid Film, 166. 2235 (1963).

[8] Awschalom, D. D. Loss, D. and Samarth, N., Ed, “Semiconductor Spintronics and Quantum Computation”, Springer, New York, (2002).

[9] Datta and Das, “Electronic analog of the electro-optic modulator”, Applied Physics. Letters., Vol 56. 665 (1990).

[10] Jayakumar, O. D., Salunke, H. G., Kadam,R. M., Mohapatra, M., Yaswant, G., and Kulshreshtha1, S. K., “Magnetism in Mn-doped ZnO nanoparticles prepared by a co-precipitation method” Nanotechnology, 17, 1278–1285 (2006).

[11] Ullah, R., Dutta, J., “Photocatalytic degradation of organic dyes with manganese-doped ZnO nanoparticles,” Journal of Hazardous Materials, 156, 194–200 (2008).

[12] Subramanian, M., Selvaraj1, V., Ilanchezhiyan, P., Kumar, G., M.,, Jayavel, R., and Soga, T., "Band Gap Variation of Mn Doped ZnO Films Prepared by Spray Pyrolysis Technique", Japanese Journal of Applied Physics, 48, 06FF07 (2009).

[13] Gao, Li. and Zhang Jian-Min., "Effects of doping concentration on properties of Mn-doped ZnO thin films", IPO Sceince, Vol 18 No 10, 1674-1056 (October 2009).

[14] Abd Rashid, A. R., Menon, P. S., "Effect of Mn Doping on the Structural and Optical Properties of ZnO Films" ICSE2010 Proc. (2010).

[15] Abd Rashid, A. R., Menon, P. S., "Effect of Mn Doping on the Structural and Optical Properties of ZnO Films" ICSE2010 Proc. (2010).

CHAPTER-II

THIN FILM DEPOSITION TECHNOLOGY

CHAPTER-II
THIN FILM DEPOSITION TECHNOLOGY

2.1 Introduction

Modern thin film technology has evolved into a sophisticated set of techniques used to fabricate many products. Thin-film deposition technique deposits a layer of thin material onto a substrate or onto previously deposited layers. "Thin" is a relative term, but most deposition techniques allow layer thickness to be controlled within a few tens of nanometers, and some (molecular beam epitaxy) allow single layers of atoms to be deposited at a time. Applications include very large scale integrated (VLSI) circuits, solar cell, sensors, optics (for reflective or anti-reflective coatings), electronics (layers of insulators, semiconductors, and conductors form integrated circuits), packaging (polyethylene terephthalate PET film) as well as protective and decorative coatings. Similar processes are sometimes used where thickness is not important: for instance, the purification of copper by electroplating and the deposition of silicon and enriched uranium by a CVD-like process after gas-phase processing. Deposition techniques fall into two broad categories, depending on whether the process is primarily chemical or physical. Generally thin films are prepared by depositing the film material, atom by atom onto a substrate. One of the examples is the condensation of vapor to give a solid or liquid film. Such process of deposition involves a phase transformation. In this chapter, some of the commonly used thin film deposition techniques are described briefly and our intension is to prepare thin films by the spray pyrolysis method, so this method has been discussed in some details. The following is a brief description of some common methods of thin film deposition technique for research, development and production purposes.

2.2 Classification of the thin film deposition techniques

Thin films are deposited by many techniques to develop the film quality according to their applications. There are two main categories of the thin film deposition techniques:

(i) Chemical deposition process

(ii) Physical deposition process.

Physical and chemical both deposition techniques include several types of deposition techniques to produce thin films. Figure 2.1 illustrates the classification of the different deposition techniques. Some most used deposition techniques are described below.

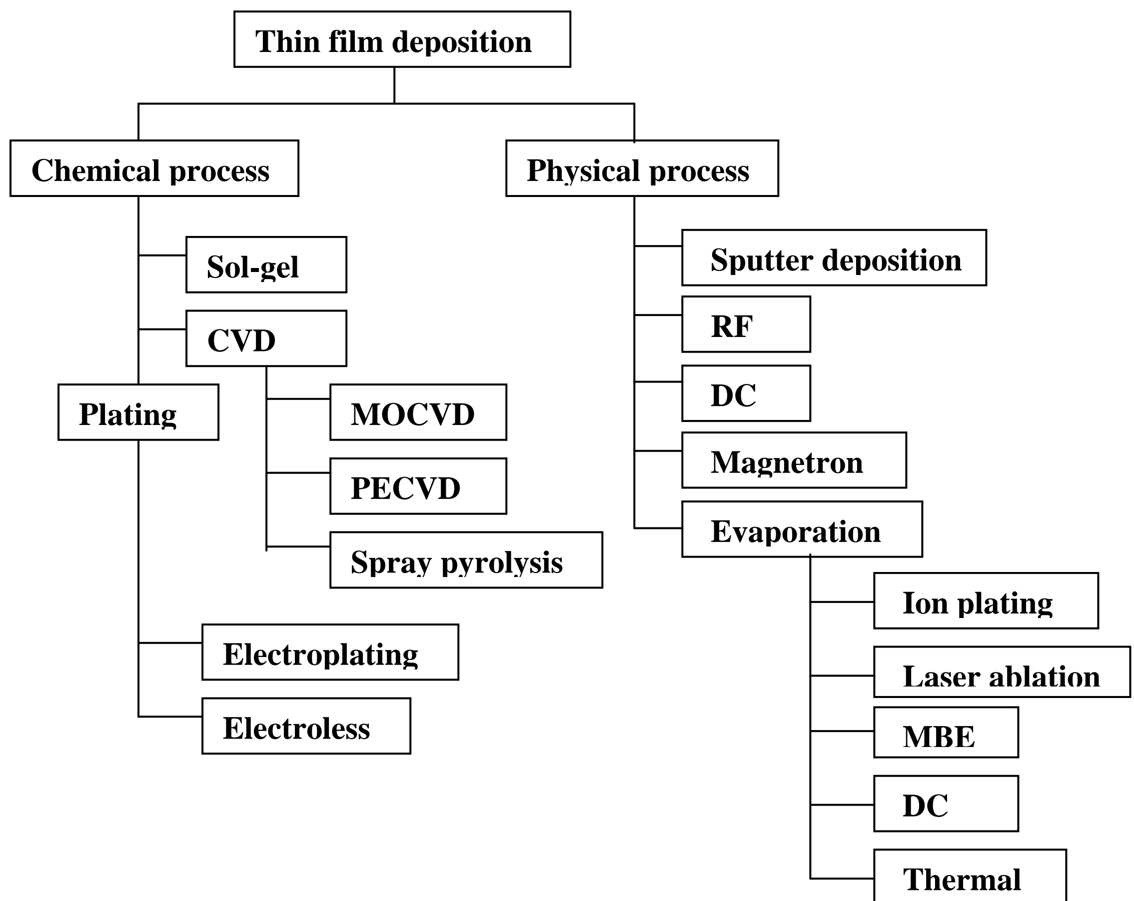

Fig. 2.1: Classification of the most common thin film deposition techniques.

2.2.1 Chemical deposition

Here, a fluid precursor undergoes a chemical change at a solid surface, leaving a solid layer. An everyday example is the formation of soot on a cool object when it is placed inside a flame. Since the fluid surrounds the solid object, deposition happens on every surface, with little regard to direction; thin films from chemical deposition

techniques tend to be conformal, rather than directional. Chemical solution deposition (CSD) and chemical vapor deposition (CVD) are chemical deposition techniques.

2.2.2 Physical deposition

Physical deposition uses mechanical or thermodynamic means to produce a thin film of solid. An everyday example is the formation of frost. Since most engineering materials are held together by relatively high energies, and chemical reactions are not used to store these energies, commercial physical deposition systems tend to require a low-pressure vapor environment to function properly; most can be classified as physical vapor deposition (PVD).

The material to be deposited is placed in an energetic, entropic environment, so that particles of material escape its surface. Facing this source is a cooler surface which draws energy from these particles as they arrive, allowing them to form a solid layer. The whole system is kept in a vacuum deposition chamber, to allow the particles to travel as freely as possible. Since particles tend to follow a straight path, films deposited by physical means are commonly directional, rather than conformal. Examples of physical deposition include: thermal evaporation, sputtering, spray pyrolysis etc.

2.2.3 Thermal or vacuum evaporation

The thermal evaporation [1] is the simple, convenient and most widely used method for the preparation of thin films. In this method, materials are vaporized by heating it to a sufficient high temperature and the condensation of the vapor into a relatively cooler substrate yielding thin solid films. A “boat” typically made of tungsten, which has a high melting point, has a little dimple into which the material to be evaporated is placed. The boat is heated in vacuum to a high enough temperature so that the vapor pressure of the evaporated material is appreciable, and the vapor is allowed to condense on a “cold” substrate. “E-beam” evaporation is a variation in which electrons are accelerated and directed at the target material, causing it to heat up. This technique allows more precise control of deposition rates and film composition

as shown in Fig. 2.2. Thermal evaporation may be performed directly or indirectly by a variety of physical method. Several variants are:

(i) Resistive heating
(ii) Exploding wire technique,
(iii) Flash evaporation,
(iv) Arc evaporation,
(v) Laser evaporation,
(vi) R.F. heating and
(vii) Electron beam evaporation.

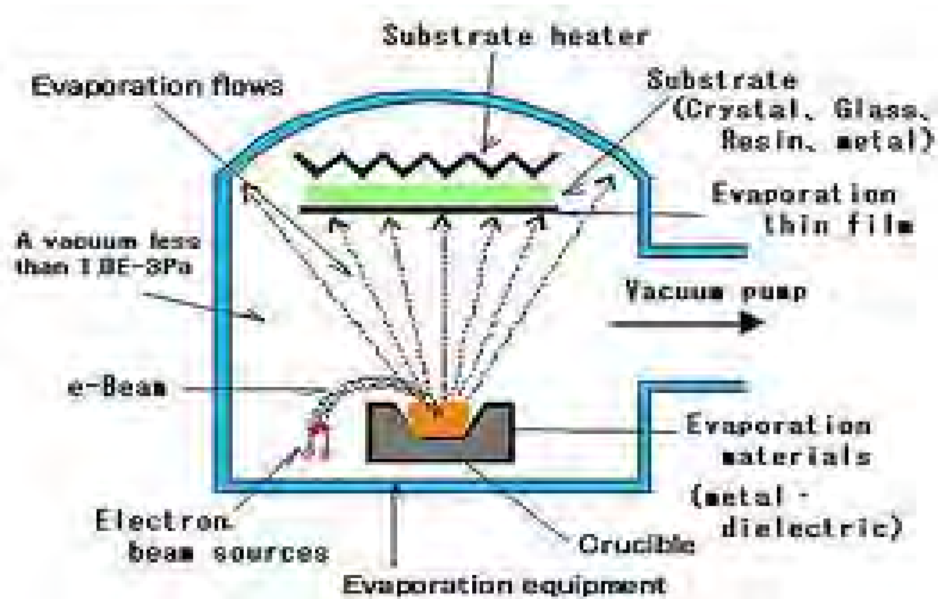

Fig. 2.2: Electron beam evaporation method.

2.2.4 Dipping and withdrawing

The dipping technique [2] consists essential of inserting the substrates into a solution containing hydrolysable metal and putting it out at a constant speed into on atmosphere containing water vapor. In this atmosphere hydrolysis and condensation processes take place. Finally, the films are hardened. This technique has been used commercially to deposit large area coating of zinc oxide.

2.2.5 Chemical vapor deposition (CVD) method

CVD is a materials synthesis process whereby constituents of the vapor phase react chemically near or on a substrate surface to form a solid product. The deposition technology has become one of the most important means for creating thin films and coatings of a very large variety of materials essential to advanced technology, particularly solid-state electronics where some of the most sophisticated purity and composition requirements must be met [3]. The main feature of CVD is its versatility for synthesizing both simple and complex compounds with relative ease at generally low temperatures. Both chemical composition and physical structure can be tailored by control of the reaction chemistry and deposition conditions. Fundamental principles of CVD encompass an interdisciplinary range of gas-phase reaction chemistry, thermodynamics, kinetics, transport mechanisms, film growth phenomena, and reactor engineering. The coating system is shown in Fig. 2.3.

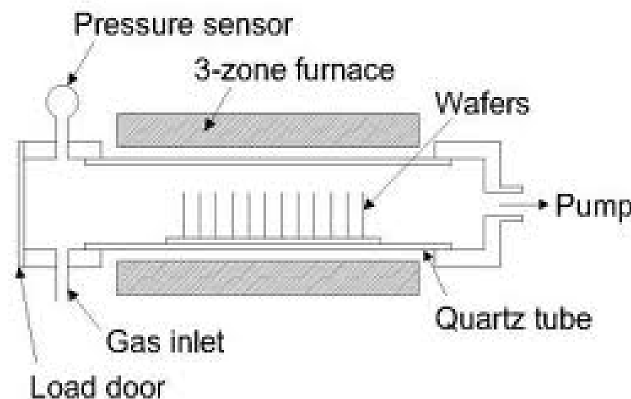

Fig. 2.3: Schematic diagram of chemical vapor deposition process.

2.2.6 Sputtering

In sputtering, atoms are removed from one surface by energetic ion bombardment and allowed to collect on another surface shown in Fig. 2.4. Noble gas ions, typically argon, are used to bombard the surface of the material from which one wishes to make a thin film. Incident ions with large kinetic energy collide with surface atoms and give them enough kinetic energy to leave the surface and travel to the substrate.

It is somewhat like shooting cannon balls at a cement wall causing chunks to fly off. Eventually the sputtered atoms accumulate in a layer on the substrate, forming a thin film [4].

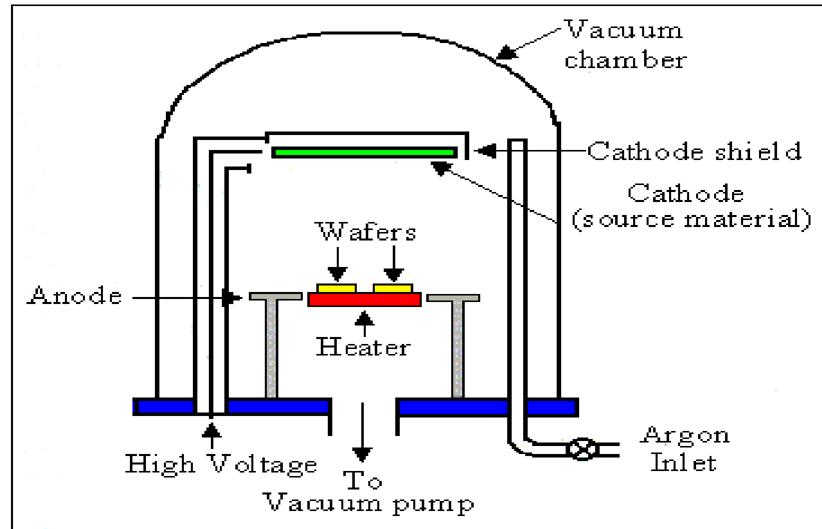

Fig. 2.4: Schematic diagram of sputtering process.

2.2.7 Epitaxial growth

An advantage of epitaxy is the high growth rate of material, which allows the formation of films with considerable thickness (>100μm). Epitaxy [5] is a widely used technology for producing silicon on insulator (SOI) substrates. The technology is primarily used for deposition of silicon. A schematic diagram of a typical vapor phase epitaxial reactor is shown in Fig. 2.5. This technology is quite similar to what happens in CVD processes, however, if the substrate is an ordered semiconductor crystal (i.e. silicon, gallium arsenide), it is possible with this process to continue building on the substrate with the same crystallographic orientation with the substrate acting as a seed for the deposition. If an amorphous/polycrystalline substrate surface is used, the film will also be amorphous or polycrystalline. Epitaxial films are grown by three techniques, such as

(a) Liquid phase epitaxy
(b) Vapour phase epitaxy
(c) Molecular beam epitaxy.

Fig. 2.5: Schematic diagram of epitaxial growth layer.

2.2.8 Molecular beam epitaxy (MBE)

Molecular beam epitaxy [6] is the ultimate and most expensive technique. In this technique ideal condition is achieved by reducing the deposition rate to the lowest value, increasing the substrate temperature to the highest value about 900°C, and creating the best vacuum of 10^{-8} or 10^{-9} millibar. This condition is best suited as when the higher energies given to molecules or atoms, they go and sit in the place. It is ideally suited for giving sufficient energy to become crystalline films. Single crystal films control the growth rate layer by layer and one have the best control on this technique as shown in Fig. 2.6. One of the advantages of this method rests on the control of the growth in real time thanks to the in situ use of the high energy electron diffraction in grazing incidence.

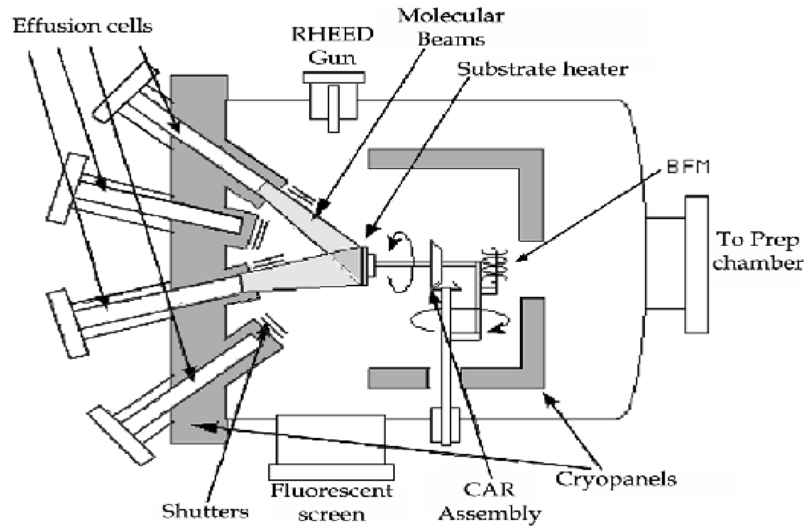

Fig. 2.6: Schematic diagram of molecular beam epitaxy method.

2.2.9 Electroplating

In electroplating a metallic coating is electrodeposited on the cathode of an electrolytic cell consisting of a positive electrode (anode), a negative electrode (cathode), and an electrolyte solution (containing the metal ions) through which electric current flow Fig. 2.7.

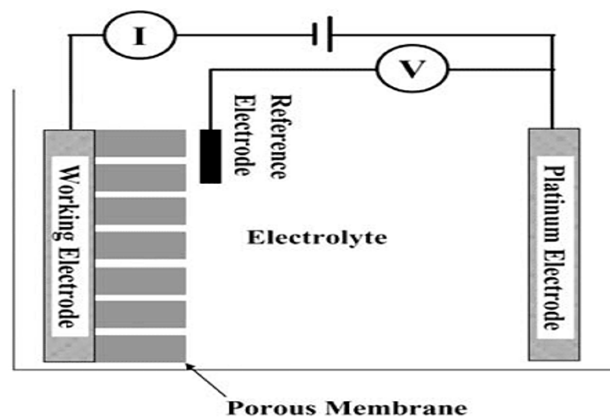

Fig. 2.7: Schematic diagram of electroplating process.

The quantitative aspects of the process are governed by Faraday's laws. Important electroplating variables include current efficiency, current density, current distribution, pH, temperature, agitation, and solution composition. Numerous metals and metal alloys have been successfully electroplated from aqueous solutions [7].

However, the technically most useful electroplated metals are chromium, copper, nickel, silver, gold, rhodium, zinc, and a series of binary alloys including chromium/nickel composites. Electroplating is widely used in industry and can produce deposits that range from very thin films to very thick coatings (electroforming).

2.2.10 Sol gel method

In the sol-gel process [8] the precursor is dissolved in a solvent (forming a sol or gel depending on the reactor conditions) and precipitates due to chemical reactions. The sol-gel process consists on 4 basic steps: hydrolysis, condensation and polymerization of particles, growth of particles and agglomeration and formation of networks. The outcome of the process depends on several factors that influence the hydrolysis and condensation rates. Among them, there are few that are considered to have a greater impact: pH, nature and concentration of catalysts, H_20/precursor molar ratio and temperature. This production method could be used to produce different nanostructures such as nano-particles, nano-porous materials or nano-fibres, while the creation of thin films can use a number of methods (e.g. spin coating, dip coating). Some of the bottlenecks highlighted herein are common to all these nanostructures production.

2.2.11 Pulsed laser deposition (PLD)

Pulsed laser deposition is a thin film deposition technique where a high power pulse laser beam is focused inside a vacuum chamber to strike a target of the material that is to be deposited. This material is vaporized from the target (in a plasma plume) which deposits it as a thin film on a substrate (such as a silicon wafer facing the target). This process can occur in ultra high vacuum or in the presence of a background gas, such as oxygen which is commonly used when depositing oxides to fully oxygenate the deposited films. When the laser pulse is absorbed by the target, energy is first converted to electronic excitation and then to thermal, chemical and mechanical energy resulting in evaporation, ablation, plasma formation and even exfoliation [9]. The ejected species expand into the surrounding vacuum in the form of a plume containing many energetic species including atoms, molecules, electrons,

ions, clusters, particulates and molten globules, before depositing on the typically hot substrate. The schematic diagram of PLD is shown in Fig. 2.8.

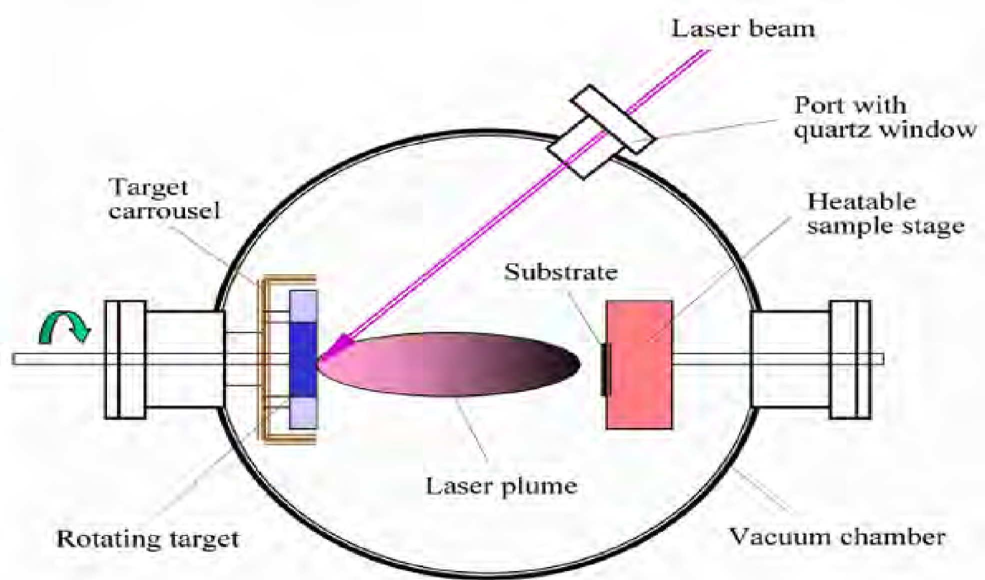

Fig. 2.8: Schematic diagram of pulsed laser deposition process.

2.2.12 Thermal oxidation technique

Thermal oxidation is a technique of oxidation of the substrate surface in an oxygen rich atmosphere as shown in Fig 2.9. It uses very high temperatures (approximately 700-1300ºC) to increase the growth rate of oxide layers. This high temperature issued to speed up the oxidation process. The process consists of exposing the raw material substrate to an oxidizing environment (O_2 dry oxidation or H_2O wet oxidation) and occurs at the surface of the substrate where the raw material is progressively replaced by the correspondent oxide. The oxide growth rate is positively affected by time, temperature, and pressure [10].

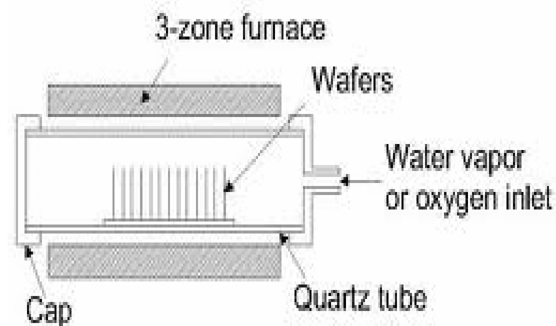

Fig. 2.9: Schematic diagram of thermal oxidation process.

2.2.13 Spray pyrolysis (SP)

The spray pyrolysis technique is a simple, low cost and powerful method for the preparation of thin films as shown in Fig. 2.10. It is a process in which a thin film is deposited by spraying a solution on a heated surface, where the constituents react to form a chemical compound. This technique involves spraying a solution usually in aqueous, containing soluble constituent atoms of the desired compound onto a heated substrate. Every sprayed droplet reaching the substrate undergoes pyrolytic decomposition and forms a single crystallite or a cluster of crystallites of the products. The other volatile by products and the excess solvent escape in the vapor phase. This method is cheaper and more convenient. The spray deposition has been used to prepare coatings for the cover glass required for flat plate collectors and

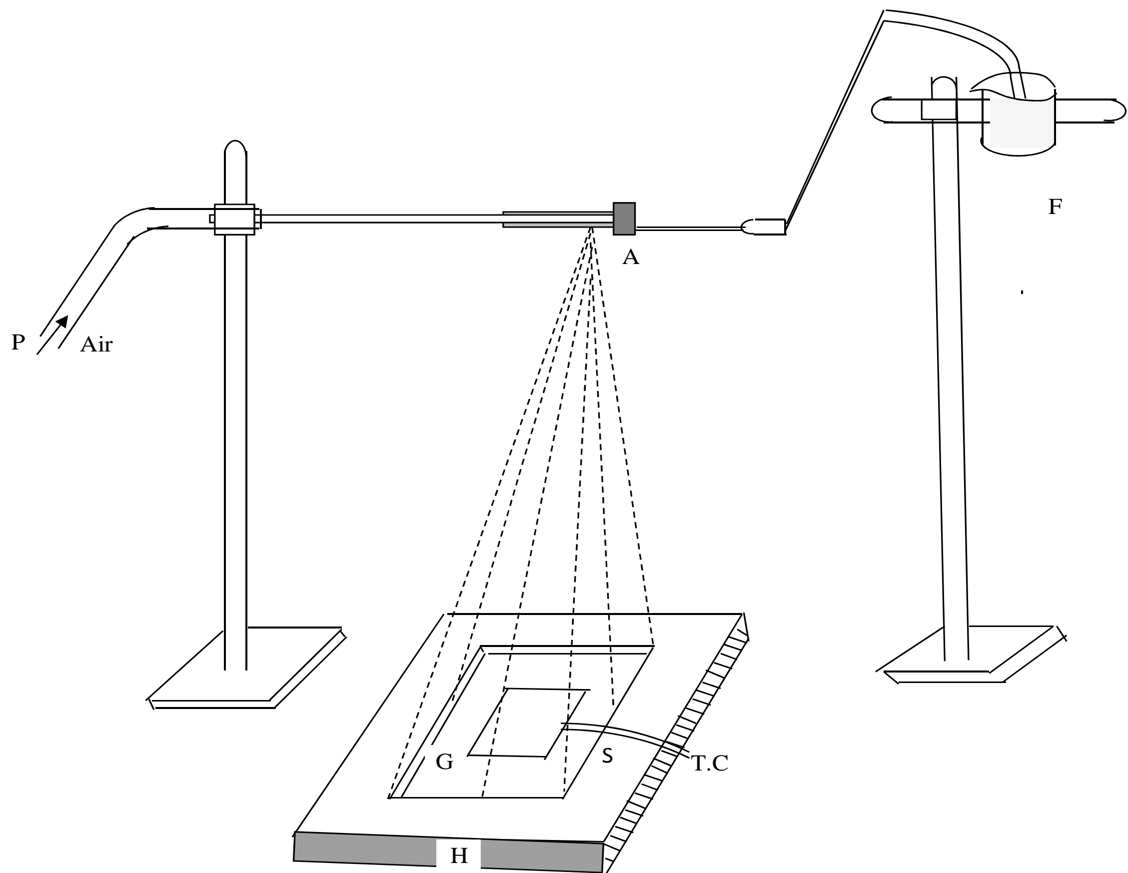

A = Lower tube G = Metal plate H = Heater S = Substrate P = Upper tube
F = Beaker T.C. = Digital multimeter with a thermocouple.

Fig. 2.10: Schematic diagram of spray pyrolysis technique.

other tube used in the focusing type cylindrical collectors. This method is mainly used in the ceramic industry. When compressed air is passed through P at a constant pressure, a fine aerosol was produced and was automatically carried to the reactor zone where film was deposited on the heated substrate. The details mechanism of spray pyrolysis technique has been discussed in chapter three.

References

[1] Kuroyangi, A., “Properties of aluminum-doped ZnO thin films grown by electron beam evaporation”, Japanese Journal of Applied Physics, 28. L219 (1989).

[2] Hamberg, I. and Granquist, G.C., “Evaporated Sn-doped In_2O_3 films: Basic optical properties and applications to energy-efficient windows”, Japanese Journal of Applied Physics. 60, R123 (1986).

[3] Han., O., Fand, P.O. Brien, “CVD Diamond for Electronic Devices and Sensors”, Thin Solid Films, 95, 173 (1989).

[4] Deok-Kyu Kim., Hong-Bae Kim., “Dependence of the properties of sputter deposited Al-doped ZnO thin films on base pressure” Journal of alloys and compounds, 522, 69-73 (2012).

[5] MNX; microsystem design and fabrication partner and nanotechnology exchange, (2007).

[6] Campbell, D. S., “handbook of thin-film deposition processes and techniques principles, methods, equipment and applications.” (2004).

[7] Aleksandrov, L., “Thin Film Science and Technology.” Elsevier, New York. 5 (1984).

[8] NMR; Nanoroadmap project, “Roadmaps at 2015 on nanotechnology application in the sectors of: Materials, Health & Medical Systems.” Energy, 2005.

[9] Kim, H., Horwitz, J. S., Kim, W. H., Kafafi, Z., D. B. Chrisey. 780 (2003) 21-32.

[10] Jaeger, Richard C., "Thermal Oxidation of Silicon". Introduction to Microelectronic Fabrication. (2001).

CHAPTER-III

THEORETICAL STUDY

CHAPTER-III
THEORETICAL STUDY

This chapter includes theoretical studies of thin film formation, structural, optical, electrical properties and thermoelectric power of thin films.

PART A: FORMATION OF THIN FILM

3.1 Introduction

The ideal condition of the film formation involves the deposited of the material atom by atom (or molecule by molecule) and layer by layer and there should be a sufficient time interval between the two successive depositions of atoms and also layers so that these can occupy the minimum potential energy configuration with respect to the substrate and subsequently on previously deposited layers. In a thermodynamically stable film all atoms (or molecules) should be in their minimum potential energy sites and the incoming atoms (or molecules) will take up positions and orientations energetically compatible with the neighboring atoms of the substrate or to the previously deposited layers. Hence the occupation sites of freshly arrived atoms or molecules will be determined energetically both by the substrate and the previously deposited atoms or layers. With the build up of layers, the effect of the substrate or the initial layers will gradually diminish but the influence of the freshly formed layers will always be present on the incoming atoms or molecules to determine their occupation sites. However, all deposition processes are carried out in environments which are far from the idealized deposition conditions and hence neither the successive atomic or molecular layers have sufficient interval of time for achieving the thermo dynamical equilibrium condition nor a layer is completed before the formation of the second or even the third or other layers start. These deviations from the idealized condition of depositions result in the formation of meta-stable films some typical growth feature, surface asperities, etc. Moreover, the thermo dynamical conditions may change with time requiring a change in equilibrium [1].

3.2 Different stages of film formation

There are three mechanism of thin film condensation which can be distinguished, depending on the strength of interaction between the atoms of the growing film and between the atoms of the film and substrate. These are:

(i) The layer-by-layer growth (Vander Merwe mechanism).
(ii) A three dimensional nucleation, forming, growth and coalescence of islands (Volmer-Weber mechanism).
(iii) Absorption of a monolayer and subsequent nucleation on the top of this layer (Stranski-Krastanov mechanism).

In most cases, mechanism (ii) takes place and we shall focus our attention on this mechanism in brief.

3.2.1 Condensation

Thin films are most commonly prepared by the condensation of atoms on a substrate from the vapour phase of the material. Condensation means the transformation of a gas in to a liquid or solid. Thermodynamically, the only requirement for condensation to occur is that partial pressure of the film material in the gas phase be equal or larger than its vapour pressure in the condensed phase at that temperature.

Condensation of a vapour atom is determined by its interaction with the impinged surface. The impinging atom is attracted to the surface by the instantaneous dipole and quadruple moments of the surface atoms. Consequently the atoms losses its velocity component normal to its surface in a short time, provided the incident kinetic energy is not too high. The vapour atom is then physically absorbed (called ad atom) but it may or may not be completely thermally equilibrated. It may move over the surface by jumping from one potential to the other because of the thermal activation from the surface and its own kinetic energy parallel to the surface. The ad atom has a finite stay or residence time on the substrate during which it may interact with other ad atoms to forma stable cluster and be chemically absorbed with the release of the heat of condensation. If is not absorbed the ad atom re-evaporates or desorbs into the vapour phase. Therefore, condensation is the net result of

equilibrium between the absorption and desertion process. The probability that an impinging atom will be incorporated into the substrate is called the "condensation" or "striking coefficient". It is measured by the ratio of the amount of material condensed on a surface to the total amount impinged. In fact, often the striking coefficient is so small that condensation is not observable by ordinary techniques. On the other hand, the striking coefficient is found to be strongly dependent on the total time during which the substrate was subjected to the impingement, and also on the substrate temperature. A non- unity striking coefficient is usually explained in terms of monomer re-evaporation form the areas on the substrate, which are outside, the capture zones around each stable nucleus. Langmuir and Frenkel formulated (1916-1924) condensation model. This model considers vapor →solid transformation. At high deposition temperatures, a vapor →Liquid (amorphous) →solid condensation mode may occur. Semen off (1930) suggested that heterogeneous nucleation always proceeds by nucleation of crystallites within the amorphous film in which the absorbed atoms move over the surface during their life times to form pairs which in turn, act as condensation center's for other atoms.

3.2.2 Nucleation

Nucleation is the birth stage of a film. Condensation is initiated by the formation of small cluster through the combination of several absorbed atoms. These clusters are called nuclei and the process of formation is called nucleation. There are two types of nucleation occurs during the formation of a film; homogeneous and heterogeneous nucleation. Volmar, Weber and Becker and Doring [2, 3] postulated a homogeneous nucleation theory, which takes into account the total free energy of formation of a cluster of ad atoms. It is later extended to heterogeneous nucleation by Volmer and to the particular shapes of clusters in a thin film case by Pound et al. [4]. In this theory clusters are formed by collisions of atoms on the substrate surface, and in the vapor phase its super saturation is sufficiently high. They initially developed with an increase in free energy until a critical size is reached above which growth continues with a decrease in free energy. In atomistic theory in low substrate temperature or very high super saturations, the critical nucleus may be a single atom which will

form a pair with another atom by random occurrence to become a stable cluster and grow spontaneously shown in Fig. 3.1.

3.2.3 Growth

There are several stages in the growth process from the initial nucleation of the deposits to the final continuous three dimensional film formation states. These stages of film growth have been observed by many workers from their electron microscopic and other studies. These are valid not only for deposits condensing from the vapour phase but also for others, i.e. for solutions, by electro deposition, chemical reactions anodic oxidation, etc. Even though the controlling factors may differ slightly or widely in the individual case these stages have been clearly distinguishes by Pashley et al. [5, 6] as under

(i) The island stage
(ii) The coalescence stage
(iii) The channel stage
(iv) The continuous film stage.

3.2.3.1 The island stage

The islands consist of comparatively larger nuclei or embryos and generally of three-dimensional natures with their height, however, much less than their lateral dimensions. The formation of these islands and their growth take place by direct addition of atoms either from the vapour phase or from other environment or by the diffusion controlled process of ad atoms or both. The diffusion-controlled process is more commonly observed except at low substrate temperature. According to Walton [7] critical nuclei formed from the vapour phase will consist of about six or fewer atoms. Electron microscopic observations by various workers show that the smallest stable nuclei are of radii of about 5 Å and also that most embryos prior to the formation of island structure are of sizes about 15-30 Å. Since a nucleus of about 5 Å size is made up of about 20 atoms or so, an island will be made up about 50-100 atoms or more. As these islands grow in size these often have tendencies to develop some crystallographic facets during the early stage of their growth and such faceted particles of sizes about 30-50 Å could be observed.

3.2.3.2 The coalescence stage

The coalescence involves considerable transfer of mass between islands by diffusion. Small Island disappears rapidly. The process resembles the sintering of bulk power where the individual particles assume spherical shapes due to the lowering of their surface energies. During coalescence of two islands which occurs at their necks recrystallization as well as annealing takes place leading to some definite shapes of larger islands as shown in Fig 3.1. The time of coalescence is very short about 0.6 second. This process can takes place amongst islands which are appropriately positioned and the coalesced islands generally become triangular or hexagonal as a result of the rapid decrease of the uncovered substrate surface area followed by, a slow rise of it. After the coalescence of island to larger masses some nuclei can still be observed in between the large coalesced masses. Often coalescence by bridging of two particles is pronounced.

3.2.3.3 The channel stage

As the coalescence continues with deposition there will be a resultant network of the film with channels in Fig. 3.1. These channels need not remain void and soon some secondary nuclei start to grow within this void space in the channel. With further deposition these nuclei will increase in size along with the film thickness in addition to formation of new island stage and eventually join the main islands or aggregate thus bridging the gaps. It is quite likely that the joining of secondary islands to the parent body may not be completed or these may not be on perfect matching arrangement with the main aggregate. As a result some strain may develop due to the stress in between them caused by an insufficient surface or volume mobility or even because of the non-coalescence at the peripheries. The resultant effect of mis-matching of these is the formation of grain boundaries. Some times these channels may not be completely filled up even with increasing film thickness thus leaving some holes or gaps on the aggregate mass. With increasing film thickness, these holes or gaps will decrease in size.

3.2.3.4 The continuous film stage

When these gaps are completely bridged by the secondary nuclei, films will be continuous. However, it often happens that some void space may still remain unabridged. In an ideal continuous film there should not be any gap in the aggregate mass. Such a stage in a film can be attained only when the film has attained certain average film thickness. The minimum film thickness for the continuous stage is also dependent on the nature of the deposits, modes of deposition parameter etc. For a non-metallic deposit such a stage is generally achieved when the average film thickness is between 500 to 1000 Å and for metallic films less. It depends upon the nature of the film material, substrate temperature, rate of deposition, etc. The growth of film as mentioned earlier also involves recrystallisation and often annealing processes. If the deposits do not have sufficient time for recrystallisation or annealing before the subsequent uni- or multi-coalescence takes place the film will be in a metastable state. The subsequent layers formed over them will also be in such a state. Thermal annealing treatment for a sufficiently long period of time will cause migration of diffusion hot some atoms leading to a stable phase. This is known as ageing of films. Different stages in the growth of a film are schematically shown in Fig. 3.1.

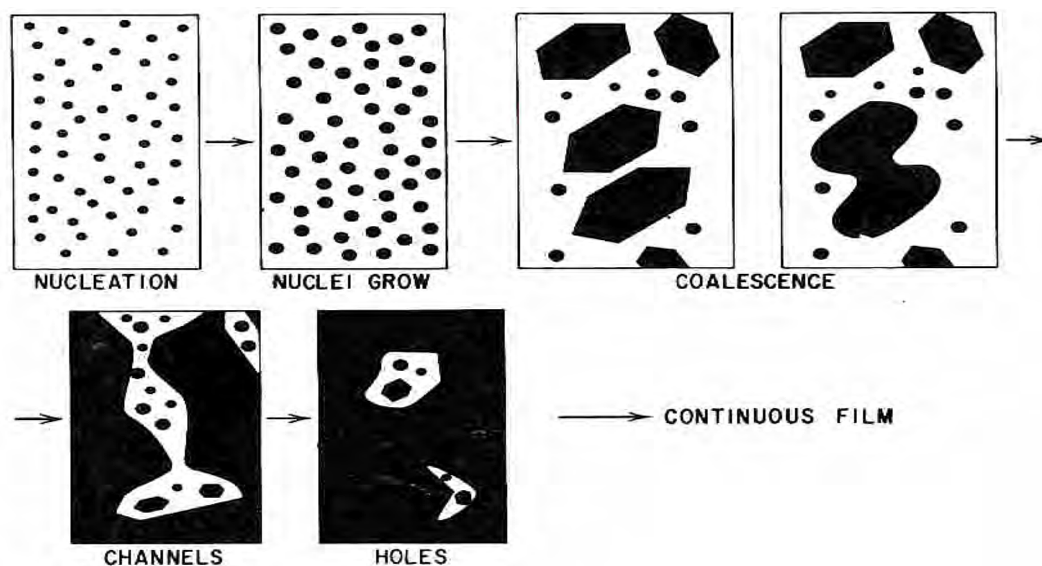

Fig.3.1: Different stages of film growth.

PART B: METHODS OF FILM THICKNESS MEASUREMENT

3.3 Introduction

Thickness dependence of electrical and optical properties of thin sold films was measured by Thomson (1901). In thin film experiments, thickness measurement is an essential job. All most all the electrical parameters except the Hall mobility and sheet resistance and also optical parameters need for their evaluation the value of film thickness should be measured with precision as far as possible. It may be measured either by in-situ monitoring of the rate of deposition or after the film is taken out of the deposition chamber. Some of the common methods of measurement of film thickness are as follows:

(i) Balance method
(ii) Electrical method
(iii) Gravimetric method
(iv) Stylus method
(v) Colour comparison
(vi) Fizeau fringes method
(vii) Newton's ring method
(viii) Optical interference method.

3.3.1 Gravimetric method

This is one of the oldest techniques for the determination of film thickness. In this method the mass of a film (m) of area, A is determined by a microbalance by weighting the substrate before and after deposition. The thickness is then calculated by assuming the density of the film material is ρ. The thickness t of the film is then given by

$$t = \frac{m}{A\rho} \tag{3.1}$$

3.3.2 Interference fringe method

Weiner was the first to use interference fringes to measure film thickness. When two reflecting surfaces are brought into close proximity interference fringes are produced, the measurement of which makes possible a direct determination of film thickness and surface topography with high accuracy. In this method, two types of fringes are utilized for thickness measurement. The first produces Fizeau fringes of equal thickness, using a monochromatic light source. The second uses a white light source and produces fringes of equal chromic order. The second method is preferred for films thinner than a few hundred angstroms since it is capable of higher resolving power. The former types slightly simpler experimentally, that this method (Fizeau fringes) was used in the present work for the measurement of film thickness in which sodium light was used as a monochromatic source.

When two reflecting surfaces are brought into close proximity, interference fringes are produced and the measurement of which makes it possible a direct determination of the film thickness. A low power microscope, monochromatic source, glass plates and an interferometer were used for experimental set up. The Fizeau fringes of equal thickness are obtained in an optical apparatus of the type shown in Fig. 3.2. The fringe spacing and fringe displacement across the step are measured and used to calculate the film thickness. If h be the fringe displacement and d the fringe spacing then the film thickness t is given by,

$$t = \frac{h}{d} \times \frac{\lambda}{2} \text{ (nm)} \tag{3.2}$$

where λ is the wavelength of the monochromatic light. The thickness of the film was calculated by using equation (3.2).

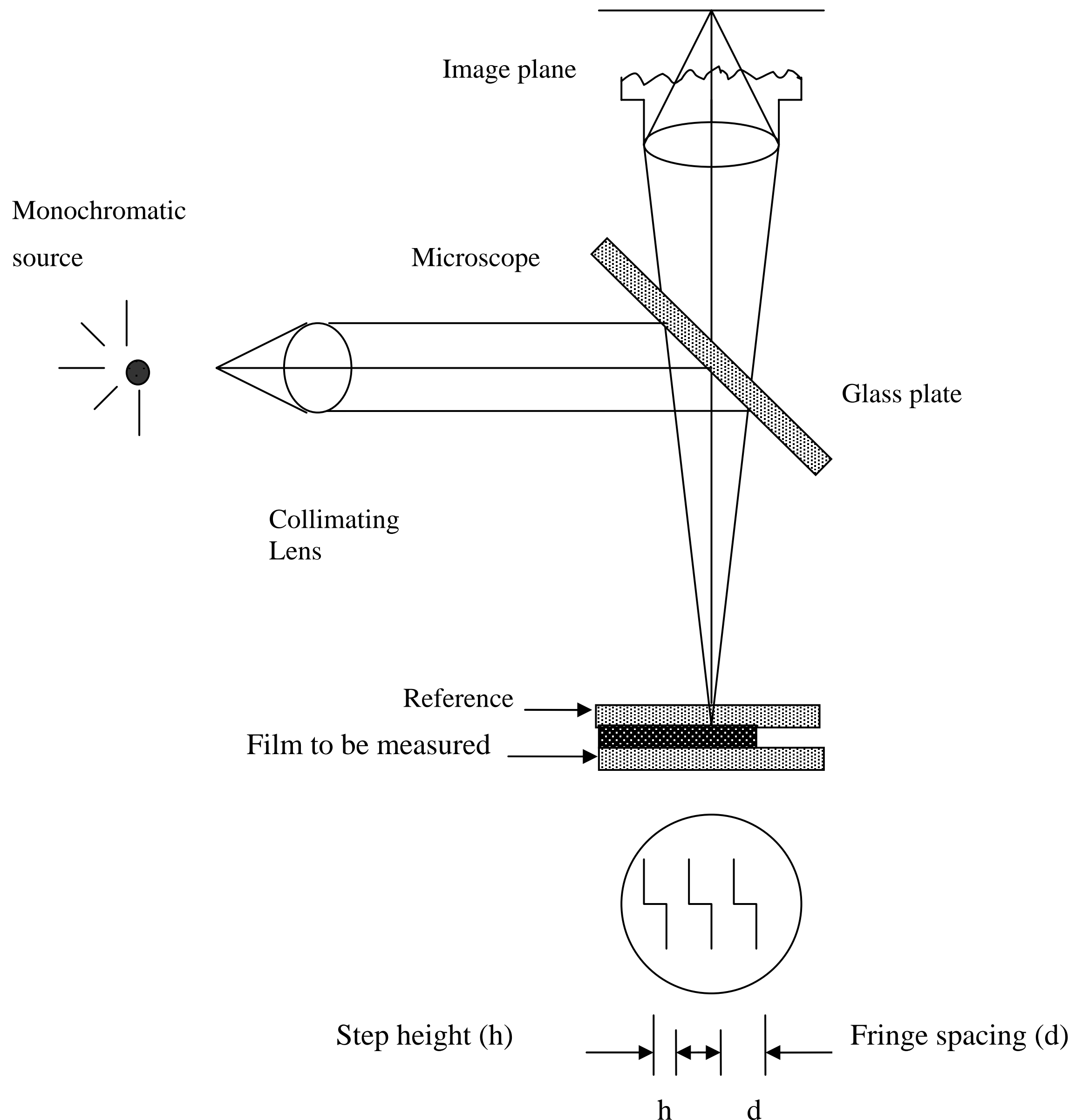

Fig.3.2: Interferometer arrangements for producing Fizeau fringes of equal thickness.

3.3.3 Newton's ring method

When a plane convex lens of large radius of curvature is placed on a plane glass substrate, a thin film of gradually varying thickness of formed. When the point of contact to viewed with monochromatic light it is found to be surrounded by alternate dark and bright ring. When it is viewed with white light it to found to be surrounded

by several colored rings with the center as dark. Let us consider a particular ring formed at a point B. The radius of the ring, PB = r'_n. Let the thickness of the air film at a point B is t' i.e., AB = t'. From the right angle triangle OAE we get,

$$OA^2 = OE^2 + AE^2$$

or, $$OA^2 = (OP - PE)^2 + PB^2$$

or, $$R^2 = (R - t')^2 + r_n'^2$$

or, $$R^2 = R^2 - 2Rt' + t'^2 + r_n'^2$$

But t' is very small, so we can neglect the term t'^2. Therefore

$$2Rt' = r_n'^2$$

or, $$t' = \frac{r_n'^2}{2R} \qquad (3.3)$$

Now if we set a thin film of uniform thickness between the lens and the glass substrate as shown in Fig. 3.3.

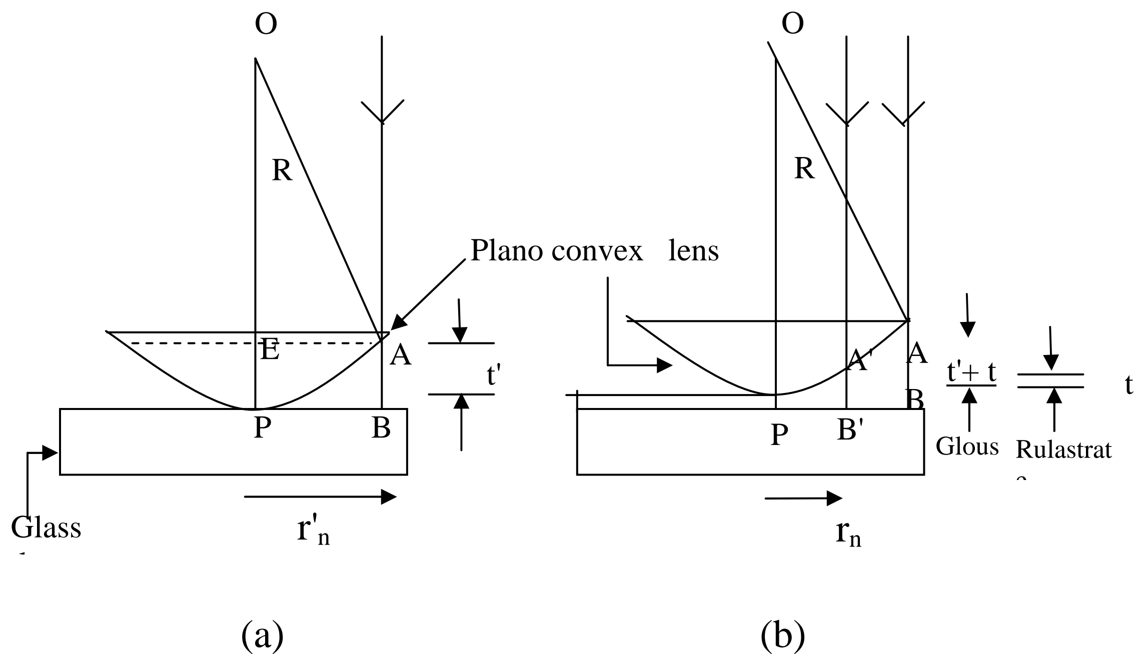

Fig.3.3: Schematic diagram for measurement of thickness by Newton's ring method (a) arrangement without film (b) arrangement with film.

Then due to the film thickness t, the thickness of the air film will be increased by an amount t and the ring for film thickness t will be formed at another point B' closer to the contact point P and in that case we get,

$$t + t' = \frac{r_n^{\ 2}}{2R} \tag{3.4}$$

where r_n is the radius of the ring at B'. Subtracting equation (3.3) from equation (3.4) we get,

$$t = \frac{r_n^{\ 2} - r_n'^2}{2R}. \tag{3.5}$$

Thus measuring the radius of n-th ring without film and with film we can calculate the thickness of the film using equation (3.5). The radius of the selected ring has been measured by measuring the chord length, and the perpendicular distance between the midpoints of the arc interested by the chord. A traveling microscope has been used for this purpose. An extra device with adequate traveling facility and micrometer has been attached to the vertical arm of the microscope so that it can move in YOY' direction in addition to XOX' direction. Movement in the ZOZ' direction is also kept functioning. If l is the length of the chord and h is the perpendicular then the radius can be measured using the relation,

$$r = \frac{l^2}{8h} + \frac{h}{2} \tag{3.6}$$

PART C: STUDY OF STRUCTURAL AND OPTICAL PROPERTIES OF THIN FILM

3.4 X-ray diffraction

To understand the physical nature of a material, it is important to know the structure of the material. X-ray diffraction is a nondestructive important experimental tool to investigate the crystal structure of a synthesized material. There are many techniques among which powder method is one of the easier and versatile techniques. From which only the powder method is discussed below.

3.4.1 The Powder method

A method of X-ray diffraction analysis in which a collimated, monochromatic beam of X-rays are directed at a sample consisting of an enormous number of tiny crystals having random orientation, producing a diffraction pattern that is recorded on film or with a counter tube is called powder method. The most common method of structure determination is the technique of X-ray diffraction.

The powder method derived by Debye and Scherer and independently by Hull in 1919 is the most widely used method in the field of applied X-rays. When the crystalline material is not available in the form of discrete single crystals then X-ray diffraction patterns are obtained by aggregation of crystals usually of the form of fine powder using a powder camera or diffractometer. Basically the method involves diffraction of monochromatic X-rays by a powder or a fine-grained polycrystalline specimen and if properly employed can yield a great deal of structural information about the material under investigation. Each particle, a grain in the specimen, is tiny crystal oriented at random with respect to the incident beam. There is fair change that a certain (hkl) plane will be correctly oriented to reflect the incident beam. Thus an angular variation of θ is obtained, not by rotating a single crystal about one of θ its axis but through the presence of many small crystals randomly oriented in space in the specimen. This variation can be determined from Bragg's law.

Bragg's law states that when X-rays hit an atom, they make the electronic cloud move as does any electromagnetic wave. The movement of these charges re-radiates waves with the same frequency (blurred slightly due to a variety of effects); this phenomenon is known as the Rayleigh scattering (or elastic scattering). The scattered waves can themselves be scattered but this secondary scattering is assumed to be negligible. A similar process occurs upon scattering neutron waves from the nuclei or by a coherent spin interaction with an unpaired electron. These re-emitted wave fields interfere with each other either constructively or destructively (overlapping waves either add together to produce stronger peaks or subtract from each other to some degree), producing a diffraction pattern on a detector or film. The resulting wave interference pattern is the basis of diffraction analysis. Both neutron and X-ray

wavelengths are comparable with inter-atomic distances (~150 pm) and thus are an excellent probe for this length scale. The interference is constructive when the phase shift is a multiple of 2π; this condition can be expressed by Bragg's law,

$$2d_{hkl}\sin\theta = n\lambda \quad (3.7)$$

where,

n is an integer determined by the order given,

λ is the wavelength of X-rays or moving electrons, protons and neutrons,

d_{hkl} is the spacing between the planes in the atomic lattice, and

θ is the angle between the incident ray and the scattering planes.

If we know the wavelength of the monochromatic radiation, we may calculate the values of h, k and l for each reflection and determine the type of unit cell and lattice parameters.

In powder diffractometry, diffraction peaks appear at 2θ position, which is recorded by a chart recorder. From the chart recorded diffraction pattern the Bragg angle as well as the highest peak intensity can be read out. The d value corresponding to each peak can be calculated by using the Bragg's relation. The interpretation of the powder diffraction pattern requires identification, i.e. determination of (hkl) values corresponding to each diffraction peak. This is known as indexing which leads to the determination of the crystal structure. Below we describe the indexing of powder pattern by the reciprocal lattice concept.

3.4.2 Calculations of lattice parameters

The lattice parameters of ZnMnO are used as reference to calculate the parameter of the prepared $Zn_{1-x}Mn_xO$ samples. The d values coincided with those of ZnMnO (JCPDS data card 36-1451) with preferential orientation along (100), (002) plane and the standard values of lattice parameters *are a* = 3.23 Å *and c* = 5.17 Å.

3.4.3 Calculations of crystallite size

The X-ray diffraction patterns clearly indicate that the samples are of crystalline type; the reflection type profiles were subjected to calculate crystal or crystallite size perpendicular to the different crystallographic planes. The grain sizes, ξ, of the samples were determined quantitatively using the formula [11].

$$\xi = k\lambda/B\cos\theta \tag{3.8}$$

where, λ is the wavelength of the incident X-ray beam, k is a constant nearly equal to unity (about 0.94) and θ is usual Bragg angle. The unit of ξ is same as that of the λ and expressed in nano-meters. The breadth B of a diffraction line may be measured by means of on ionization chamber or by densitometry of a pattern recorded photographically. In general, B is obtained by measuring so called full width at half-maximum (FWHM) of a diffraction peaks expressed in radians.

3.5 Optical properties of thin films

Optical properties of a solid emanate from its interactions with electromagnetic waves and are manifested in optical frequencies. The effect of such interactions in the audio frequency region results in the dielectric behaviour and in the optical frequencies, optical behaviour. Optical properties of films have been studied extensively primarily because of their applications in various optical and electro-optical devices. The optical study of a solid concerns not only with the physical phenomena such as reflection, refraction, transmission, absorption, polarization, interference of light but also the interactions of photon energy with matter and the consequent changes in the electronic states. From reflection, transmission and absorption processes it is possible to evaluate the optical constants refractive index n, extinction coefficient k and absorption coefficient α and in turn also the complex dielectric constant e^* of a solid. The study of the refractive index provides an understanding of the chemical bonding [8], photoemission properties and electronic structure of the material [9]. On the other hand, absorption studies provide a simple means for the evaluation of absorption edge, optical energy band gap, optical transitions which may be direct or indirect, allowed or forbidden and also the nature of the solid material.

3.6 Absorption co-efficient

When a semiconductor is illuminated by light, photon strikes the surface, a function of photons is reflected and the remaining photon enters the semiconductor. Some of these are absorbed within the semiconductor and the remainder transmitted through

the semiconductor. The absorption of radiation by any medium occurs through the excitation of electrons and photons.

For semiconductor, it is convenient to consider several types of absorption arising from,

(i) Electronic transitions between different energy bands
(ii) Electronic transitions within any energy band
(iii) Electronic transition to localized states of impurity atoms
(iv) Lattice vibrations
(v) Vibrations of impurity atoms.

In the fundamental absorption region the transmission T is given the relation,

$$T = A\exp\left(-\frac{4\pi kt}{\lambda}\right) \tag{3.9}$$

where A is constant, k is the extinction co-efficient and t is the thickness. For $k^2 << n^2$ the principal variation of T occurs in the exponential term and pre exponential term A. Therefore

$$T \approx exp(-\alpha t) \tag{3.10}$$

where, $\alpha = \frac{4\pi k}{\lambda}$ is the absorption coefficient of the film. Then

$$\alpha = \frac{1}{t}\ln\frac{1}{T} \tag{3.11}$$

3.7 Optical bandgap

The difference in energy between the top of the valence band and bottom of the conduction band is known as bandgap or forbidden energy gap. For conduction of electrons energy must be equal to or greater than the forbidden energy gap. In general two types of bandgap are found in the crystal.

(i) Direct bandgap
(ii) Indirect bandgap.

3.7.1 Direct bandgap of semiconductor

If the maximum of the valance band and the minimum of conduction band energy exist for the same value of crystal momentum P in a semiconductor, then the semiconductor is called direct bandgap semiconductor. The form of the absorption process for a direct bandgap semiconductor is shown in energy momentum sketch of Fig. 3.4 (b). Since the momentum of photon small compared to the crystal momentum, the latter essentially is conserved in the transition. The energy difference between the initial and the final state equal to the energy of the original photon, i.e.,

$$E_f - E_i = h\nu \tag{3.12}$$

in terms of parabolic band.

$$E_f - E_c = \frac{P^2}{2m_c^*} \tag{3.13}$$

Therefore the specific value of crystal momentum at which the transition occur is given by

$$\left(E_f - E_i\right) - \left(E_C - E_V\right) = \frac{P^2}{2}\left[\frac{1}{m^*_c} + \frac{1}{m^*_n}\right] \tag{3.14}$$

$$h\nu - E_g = \left[\frac{1}{m^*_c} + \frac{1}{m^*_n}\right] \tag{3.15}$$

where, $h\nu = E_f - E_i$ = photon energy and $E_g = E_c - E_v$ = energy gap.

As the photon energy, $h\nu$ increases, so does the value of the crystal momentum at which the transition occurs Fig. 3.4 (c). The energy form the band edge of both the initial and the final states also increases. The probability of absorption depends on the density of the electron at the energy corresponding to the initial state as well as the density of empty states at the final energy. Since both these quantities increases with energy away from the band edge the absorption co-efficient increase rapidly with increasing photon energy above E_g. A simple theoretical treatment gives the result, as

$$\alpha(h\nu) \approx A^*(h\nu - E_g)^{\frac{1}{2}} \tag{3.16}$$

where A^* is a constant having the numerical value of 2×10^4 when α is expressed in cm^{-1} and $h\nu$ and E_g are in electron volts (eV).

3.7.2 Indirect band gap semiconductor

In the case of an indirect bandgap semiconductor, the minimum energy in the conduction band and the maximum energy in the valance band occur at different values of crystal momentum.

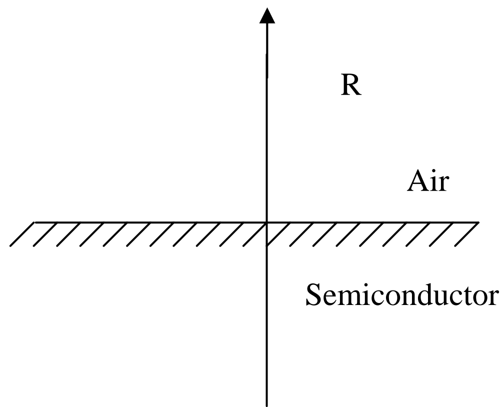

Fig. 3.4 (a) Ray of monochromatic light incident on semiconductor.

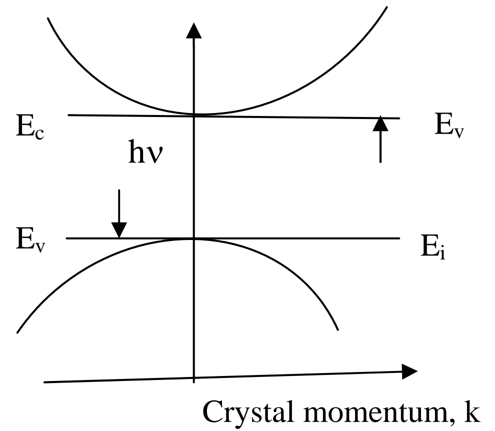

Fig. 3.4 (b) Energy-crystal momentum of a direct bandgap semiconductor.

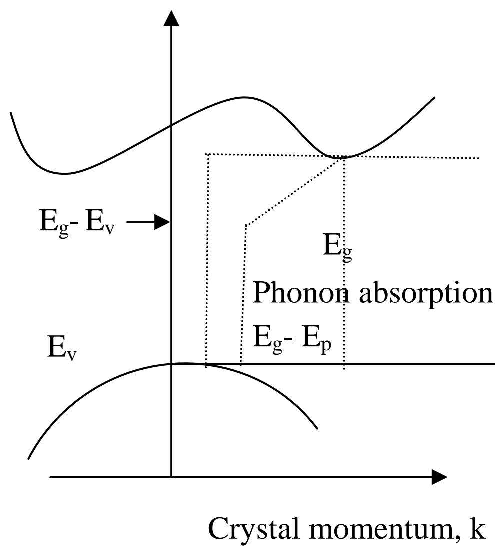

Fig 3.4 (c) Energy-crystal momentum diagram of an indirect bandgap semiconductor.

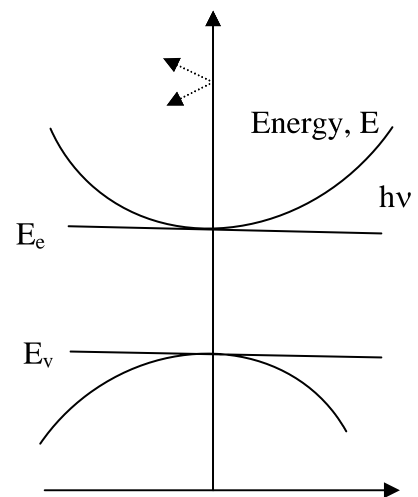

Fig. 3.4 (d) Free carrier absorption in conduction band.

Fig.3.4: Photon energies much larger than the forbidden gap are required to give transition of electrons from the valance band to conduction band.

As indicated in the energy momentum sketch of Fig. 3.4 (c), an electron can make a transition from the maximum energy in the valance band to the minimum energy in the conduction band in the presence of photons of suitable energy by the emission or absorption of phonon, Hence the minimum photon energy required to excite an electron from the valance to conduction band is

$$h\nu = E_g + E_p \tag{3.17}$$

where, E_p is the energy of an absorbed phonon with the required momentum. An analysis of the theoretical value of the absorption co-efficient gives the results,

$$\alpha_a(hv) = \frac{A(hv - E_g + E_p)^2}{\exp\left(\frac{E_p}{KT}\right)^{-1}} \tag{3.18}$$

for the transition involving phonon absorption and

$$\alpha_e(hv) = \frac{A(hv - E_g + E_p)^2}{1 - \exp\left(\frac{E_p}{KT}\right)^{-1}} \tag{3.19}$$

for one involving photon emission. Since both photon emission and absorption are possible for $h\nu > E_g + E_p$, the absorption co-efficient is then.

$$\alpha(hv) = \alpha_a(hv) + \alpha_e(hv) \tag{3.20}$$

3.8 Refractive index, extinction coefficient determination

Let us consider a thin film of thickness t having a refractive index n. If the absorption occurs then n should be replaced by n_o-ik i.e.,

$$n = n_o - ik \tag{3.21}$$

where, k is the extinction coefficient and n_o is the real part of n. The physical meaning of k is the following. When the wave has propagated over a distance equal to the wavelength in the vacuum, the amplitude is reduced by a factor exp(-2πk). The film is bounded by transparent media with refractive indices n_g (glass) and r_a (air) as shown in Fig. 3.5.

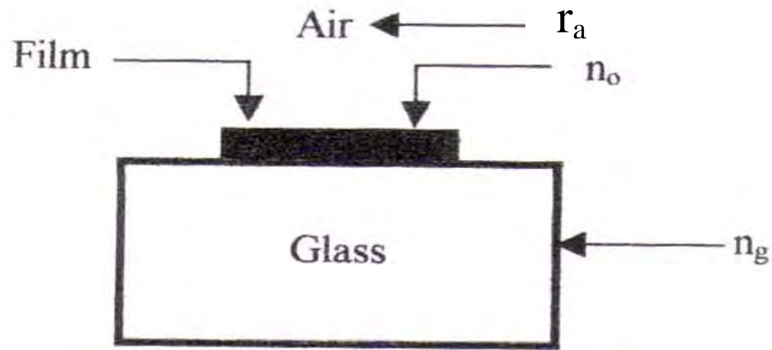

Fig.3.5: A film bounded by air and glass.

There are many methods for determination of n and measuring transmittance and reflectance of the same film can make k separate determination of n and k. We can determine absorption coefficient by using the relation,

$$\alpha = \left(\frac{4\pi k}{\lambda}\right) = \frac{1}{t}\ln\left[\frac{(1-R)^2}{T}\right] \qquad (2.22)$$

From above equation we can write,

$$k = \frac{\alpha\lambda}{4\pi} = \frac{\lambda}{4\pi t}\ln\left[\frac{(1-R)^2}{T}\right] \qquad (3.23)$$

where λ is the wavelength of incident light and T is the transmittance.
The refractive indices, n for the films having interference in the reflectance spectra can be determined by the relation,

$$n = \frac{1}{2t}\left[\frac{\lambda_1\lambda_2}{\lambda_2 - \lambda_1}\right] \qquad (3.24)$$

where t is the thickness of the film and λ_1 and λ_2 are the wavelengths of two consecutive maxima of interference pattern [10]. The same value of n can be determined by the relation,

$$n^2 = n_0 n_s \left[\frac{1 \pm \sqrt{R_{qw}}}{1 \pm \sqrt{R_{qw}}}\right] \qquad (3.25)$$

where n_o and n_s are refractive index of air and glass substrate respectively and R_{qw} is the reflectance of the quarter wavelength [11].

The refractive index n and the extinction coefficient k in the crystal are related to the reflectivity at normal incidence by the relation,

$$r = \frac{n + ik - 1}{n + ik + 1} \tag{3.26}$$

and the reflectance is given by the relation,

$$R = rr^* = \frac{(n-1)^2 + k^2}{(n+1)^2 + k^2} \tag{3.27}$$

From equation (3.24) we can write,

$$n = \frac{-2(R+1) \pm \sqrt{(2R+2)^2 - 4(R-1)(R + Rk^2 - k^2 - 1)}}{2(R-1)} \tag{3.28}$$

knowing reflectance R and extinction coefficient k, we can calculate refractive index by using equation (3.28)

3.9 Optical conductivity

The dielectric constant is an intrinsic property of a material. The ratio of the electric displacement, *D* in a dielectric medium to the applied electric field strength, *E* is known as the permittivity denoted by Є and defined as

$$Є = \frac{D}{E} \tag{3.29}$$

The relative permittivity ϵ_r is the ratio of electric displacement in a medium to the electric displacement in free space for the value of applied electric field strength i.e.,

$$Є_r = \epsilon / \epsilon_0 \tag{3.30}$$

here ϵ_0 is the permittivity of free space . The dimensionless quantity ϵ_r is also termed as the dielectric constant when it is independent of electric field strength .In case of thin film absorption occurs; this film is characterized by complex dielectric constant given as

$$Є = \epsilon_1 - i\epsilon_2 \tag{3.31}$$

where subscript ‘r’ has dropped. It follows from the Maxwell’s equations that

$$(n - ik)^2 = \epsilon_1 - i\epsilon_2 \text{ (for the case of free electron)} \tag{2.32}$$

Following above equation we can write for real and imaginary parts respectively,

$$Є_1 = n^2 - k^2 \tag{3.33a}$$

$$Є_2 = 2nk \tag{3.33b}$$

The loss angle is given by the relation,

$$\delta = tan^{-1}(\epsilon_2/\epsilon_1) \quad (3.34)$$

The electromagnetic energy absorbed by unit volume of a crystal when it interact with the light is proportional to the optical conductivity, denoted by σ_1. The optical conductivity is defined by

$$\sigma_1 = nkc / \lambda \quad (3.35)$$

where c is the velocity of light, λ is the wave length of light.

PART D: STUDY OF ELECTRICAL PROPERTIES OF THIN FILM

3.10 Introduction

All solids can broadly be classified into two categories, namely, conductors and insulators. There, however, exists a class of materials the conductivities of which lie in between the above two categories lying in the range ~10^{-3} $ohm^{-1}cm^{-1}$ and 10^6 $ohm^{-1}cm^{-1}$ and these materials are known as semiconductors. Their electrical conduction may be close to those of poor conductors or may be as low as of an insulator. The physical properties of thin films of a material are different from those of the bulk material. When the thin films are used in many practical purposes it's electrical, optical and other properties must be known. Depending on its uses, transmitivity, reflectivity, optical absorption, band gap energy, extinction co-efficient refractive index etc., are calculated within certain wavelength range of incident photon energy. It is also interesting to study the thin film resistivity and also on its dependence on film thickness, which is often referred to as size effect. The resistivity of metals at room temperature is of the order of 10^{-6} Ω-cm, in semiconductor 10^2 ~ 10^9 Ω-cm, and in insulator it ranges from 10^{14} ~ 10^{22} Ω-cm. Electrical resistivity of semiconductor strongly depends on temperature. At high temperature it may behave as conductor and at absolute zero a pure semiconductor will be an insulator.

3.10.1 Resistivity and conductivity measurement

The tendency of a material to consist of the flow of an electrical current through it and to convert the electrical energy into heat energy is called resistance. According to Ohm's law,

$$R = \frac{V}{I} \qquad (3.36)$$

Where R is the resistance of a material, V is the potential difference and I is the current flow through the material.

The resistance per unit length of unit cross section is called resistivity. It is denoted by ρ and mathematically defined as,

$$\rho = \frac{RA}{L} \qquad (3.37)$$

where A is the cross-sectional area and L is the length.

Electrical conductivity of a material is reciprocal of resistivity of the material. It is denoted by σ and mathematically defined as

$$\sigma = \frac{l}{\rho} \qquad (3.38)$$

Resistivity is an intrinsic property of a material and depends only on the crystal structure of the material. The resistivity can be obtained by measuring the resistance of a specimen of the material with well-defined regular geometric shape. There are many methods to measure resistivity. Some of them has been discussed below.

3.10.2 Methods to determine the resistivity

There are four methods commonly used for the measurement of resistivity.

(i) Direct method

(ii) Two-probe method

(iii) Four probe method

(iv) Van-der Pauw method

3.10.2 (i) Direct method

The resistivity of a thin film can be measured easily by direct method using the relation

$$\rho = R\frac{bt}{L} \tag{3.39}$$

where, b and t are the breadth and thickness of the sample. For simplicity, if we consider, b = L, the above equation becomes

$$\rho = Rt \tag{3.40}$$

measuring the resistance, R and thickness, t, one can easily determine the resistivity. The circuit diagram of the direct method is shown in Fig. 3.6 (a).

3.10.2 (ii) Two-probe method

In this method potential is applied between the two ends of the specimen and the voltage drop is measured between two points in the specimen. The method is generally used to determine the high resistivity i.e., low conductivity having order 10^{-14} to 10^{-18} mho-cm^{-1}. The voltage drop is measured between potential probe as shown is Fig 3.6(b).

3.10.2 (iii) Four-probe technique

Four-probe method is usually used for the determination of low resistivities. For this purpose four metal pins at a equal distance D are pressed by springs against the semiconductor sample as shown in Fig. 3.6(c). If the outside pins carry a current of intensity, I a voltage drop is measured between the inner probes of magnitude V. Assuming the sample to be much thicker that the pin distance, D the resistivity ρ is given by

$$\rho = \frac{2\pi DV}{I} \tag{3.41}$$

The effect of the contact resistance is avoided in Four-probe method.

3.10.2 (iv) Van-der Pauw method

The resistivity of a film having any arbitrary shape can be uniquely determined by Van-der Pauw's method. A brief account of this method is given below because in our measurement we have used Van-der Pauw method.

At first we select a region or the sample where four electrical contacts were made at four corners, say *A*, *B*, *C*, and *D* as shown in Fig. 3.6(d). Using silver paste or indium was used to make the contact. If a current I_{AB} entering the specimen through the

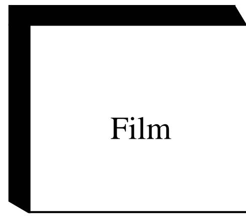

Fig. 3.6 (a) For direct method

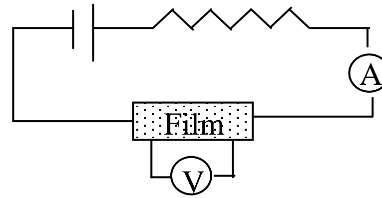

Fig. 3.6 (b) For two-prove method

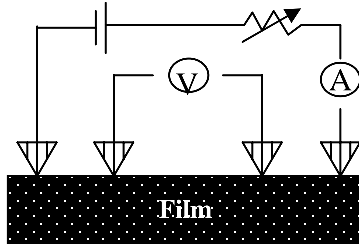

Fig. 3.6 (c) Circuit arrangement for four-prove method

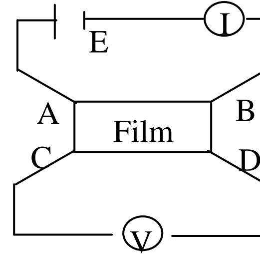

Fig. 3.6 (d) Circuit arrangement for Van - der Pauw's method

Fig. 3.6: Circuit arrangements to determine electrical resistivity.

contact A and leaving through the contact, B produces a potential difference $V_D - V_C$ between C and D then the resistance $R_{AB,\,CD}$ is defined as

$$R_{AB.CD} = \frac{V_D - V_C}{I_{AB}} = \frac{V_{CD}}{I_{AB}} \tag{3.42}$$

Similarly,

$$R_{BC.DA} = \quad = \frac{V_A - V_D}{I_{BC}} = \frac{V_{DA}}{I_{BC}} \tag{3.43}$$

$$R_{CD.AB} = \frac{V_B - V_A}{I_{CD}} = \frac{V_{AB}}{I_{CD}} \tag{3.44}$$

and $$R_{DA.BC} = \frac{V_C - V_B}{I_{DA}} = \frac{V_{BC}}{I_{DA}} \tag{3.45}$$

The resistivity of a thin film can be expressed by the equation,

$$\rho = \frac{\pi t}{\ln 2}\left[\frac{R_{AB.CD} + R_{BC.AD}}{2}\right] \times f\left[\frac{R_{AB.CD}}{R_{BC.AD}}\right] \tag{3.46}$$

$$\rho = 4.53t \times \left[\frac{R_{AB.CD} + R_{BC.AD}}{2}\right] \times f\left[\frac{R_{AB.CD}}{R_{BC.AD}}\right] \tag{3.47}$$

where t is the thickness of the film and the function f can be evaluated from the equation,

$$\left[\frac{R_{AB.CD} - R_{BC.DA}}{R_{AB.CD} + R_{BC.DA}}\right] = \frac{f}{\ln 2} are\cosh\frac{\exp(\ln 2/f)}{2} \tag{3.48}$$

If $R_{AB,CD}$ and $R_{BC,DA}$ are almost equal, f may be approximately equal to unity and then the equation (3.49) takes the form,

$$\rho = 2.265\ t\ (R_{AB,CD}+R_{BC,DA})\ \Omega\text{-}cm \tag{3.49}$$

It is very difficult to get f equal to unity, so we have taken the value of f from the chart for different ratio greater than unity.

3.12 Hall effect

One of the most important properties of all solids is the Hall Effect and this is conjunction with the electrical conductivity is a simple but powerful technique for studying the transport properties of metals and semiconductors. When a conductor is place in a magnetic field perpendicular to the direction of current flow, a field is developed across the specimen in the direction perpendicular to both the current and the magnetic field. This effect was observed by E H Hall and known as Hall effect. The experimental procedure of Hall effect is available to measure the carrier concentration and mobility and it makes possible to determine the sign of the charge carriers in the semiconductors. Number of literature deals with the Hall effect in thin films grown by various methods. These investigations show that the Hall effect in thin film strongly depends on,

(i) The state of ordering as influenced the vacuum conditions, the substrate temperature during the deposition and the annealing temperature.

(ii) Concentration of different materials in the alloy films.

(iii) The temperature

(iv) The film thickness.

Hall effect is important for the following information,

(i) To characterize the material under the consideration whether it is p-type or n-type.

(ii) For the calculation of the number of charge carriers per unit volume.

(iii) For the understanding of the mobility of charge carriers and Hall constant from where the conductivity is known.

3.12 The Hall constant and carrier concentration

When a conductor carrying a current *I* is placed in a transverse magnetic field *B*, then an electric field is induced in the conductor in the direction perpendicular to both *I* and *B*. if the current. *I* is in the X-direction and magnetic field B in the Z-direction of right handed co-ordinate system and the electric field is produced in the conductor in the Y-direction as shown in Fig. 3.8(c)
In the presence of magnetic field a magnetic force proportional to the magnetic field strength *B* and electrons average velocity of magnitude *V* also acts on the electron. This forces is at right angles to the directions of *B* and *V* and for the deflection of each electron of electrical change is build up there which, in turn, produces an additional electric field under equilibrium condition, the sideways force on the moving carries due to this field just balance that arising from the magnetic field and the electrons can more freely down the conductor. The magnitude of the transverse Hall field E_H is found by equation the sidewise forces,

$$eE_H = eVB \tag{3.57}$$

The current density J is given by

$$J = neV \tag{3.58}$$

where, n is the conduction electron density and V is the average velocity.
Putting the value of *V* from Eq. (3.58) into Eq. (3.57), we obtain

$$E_H = \left(\frac{1}{ne}\right)JB = R_H JB \tag{3.59}$$

where the Hall constant is

$$R_H = \frac{l}{ne} \tag{3.60}$$

The carrier concentration is obtained from equation (3.60) and Hall voltage V_H is obtained from equation (3.59) directly.

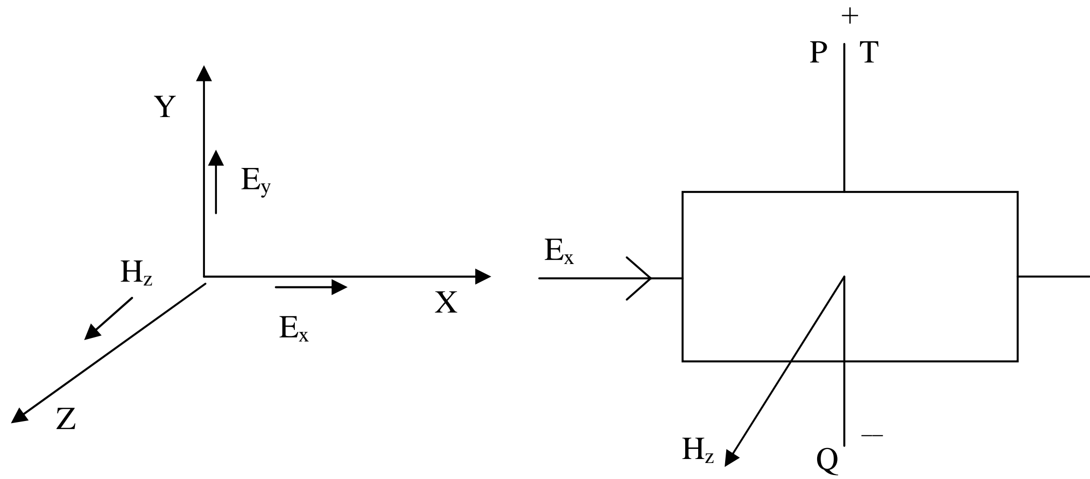

Fig. 3.7 (a) Relative direction of current, magnetic field and Hall field for negative electrons.

Fig. 3.7(b) Strip of conducting material.

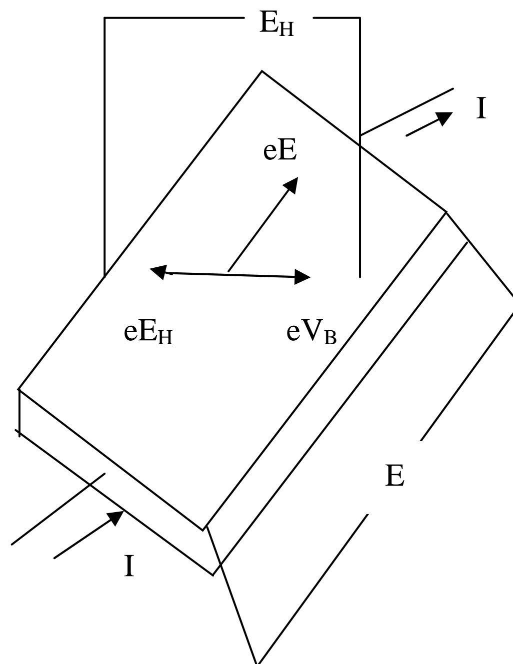

Fig. 3.7(c) The forces acting on a current carrier in a conductor placed in a magnetic field leading to the observable Hall field E_H.

Let a rectangular sample of material of width W and thickness t. The Hall voltage is produced by the applied magnetic field B is V_H, then E_H is given by

$$E_H = \frac{V_H}{W} \tag{3.61}$$

and current density J is given by

$$J = \frac{I}{Wt} \tag{3.62}$$

Therefore Eq. (2.59) becomes

$$R_H = \frac{1}{ne} = \frac{E_H}{JB} = \frac{V_H t}{IB} \tag{3.63}$$

In equation (3.63), e is the magnitude of electronic charge and algebraic sign of the sign of the Hall voltage tells whether the carriers are holes or electron conduction by holes gives the positive value for E_H. Conduction by electrons give a negative value of E_H and a negative value of Hall constant R_H.

References

[1] Goswami., A., “Thin film fundamentals” New age international (p) limited, Publisher, New Delhi India. 140 (1996).

[2] Volmer., M. and Weber, A., “Partical Formation: Thory of neucleation and system”, Physical Chemistry, 119 ,277 (1925).

[3] Becker, R., and Doring,W., “The kinetic treatment of nuclear formation in supersaturated vapors” Annalen der Physik, 24, 719 (1935) .

[4] Pound, G. M., Simmad,M. T. and Yang, L. “Heterogeneous nucleation of film growth”, Journal of Chemical Physics 22 1215 (1954).

[5] Pashley, D. W., Stowell, M. J., Jacobs, M. H. and Law, T. “The growth and structure of gold and silver deposits formed by evaporation inside an electron microscope”, Philosophical Magazine.10, 127 (1964).

[6] Pashley. D. W., “The study of epitaxy in thin surface films”, Advance Physics, 14, 61 (1965).

[7] Walton, D. “Mechanism of condensation”,Journal of Chemical Physics, 37, 2182 (1962).

[8] Van Vechtan, J. A., “Interatomic forces and ionicity in covalent crystals”, Journal of Physical Review, 182, 801 (1969).

[9] Krolikowski, W. P. and Spicer, W. E., “Photoemission and electron states at clean surfaces”, Journal of Physica Review, 185 882 (1969).

[10] Cullity, B. D., “ Elements of X-ray diffraction” Addision-Wesley Publishing Co. Inc. 262 (1967).

[11] Carrngilia, C. K., Maria. M., et al. “Basic Concept of Coating Design” 212 (1978).

CHAPTER-IV

EXPERIMENTAL DETAILS

CHAPTER-IV
EXPERIMENTAL DETAILS

This chapter includes the experimental setup for thin film deposition equipments for spray pyrolysis technique and illustrates in details the preparation of $Zn_{1-x}Mn_xO$ thin film with doping concentrations, x = 0.01, 0.02, 0.03, 0.04, 0.05 up to 0.20 on glass substrate. The detail discussion about every experimental setup have been presented with appropriate method throughout the course of the thesis work for the analysis of the structural, optical, electrical, properties.

PART A: FILM PREPARATION

4.1 Introduction

Thin films can be prepared from several of materials such as metals, semiconductors, magnetic semiconductor, insulators, dielectrics etc. and for this purpose various preparation techniques have also been developed. Spray pyrolysis is the most commonly used technique adopted for the deposition of metals, alloys and many compounds. This chapter deals with mainly the experimental setup of different experimental apparatuses and preparation of experimental samples of $Zn_{1-x}Mn_xO$ thin film with doping concentrations, x = 0.01, 0.02, 0.03, 0.04, 0.05 up to 0.20 onto glass substrate. Various steps taken for the film deposition have been discussed below.

4.2 Experimental equipments for spray pyrolysis technique

For the fabrication and characterization of the fabricated films, we were used various kind of equipments. The experimental setups for the spray pyrolysis technique have been described below.

4.2.1 Preparation of mask

The direct deposition of thin film pattern requires a suitably shaped aperture, commonly referred to as a mask. In the case of chemical spray deposition process it is needless to say that the mask should be insert to the chemicals used for the process

and also can sustain high temperature. We found mica and stainless steel as suitable masking material. Since the thickness of the films deposited is of the order the mask should be as thin as possible so as to obtain uniformity of thickness throughout the film pattern. Masks used for film are shown in Fig. 4.1.

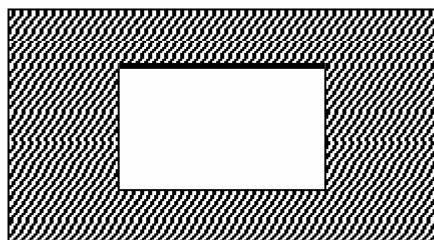

Fig.4.1: Mask used for the thin film preparation.

4.2.2 Heater

The heater H shown in Fig. 4.2 is an ordinary hot plate 2-kilowatt nichrome wire heater. The top of the plate is covered with a thick sheet of stainless steel plate G. Substrate is placed on this plate to have a uniform temperature throughout the substrate surface. A mica sheet with the same design of mask is placed in between the substrate and the mask to prevent spreading in solution beyond the opening of the mask. An electrical voltage variac controls the heater power. The temperature of the heater was measured by a pyrometer.

4.2.3 The design of reactor

Fig. 4.2 shows the design of the reactor. It is the vertical batch type reactor composed of a galvanized iron enclosure E, a heater H and heat susceptor G. For the rapid expulsion of the by-product gases there are openings at the side and at the top of the reactor. The bauble cone shape of the reactor wall E has fold action. It helps focusing the incoming aerosol towards the substrate S and also provides a chimney action to the exhaust gas upwards.

4.2.4 The fume chamber

It is a large box type chamber with a slanting top and is provided with a chimney. There is an exhaust fan with regulated power supply fitted at the mouth of the chimney. The slanting top and the sidewalls are made of glass. There are airtight doors in the front side. The chamber has purging facilities.

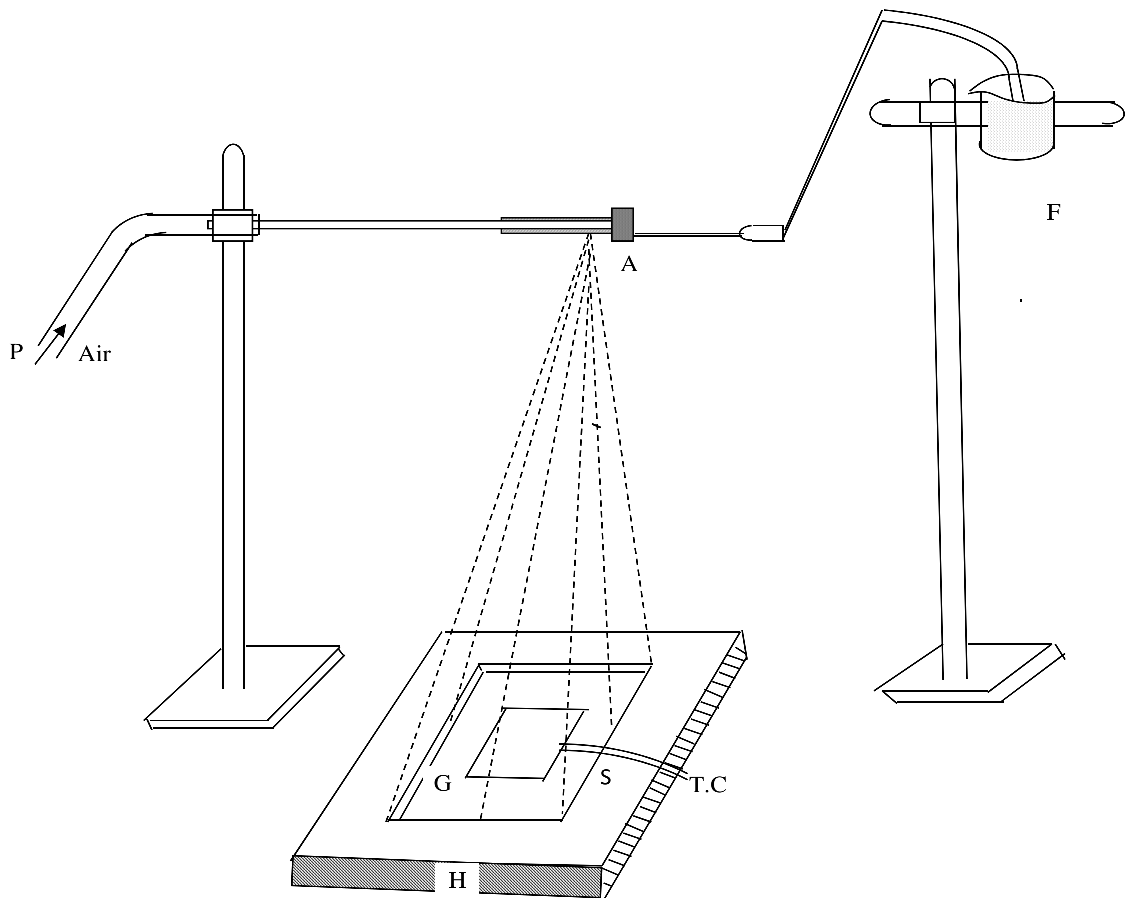

A = Lower tube G = Metal plate H = Heater S = Substrate P = Upper tube F = Beaker T.C. = Digital multimeter with a thermocouple.

Fig.4.2: Schematic diagram of spray pyrolysis technique.

The whole spray system is kept inside the fume chamber at the time of film deposition because of (a) safety grounds and (b) to check air current disturbances at

the deposition site. These two points just stated are very important for the parasol process when deposition is carried out in open-air atmosphere.

4.2.5 Air compressor

It is a reservoir type electrical air compressor. A rotary pump in this section mode draws atmospheric air and keeps it reverse in a large capacity air tank. At the outlet of the tank a pressure gauge is attached which records the pressure of the air at the time of supplying it from the tank. There is a bypass control valve which can keep the output pressure constant.

4.2.6 Nozzle

The single spray nozzle consists of capillary tubes (stainless steel) fitted at perpendicular to the other tube as shown in Fig. 4.2. When compressed air is passed rapidly through the upper tube P in direction tangential to the mouth of the lower tube ‘A’ and the other end is kept immersed in the spray liquid. Due to this partial vacuum the liquid rises up through the tube A and the compressed air drives it away in the form of the fine spray particles (aerosol). The thinner the spray nozzle the finer would be the spray particles. A very fine needle shaped capillary tube was used for the spray nozzle. Fine spray through the nozzle depends on the bore of the nozzle and it may vary from nozzle to nozzle.

4.3 Substrate and substrate cleaning

The most commonly available microscope glass slides were used as substrates in the present work. The cleanliness of substrate surface exerts a decisive influence on film growth and adhesion. A thoroughly cleaned substrate is a pre-requisite for the preparation of films with reproducible properties. The choice of cleaning techniques depends on the nature of the substrate, the type of contaminants and the degree of cleanliness required. Since our glass substrates were ordinary soda lime microscope slides and over slides and therefore residue from manufacturing and packaging, lints, fingerprints, oils and air borne particulate maters were supposed to be contaminations. The following procedure was found adequate for substrate cleaning in our laboratory. The gross contaminations of each of the substrates are first

removed by Luke warm aqueous solution of sodium carbonate. After washing in a stream of washing powder and dipped in ethanol. Taking them out of the ethanol one by one they are washed and thoroughly rinsed with de-ionized water several times and finally made dry by blowing hot air. They are then preserved in desiccators. During the whole process slide, holding forceps always held the substrates.

4.4 Working Solutions

$Zn_{1-x}Mn_xO$ (x = 0:00, 0.01, 0.02, 0.03, 0.04, 0.05 upto 0.20) thin films will deposited using spray pyrolysis technique. $Zn(CH_3COO)_2.2H_2O$ and $Mn(CH_3COO)_2.4H_2O$ were used as precursors for Zn and Mn ions, respectively. Both the precursors were dissolved in deionized water. The total concentration of the solution was kept at 0.5 mol. The films were deposited on glass substrates cleaned with acetone and deionized water. For all concentration of Mn, the substrate was maintained at 300 °C. The temperature of the substrate will be measured by a pyrometer. The spray rates will be measured by a flow meter. The flow rate of the solution during spraying will be adjusted to be about 2.5ml/min and kept constant throughout the experiment. The distance between the spray nozzle and the substrate will be maintained about 25 cm.

4.5 Sample deposition

It has been stated earlier that the spray pyrolysis method for preparation of $Zn_{1-x}Mn_xO$ with x = 0.1, 0.2, 0.3, 0.4 0.05 upto 0.20 thin film is an economically attractive method, which consists basically of spraying a solution on a heated substrate. The apparatus needed to carry out the chemical spray process consists of a device to atomize the spray solution on a substrate heater. Fig. 4.2 shows a typical experimental set up. A considerable amount (above 100 ml) of spray solution taken in the container F fitted up with the spray nozzle A. The clean substrate with a suitable mask was put on the susceptor of the heater H. The distance between the tip of the nozzle and surface of the substrate was 22 cm. Before supplying the compressed air the heater was kept for sometime so that the substrate and the reactor wall attain the requisite temperature. The substrate temperature T_s was to be kept at a level slightly higher than the required substrate temperature because at the onset of

spraying a slight fall of temperature likely. The temperature of a substrate was controlled by controlling the heater power by a variac. When compressed air is through P at a constant pressure (0.5 bar), a fine aerosol was produced and was automatically carried to the reactor zone where film was deposited on the heated substrate. By trial we have adjusted a situation such that 5 to 7 minutes of spray produces thin films of requisite thickness (400-580 nm) at a substrate temperature of 300°C. Finally we were fabricated $Zn_{1-x}Mn_xO$ thin film with x = 0.1, 0.2, 0.3, 0.4 0.05 upto 0.20 at 300 °C substrate temperature at air ambient onto glass substrate and it was maintained substrate to source distance 25 cm. Possible reaction of the material when pyrolysis was occur as follows:

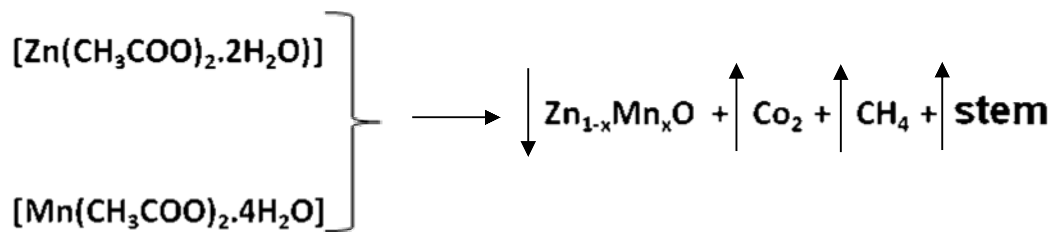

4.6 Deposition rate and thickness control

The rate of flow of the solution can be controlled by suitably designing the nozzle A and adjusting the airflow rate. In the present spray deposition process, the deposition time is the main thickness-controlling factor, provided the other parameters remain constant. Since the deposition is carried out in normal atmosphere a direct and inset control of thickness is not so essay. To control the film thickness therefore calibration chart may be used. The charts are generally plots of deposition time versus thickness, and can be prepared at different constant substrates temperatures prior to the preparation of particular experimental samples using the different solution and deposition variables. Since the rate of deposition in present setup is rather small, the thickness control is therefore not difficult.

PART B: EXPERIMENTAL MEASUREMENT

4.7 Measurement of film thickness

In the present work, $Zn_{1-x}Mn_xO$ films were deposited by spray pyrolysis technique on glass substrate at constant substrate temperature and films of different thickness were grown. The thicknesses of the films were measured by Newton's ring method which is described in chapter three. The thicknesses of the films were varied by varying deposition time. Films prepared by spray pyrolysis process were found to be physically stable and adhered to the glass substrate well.

4.8 Structural study by XRD analysis

X-ray diffraction (XRD) patterns of $Zn_{1-x}Mn_xO$ thin films deposited on glass substrate were taken using X-ray diffractomet. X- ray diffraction of all the samples have been recorded using monochromatic CoK_α radiation of wavelength $\lambda = 1.709$ Å, . From the XRD patterns crystal parameters such as crystal structure, lattice constants, grain size, etc. have been evaluated.

4.9 Measurement of absorbance and transmittance

Optical reflectance and transmittance of thin film samples were measured by using a double beam UV-Visible spectrophotometer at room temperature. The sample with the substrate was placed in the incident beam and another empty substrate in the reference beam of the instrument. The optical transmission spectra of the film with respect to glass substrate were then taken for wavelength range 300 to1100 nm.

4.10 Measurement of absorption coefficient and optical bandgap

Absorption coefficient and optical bandgap have been calculated using reflectance and transmittance spectra taken at room temperature directly. The value of absorption coefficient is calculated by using the relation,

$$\alpha = \frac{1}{t}\ln\left[\frac{(1-R)^2}{T}\right] \quad (4.1)$$

According to Bardeen et al. [1] the relationships that exist for possible transition across the energy gap of a semiconductor show that the absorption co-efficient α is proportional to the following expression for the condition given below,

$$\alpha = \frac{A(h\nu - E_g)^n}{h\upsilon} \tag{4.2}$$

where, A is a constant, hυ is the photon energy, *n* is an index related to the density of state (n = 1/2 for direct allowed transition and n = 2 for indirect allowed transition) and E_g is the optical bandgap of the semiconductor. By plotting $(\alpha h\upsilon)^n$ against hν for the various value of n it is possible to determine which of these conditions dominate and hence determine the appropriate energy gap of the sample.

4.11 Attachment of conducting wire with films

Generally two methods are used to attach the conducting wire with the thin films, namely solid phase bonding and alloying bonding. The solid phase bonds are formed by thermo compression and ultrasonic means, whereas the alloy bonds are formed by soldering. Soldering is the simplest and most commonly used process in joining leads to thin films and in the present work indium was used as soldering material to make electrical contact shown in Fig. 4.3.

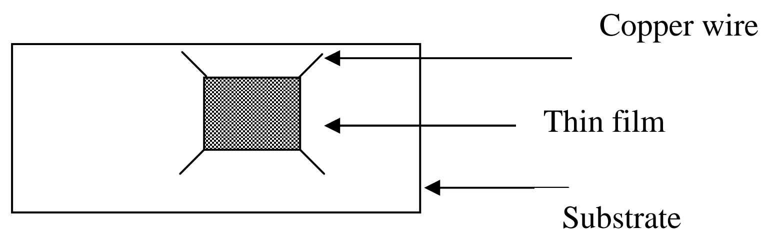

Fig. 4.3: Diagram of film with lead attachment

4.12 Measurement of resistivity, conductivity and activation energy

Van-der Pauw's method [2] was used to measure the resistivity and the electrical conductivity of the specimen, which is described in Part-D of chapter three. The circuit arrangements used for the resistivity and conductivity measurement are shown in Fig. 4.4. The currents were passed through the terminals A and B, B and C the corresponding potential difference were measured between the terminals C and D

and D and A respectively with the variation of temperature. Temperature was measured directly by a digital temperature measuring multimeter (model KT105).

The resistivity ρ and hence, the conductivity σ was calculated using the equation,

$$\rho = 2.265t\ (R_{AB,CD}+R_{BC,DA}) \quad (4.3)$$

and hence, the conductivity σ was calculated using the equation,

$$\sigma = 1/\rho \quad (4.4)$$

where, t is thickness of the film, $R_{AB,CD} = V_{CD}/I_{AB}$ and $R_{BC,DA} = V_{DA}/I_{AB}$.

Activation energy ΔE was calculated from the slope of $ln\sigma$ versus $1/T$ plot based on the equation,

$$\sigma = \sigma_o \exp(-E_a/2k_BT)$$

or, $$\Delta E = -2k_B ln\sigma/(1/T) \quad (4.5)$$

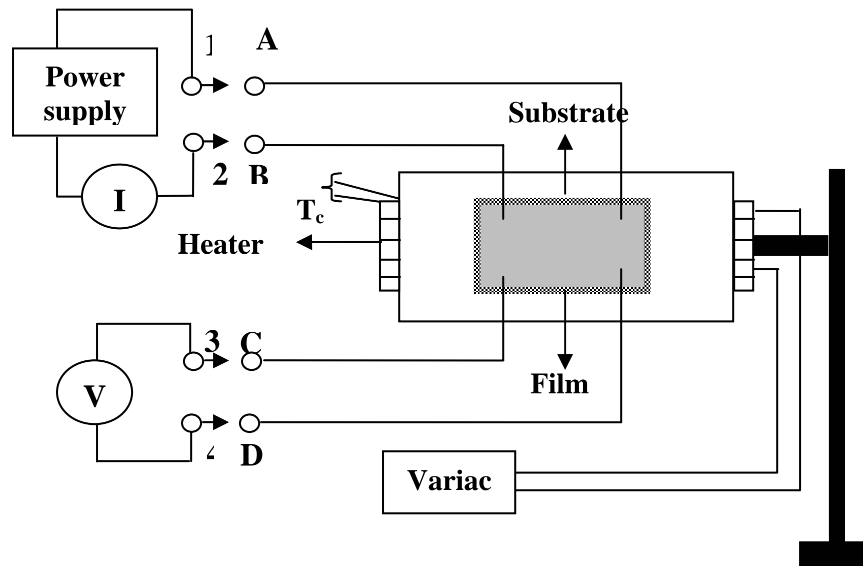

Fig. 4.4: Schematic diagram for the measurement of film resistivity. 1, 2, 3 and 4 are meter terminals and A, B, C and D are the film terminals.

References

[1] Barden,J., Blatt, F. J. and Hall, "Photoconductivity Confer," Eds. R. Wreckarridge, B. Russel and Halmn, New York.(1965).

[2] Van-der-Pauw., "A Method of Measuring Specific Resistivity and Hall Effect of Discs of Arbitrary Shape", Philips Research Report. 13.1(1958).

CHAPTER-V
RESULTS AND DISCUSSION

CHAPTER-V
RESULTS AND DISCUSSION

In this chapter the results of structural, optical, and electrical, properties of $Zn_{1-x}Mn_xO$ thin films with doping concentrations, x = 0.01, 0.02, 0.03, 0.04, 0.05 up to 0.20 have been discussed. Films were fabricated onto glass substrate by spray pyrolysis technique at 300 °C substrate temperature. Then the experimental results of $Zn_{1-x}Mn_xO$ thin films have been presented. The possible explanations and discussion of the experimental results are also given in this chapter.

5.1 Thickness Measurement

The thicknesses of the films were measured by the setup of Fizeau fringes method. The thickness of $Zn_{1-x}Mn_xO$ thin films for x= 0.00, 0.01, 0.03, 0.04, 0.05 0.06, upto 0.20 were found to be 400 to 550 nm respectively.

5.2 Surface morphology of $Zn_{1-x}Mn_xO$

Scanning electron microscopy is widely used to obtain the surface morphological information of thin films. Surface morphology of the undoped and Mn doped ZnO thin films on glass substrate were studied by scanning electron microscopy (SEM). The SEM images are of the as deposited film as in Fig.5.1 (a). From this figure it is observed that the film surface is very smooth but only a few space shown circular disc like shape consisting of a number of rope like nanostructure arranged or overlapped around the nucleation centre.

Different results were obtained for Mn doped ZnO thin films as in fig.5.1 (b, c, d, f) respectively. Those pictures shows randomly oriented nano rops on the film surface. With increasing Mn concentration nano rops are clearer as well.

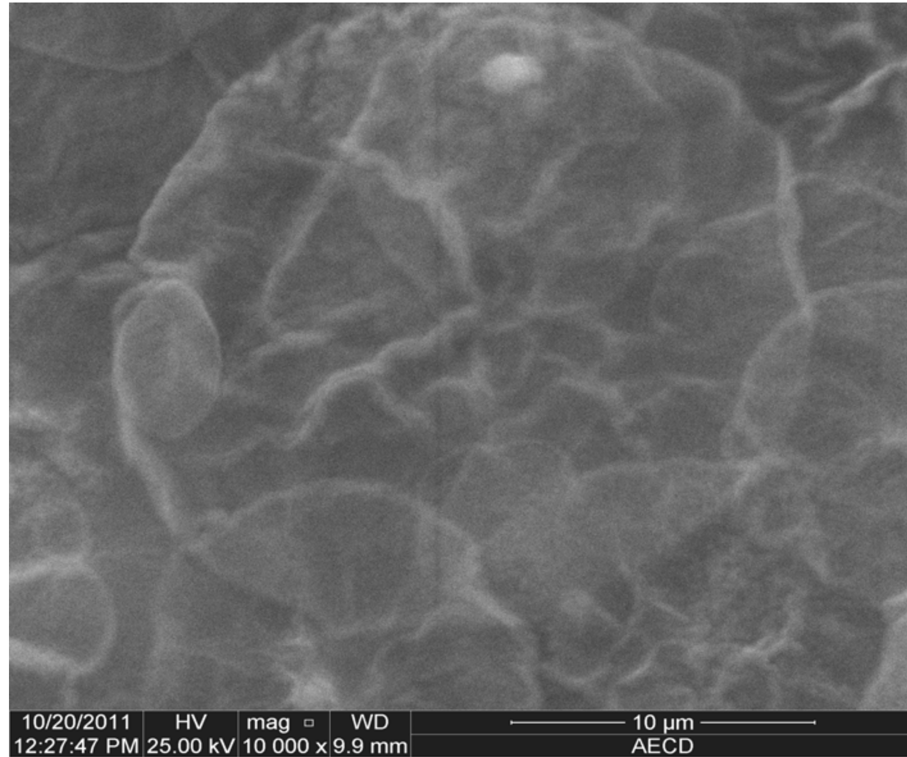

Fig.5.1a: SEM image of (10000X magnification) ZnO thin film for (a) x=0.00

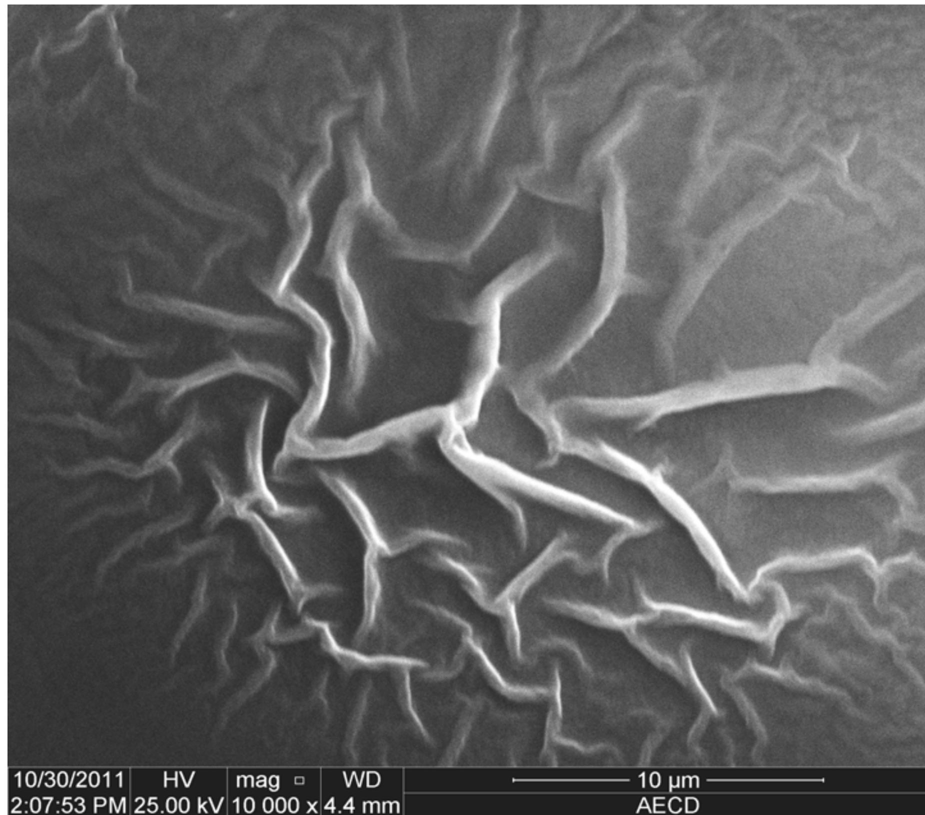

Fig.5.1b: SEM image of (10000X magnification) $Zn_{1-x}Mn_xO$ thin film for (b) x=0.02

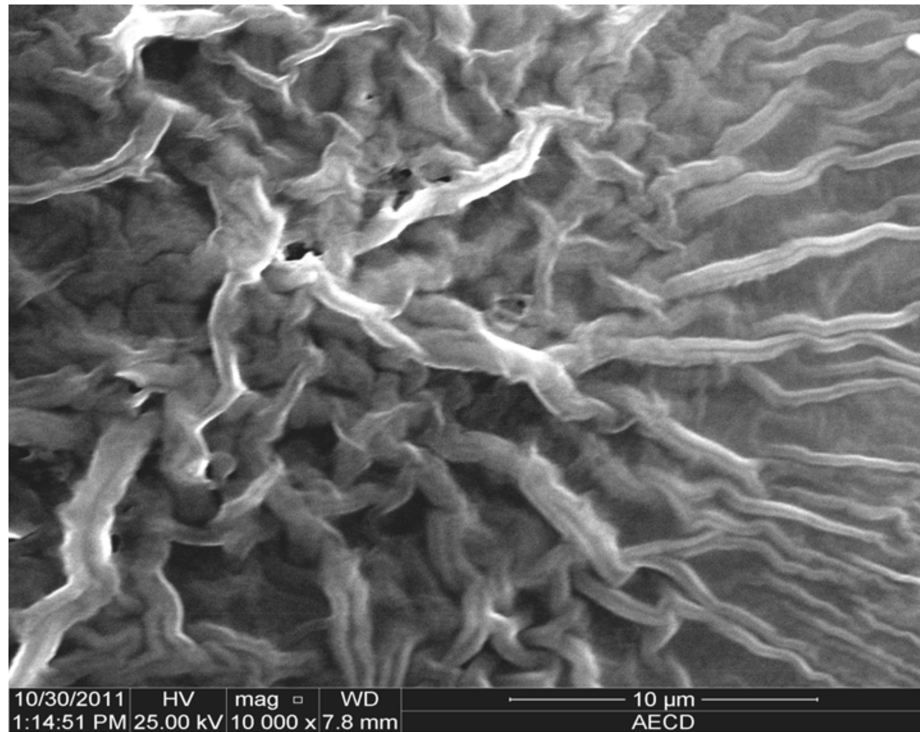

Fig.5.1c: SEM image of (10000X magnification) $Zn_{1-x}Mn_xO$ thin film for (c) x=0.04

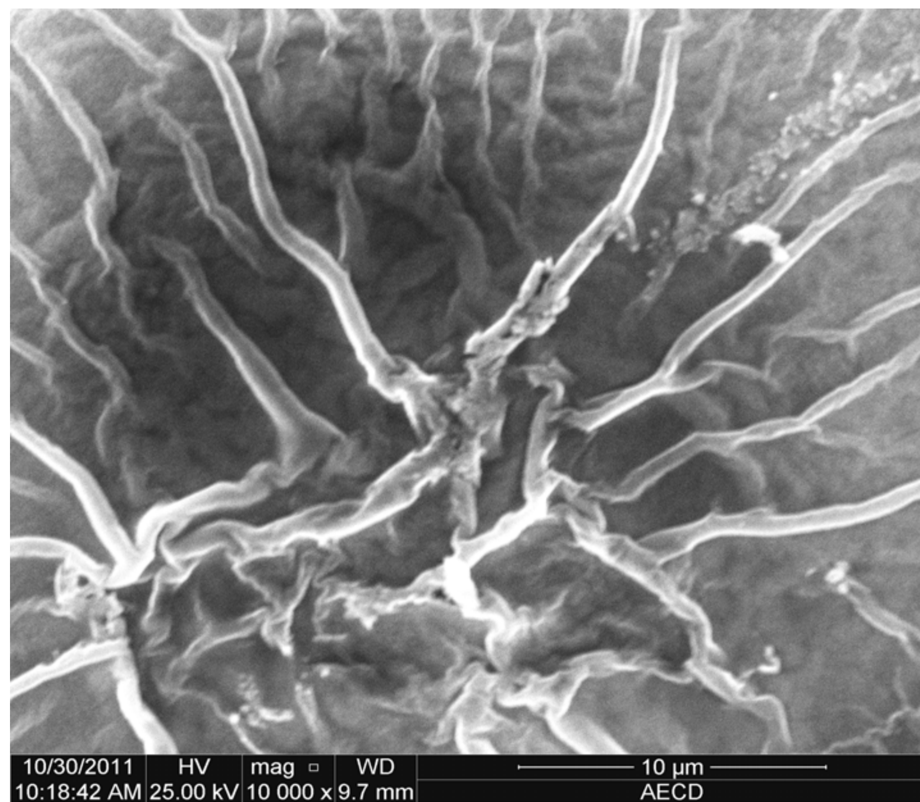

Fig.5.1d: SEM image of (10000X magnification) $Zn_{1-x}Mn_xO$ thin film for (d) x=0.06

Fig.5.1e: SEM image of (10000X magnification) $Zn_{1-x}Mn_xO$ thin film for (e) x=0.10

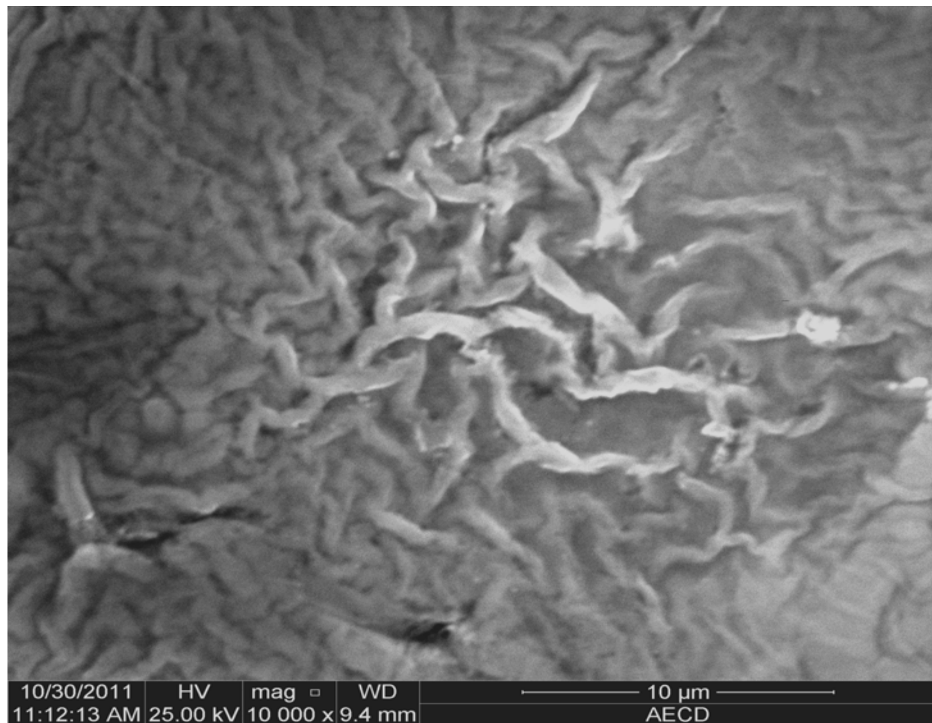

Fig.5.1f: SEM image of (10000X magnification) $Zn_{1-x}Mn_xO$ thin film for (f) x=0.20

Under higher magnifications of 10000X, the SEM micrograph of the Mn doped ZnO shows high density of closely packed smooth over a large area around the nucleation center. The fibers are oriented of various lengths.

In the case of 4% Mn doping concentration the disc likes structures completely disappear and very straight nono-rops were observed shown in figure 5.1(c).

5.3 Compositional studies

The composition of $Zn_{1-x}Mn_xO$ films was confirmed by energy dispersive X-ray spectroscopy (EDX). Fig. 5.2(a-d) shows the EDX spectra of $Zn_{1-x}Mn_xO$ thin films. Table 5.1 shows the composition of elements in film of the sprayed solution. A strong peak is observed which corresponds to Si (Substrate) and Ca peak is also responsible for substrate. An Oxygen peak is also observed which is due to incorporation of oxygen into the substrate from the air when pyrolysis was occurring. Two different peaks corresponding to Zn and Mn in the spectrum, which confirms the $Zn_{1-x}Mn_xO$ thin film. For different concentrations of Mn in the solution, there is also Mn peak in the spectra. At high operating voltage the electron beam penetrates the film and reaches the glass surface, which results the Si and Ca peak are produce. Figures 5.2 (b-d) are shown the EDX analysis spectrum for $Zn_{1-x}Mn_xO$ thin films.

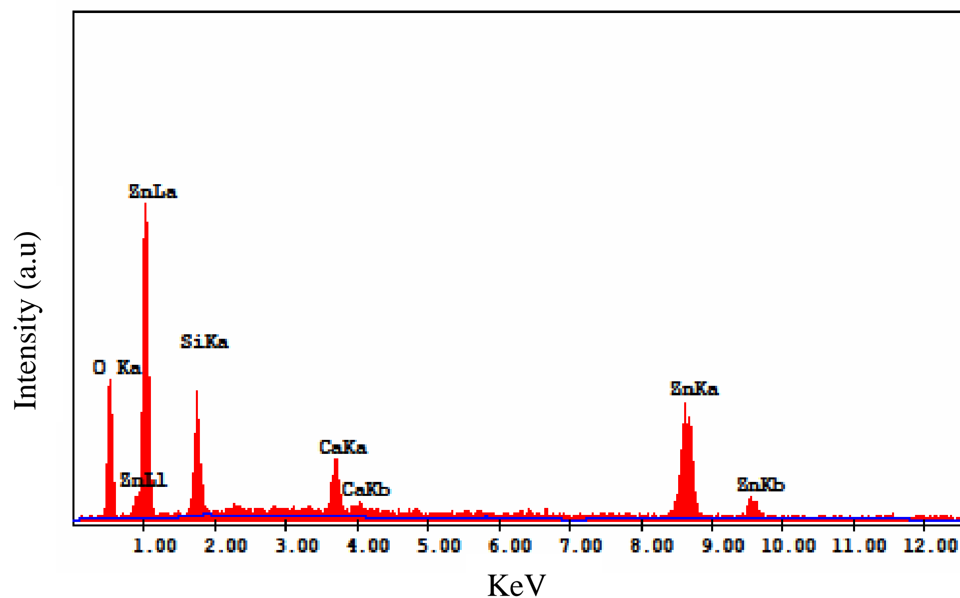

Fig 5.2a: EDX spectrum of as-deposited ZnO thin film.

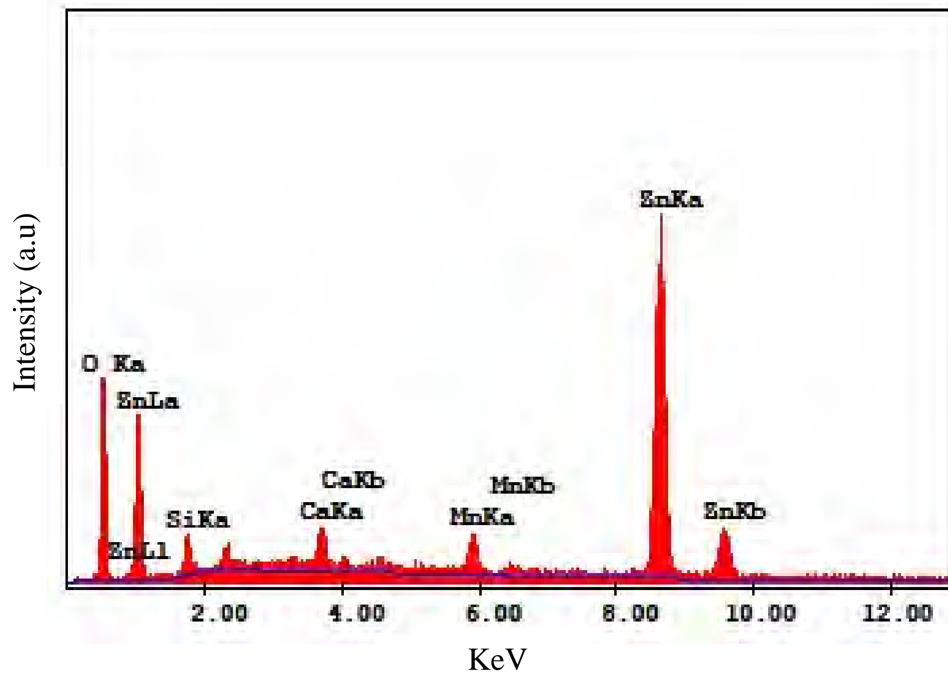

Fig 5.2b: EDX spectrum of $Zn_{1-x}Mn_xO$ thin film for x=0.04.

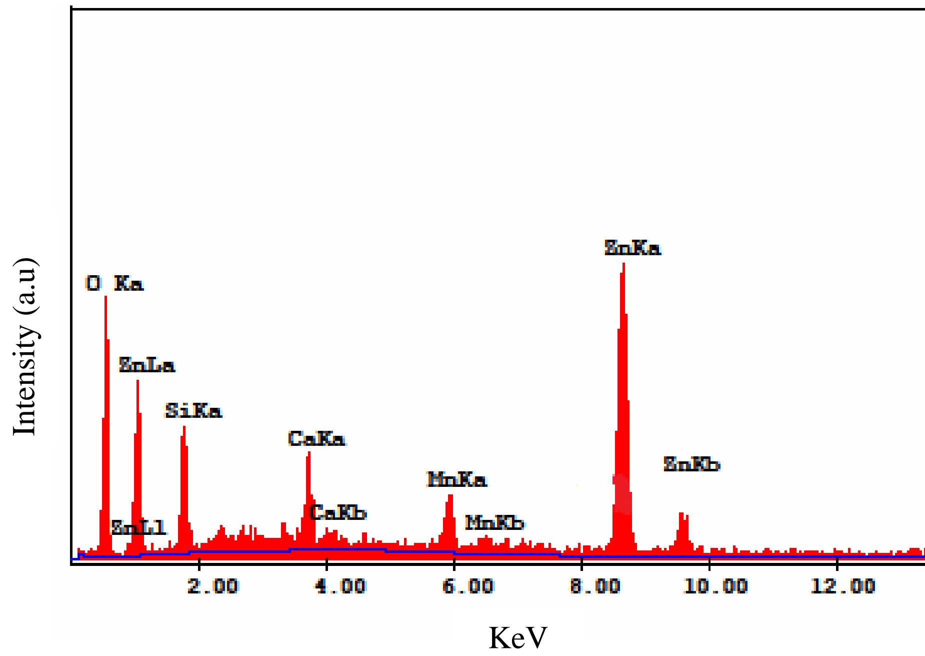

Fig 5.2c: EDX spectrum of $Zn_{1-x}Mn_xO$ thin film for x=0.06.

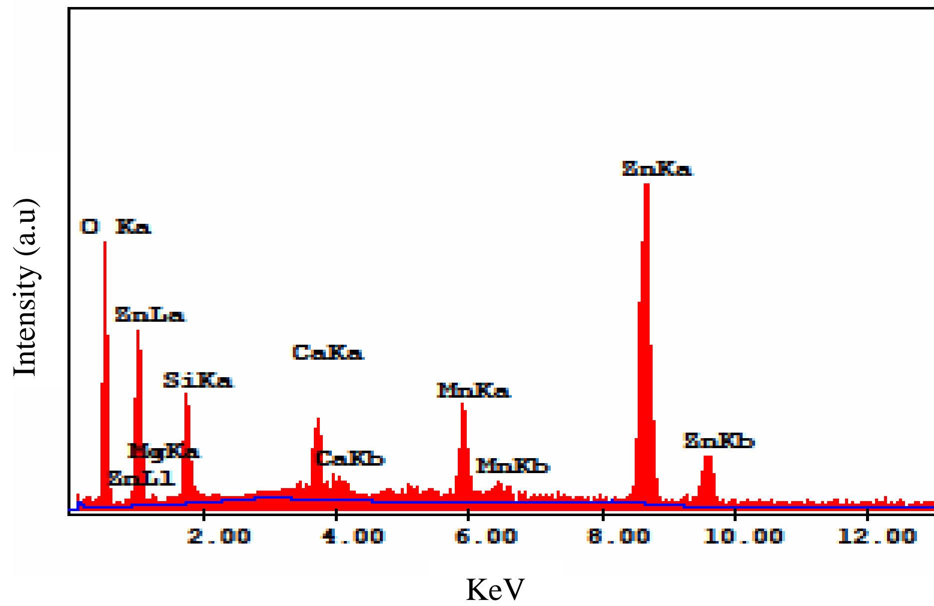

Fig.5.2d: EDX spectrum of $Zn_{1-x}Mn_xO$ thin film for x=0.10.

Table-5.1: Elemental analysis data for $Zn_{1-x}Mn_xO$ thin films.

Concentration of Mn	Elements	Wt %	At %
X=0.00	O	5.85	11.49
	Si	2.27	6.41
	Ca	2.42	3.28
	Zn	89.46	69.83
	Total	100	100

Concentration of Mn	Elements	Wt %	At %
X=0.04	O	4.53	12.93
	Si	1.69	1.42
	Ca	2.11	1.60
	Mn	3.54	2.62
	Zn	88.13	81.43
	Total	100	100

Concentration of Mn	Elements	Wt %	At %
X=0.06	O	5.19	17.42
	Si	2.04	4.41
	Ca	2.31	3.10
	Mn	4.87	4.79
	Zn	85.59	70.33
	Total	100	100

Concentration of Mn	Elements	Wt %	At %
X=0.10	O	7.97	23.68
	Si	6.30	10.66
	Ca	4.73	5.61
	Mn	8.23	7.12
	Zn	72.78	52.93
	Total	100	100

In this table we have seen that, the average atomic percentage of Zn, O, and Mn was 81.43, 12.93, and 2.62 respectively for 4% of Mn concentration which reveals that the as-deposited films are very nearly-stoichiometric.

5.4 Structural study by XRD analysis

To determine the structure of ZnO and Mn doped ZnO thin films, samples were deposited on glass substrate by spray pyrolysis method at 300°C substrate temperature. The XRD patterns of the films were taken with a diffractometer, using CoK_{α} radiation (of wavelength, λ = 1.7901 Å) source. XRD scan was taken in between 20° to 60° of 2θ scale. The XRD patterns of $Zn_{1-x}Mn_xO$ thin films are shown in Fig. 5.3. From XRD patterns, it is clear that the films are of amorphous with crystalline nature in all cases. The peaks observed at 2θ and corresponding (hkl) values are tabulated in Tables-5.2, for doping concentrations, x = 0.00, 0.02, 0.04, 0.06, 0.10 and 0.20, respectively. The XRD patterns could be indexed with

hexagonal structure. The lattice constants were calculated and found, a = 3.23 Å and c = 5.17 Å that matched well with standard values a = 3.24 Å and c = 5.20 Å. These results are in close agreement with the stoichiometric $Zn_{1-x}Mn_xO$ of a hexagonal structure [1, 2]. Crystallite size was calculated using the relation,

$$\xi = 0.94\lambda/B\cos\theta \qquad (5.1)$$

where, ξ is the crystallite size, λ is the wavelength of the X-ray used, θ is the diffraction angle and B is the full width at half maximum (FWHM) [3]. The diffraction peaks at 2θ values have been chosen for calculation of crystallite sizes for x= 0.00, 0.02, 0.04, 0.06, 0.10 and 0.20 of $Zn_{1-x}Mn_xO$ system. The calculated values of crystallite sizes of $Zn_{1-x}Mn_xO$ system for different Mn concentration are given in Tables-5.2.

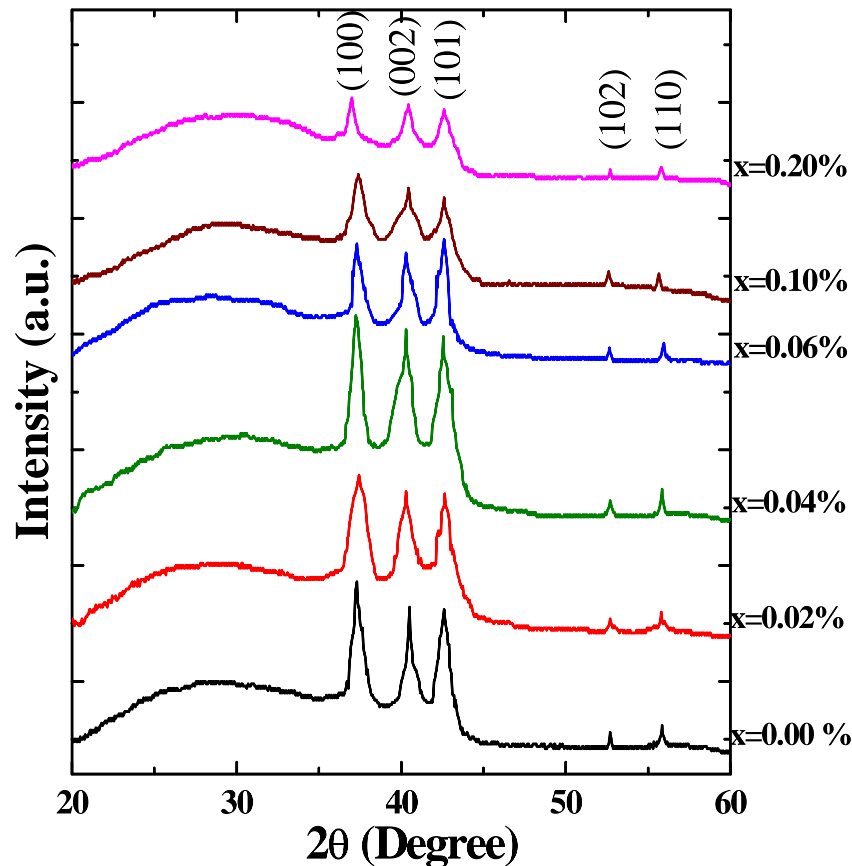

Fig 5.3: X-ray patterns of as-deposited $Zn_{1-x}Mn_xO$ thin films

Table-5.2: Crystallite size of as-deposited $Zn_{1-x}Mn_xO$ thin films.

Composition X in %	For (100) reflection			For (002) reflection			Ave. Grain size (nm)	c/a ratio
	2θ°	d_{hkl}(Å)	a (Å)	2θ°	d_{hkl}(Å)	c (Å)		
x=0.00	37.30	2.7990	3.2320	40.50	2.5861	5.1722	14	1.60
x=0.02	37.45	2.7882	3.2195	40.30	2.5984	5.1986	09	1.60
x=0.04	37.25	2.8026	3.2362	40.30	2.5984	5.1986	15	1.60
x=0.06	37.30	2.7990	3.2320	40.30	2.5984	5.1986	16	1.60
x=0.10	37.40	2.7918	3.2237	40.45	2.5891	5.1783	18	1.60
x=0.20	37.00	2.8209	3.2573	40.45	2.5891	5.1783	22	1.60

With increasing Mn concentration the intensity of the (001) peak increases up to 4 % and then it decreases with increase in full width at half maximum (FWHM). This is due to the lattice disorder and train induced by Mn^{2+} substitution in the host lattice [4].

5.5 Optical properties

5.5.1 Transmittance and absorbance

The optical, transmittance and absorbance versus wavelength curves of $Zn_{1-x}Mn_xO$ thin films with x= 0.00, 0.02, 0.04, 0.06, 0.10 up to 0.20 deposited onto glass substrates were taken in the wavelength range over 300 nm to 1100 nm. The transmittance and absorbance of thin films are shown in Fig. 5.4, and Fig. 5.5, respectively. Figure 5.4 shows that variation of transmittance as a function of wavelength for different composition of Mn doped ZnO films. These spectra show high transmittance near about 80% in the wavelength range from 800-1100 nm. Transmittance show a decreases upto 4% and then increases with higher persentage of Mn concentration at UV-VIS region. Figure 5.5 shows variation of Absorbance as a function of wavelength for different composition of Mn doped ZnO films. These spectra show high absorbance in the wavelength range from 350-500 nm. Finally absorbance becomes very smaller and remains steady above 700 nm wave length regions. Absorbance increases upto 4% and decreases with higher percentage of Mn concentration. From these graphs, it is clear that the absorption edge shifted to the longer wavelengths when ZnO thin flims was doped with Mn.

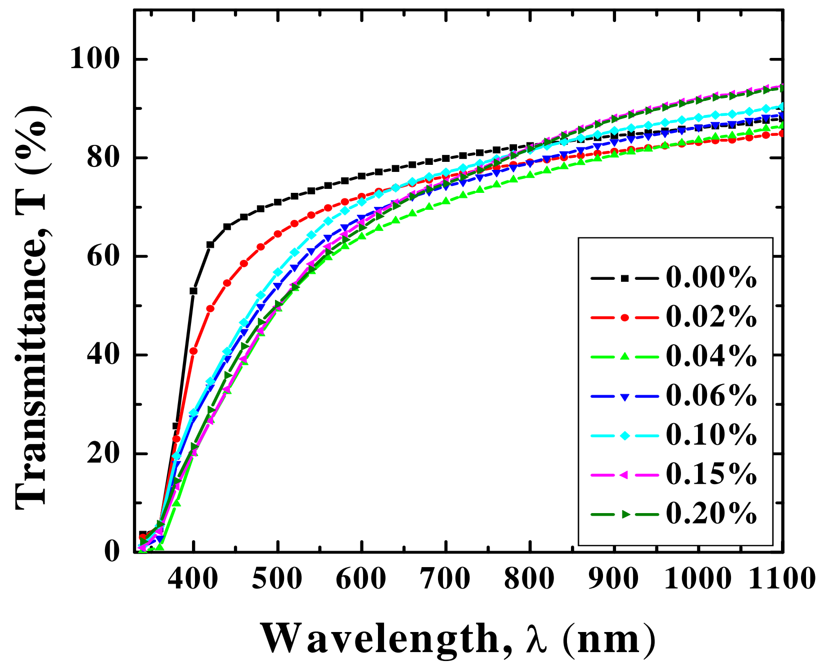

Fig.5.4: Variation of transmittance as a function of wavelength for $Zn_{1-x}Mn_xO$ films for different concentrations.

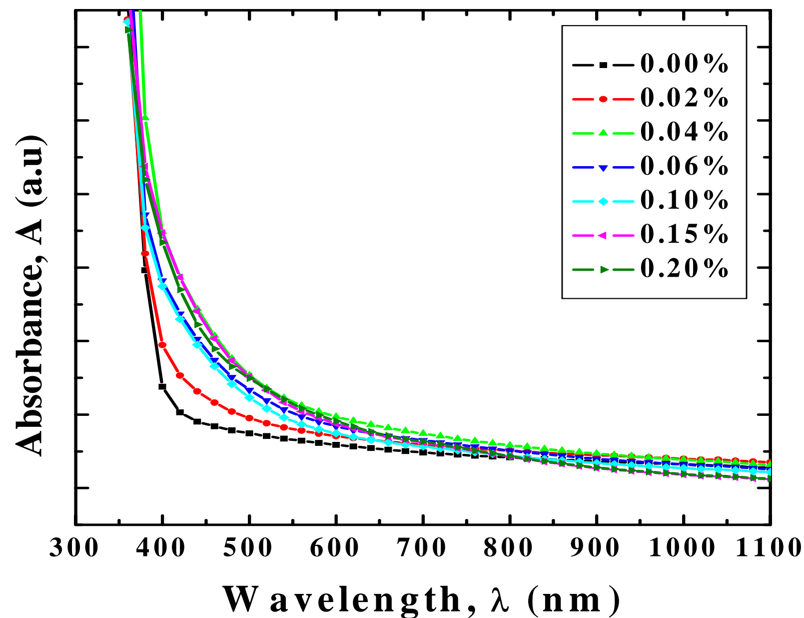

Fig.5.5: Variation of absorbance as a function of wavelength for $Zn_{1-x}Mn_xO$ films for different concentrations.

5.5.2 Optical bandgap

The direct band gap energy of the films have been obtained from intercept on the energy axis after extrapolation of the straight line section of $(\alpha h\nu)^2$ vs hν curve from the relation.

$$\alpha h\nu = A\,(h\nu - E_g)^n \qquad (5.3)$$

where A is a constant, hν is the photon energy and E_g is the optical band gap of the semiconductor and n is index related to the density of states for the energy band and is determined by the nature of optical transition involved in the absorption process. For the determination of band gap we have considered the direct allowed transitions. Variation of $(\alpha h\nu)^2$ (direct allowed transition) with hν for x=0.00, 0.02, 0.04 and x=0.06, 0.10, 0.15, 0.20 of $Zn_{1-x}Mn_xO$ thin films are shown in Fig. 5.6. and Fig.5.7 respectively. The bandgaps of the samples were obtained from intercepts on energy axis after extrapolation of the straight-line section in the high-energy region of $(\alpha h\nu)^2$ versus hν curve.

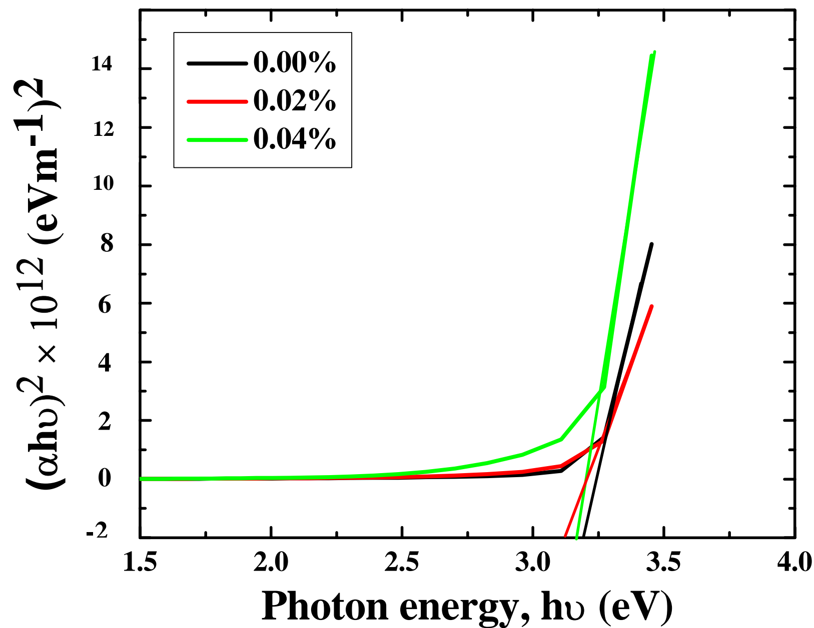

Fig. 5.6: Variation of $(\alpha h\nu)^2$ with hν for x=0.00, 0.02, 0.04 of $Zn_{1-x}Mn_xO$

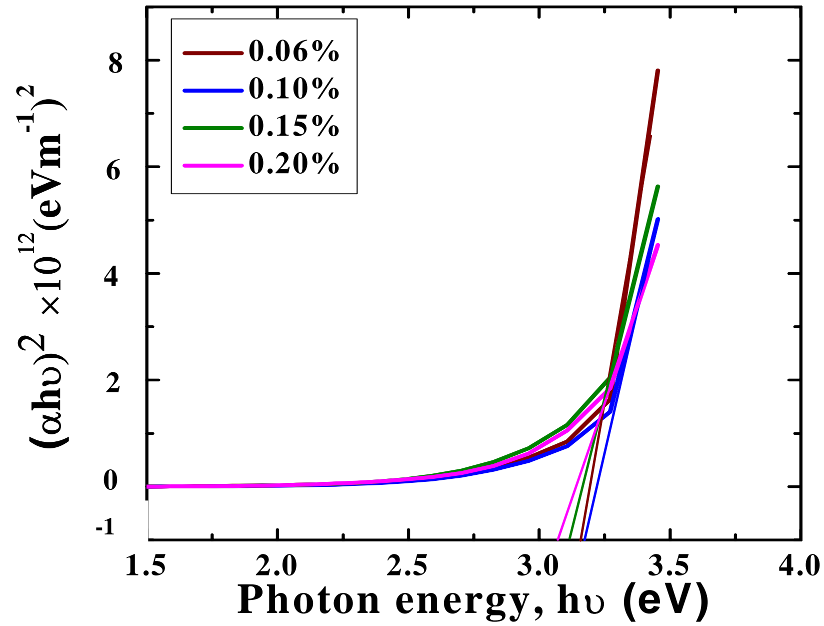

Fig. 5.7: Variation of $(\alpha h\nu)^2$ with hν for x=0.06, 0.10, 0.15, 0.20 of $Zn_{1-x}Mn_xO$

Table-5.3**:** Variation of bandgap with doping concentration of $Zn_{1-x}Mn_xO$ thin films.

Sample	Concentration of Mn	Direct band gap energy, ΔE_g (eV)
$Zn_{1-x}Mn_xO$	x=0.00	3.24
	x=0.02	3.23
	x=0.04	3.21
	x=0.06	3.22
	x=0.10	3.23
	x=0.15	3.12
	x=0.20	3.10

The variation of direct bandgap with doping concentrations is shown in Fig. 5.8 which shows that the interesting band gap tuning for deferent of doping concentrations.

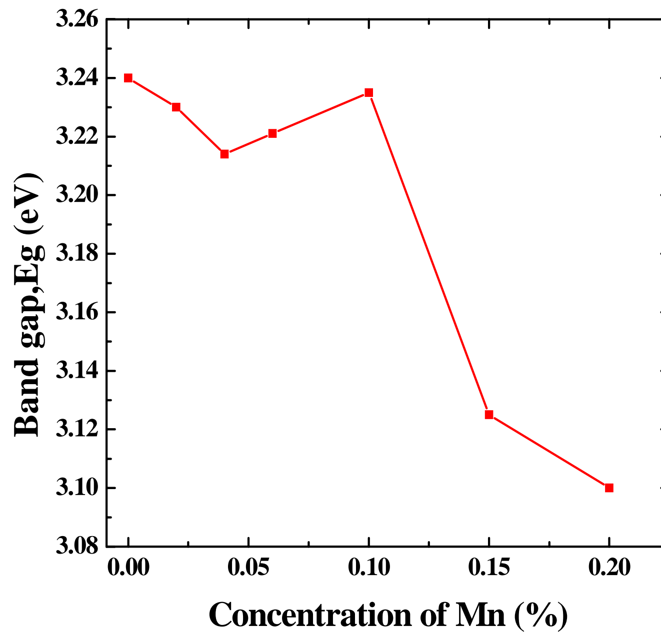

Fig. 5.8: Variation of band gap of $Zn_{1-x}Mn_xO$ films for different doping concentrations.

The optical band gap decreases when the Mn concentration increases from 0 to 4%, and then increases upto 10%. For 15% Mn doped ZnO film, the band gap then shows a sharp decrease as presented in Fig.5.8 Band gap decrease in the lower Mn concentration is due to the sp–d interaction between the Mn^{2+} and Zn^{2+} ions [6]. Besides that, the ionization energy of Zn is very high compared to other metals which are due to its fully filled d-orbital. The band gap variation can be explained by the strain which was induced by the substitution of Mn ions for Zn ions [7].

5.5.3 Refractive index and optical conductivity

The refractive index and optical conductivity are determined by using the transmission and reflection data. The refractive index has been calculated using the following relations,

$$n = \left(\frac{1+R}{1-R}\right) + \sqrt{\left(\frac{4R}{(1-R)^2} - k^2\right)} \qquad (5.4)$$

where, n is the refractive index, k is the extinction and R is the optical reflectance.

The variation of refractive index and optical conductivity with wave length and photon energy of $Zn_{1-x}Mn_xO$ thin films are shown in Fig. 5.9 and Fig. 5.10, respectively. The variation of refractive index with wavelength for various concentrations is shown in Figure 5.9. From this Fig., it is observed that the refractive index increases in between 350 to 540 nm wavelength region and then decreases rapidly with increasing wavelength from 540 to 1100 nm.

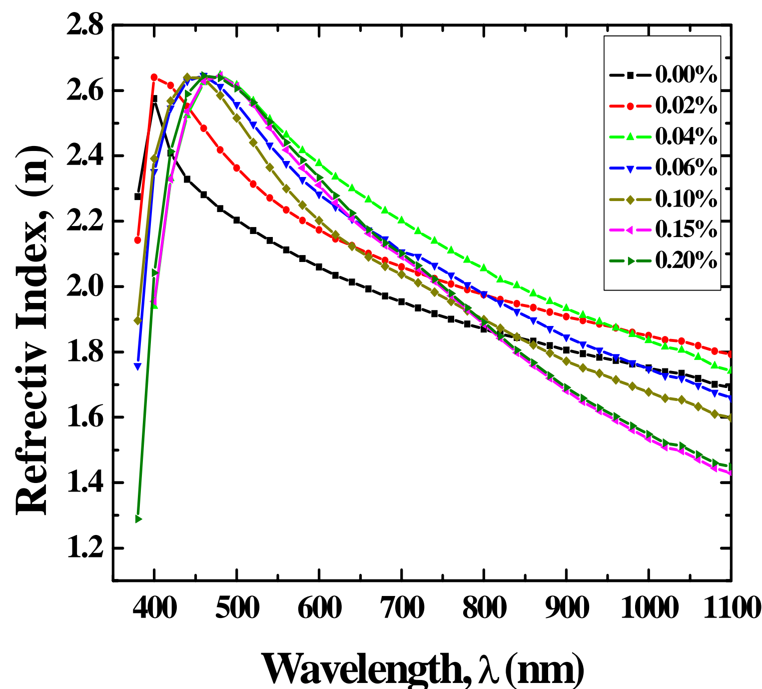

Fig.5.9: Variation of refractive index as a function of wavelength of $Zn_{1-x}Mn_xO$ films for different Mn concentrations.

Fig.5.10 shows the variation of optical conductivity with the incident photon energy. The optical conductivity was determined by using the relation

$$\sigma = \alpha nc/4\pi \quad (3.2)$$

where c is the velocity of light, α is absorption coefficient and n is refractive index. Figure 5.10 shows that the optical conductivities are increases with photon energy and it is also observe that conductivities are increases with the deferent Mn concentration. This means that photons having lower energy are absorbed while photon having higher energy can transmit through the thin films.

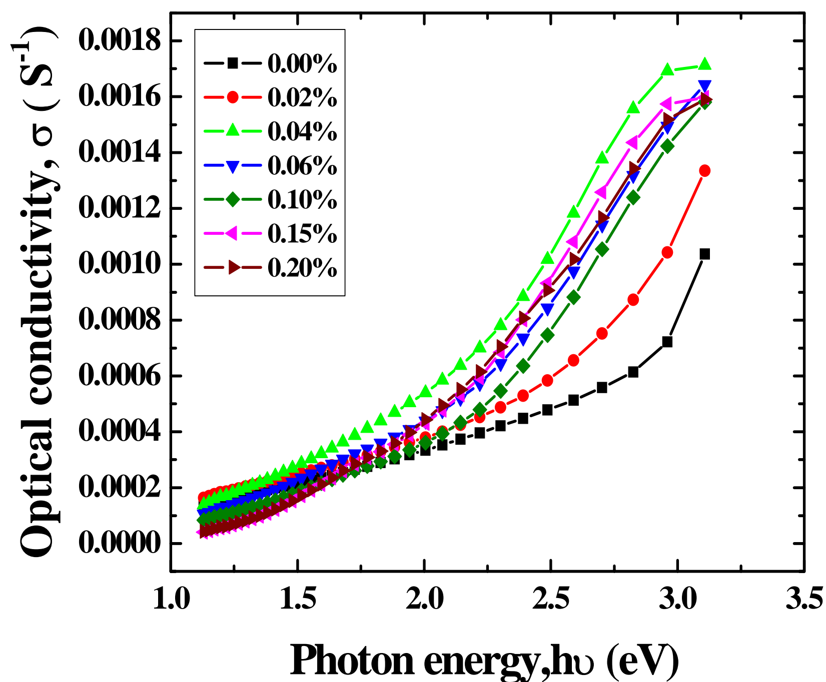

Fig.5.10: Variation of optical conductivity as a function of wavelength of $Zn_{1-x}Mn_xO$ films for different concentrations.

The optical conductivity increases at high photon energies (2eV to 3eV) is may be due to the high absorbance of thin films.

5.6 Electrical properties

5.6.1 Variation of resistivity with temperature

The Variation of resistivity with temperature of $Zn_{1-x}Mn_xO$ thin film are shown in Fig 5.11. The resistivities have been measured by the Vander Pauws method. The resistivity has been performed over a range from room temperature to 440 K. Resistivity measurements were then resumed by decreasing the temperature slowly to room temperature.

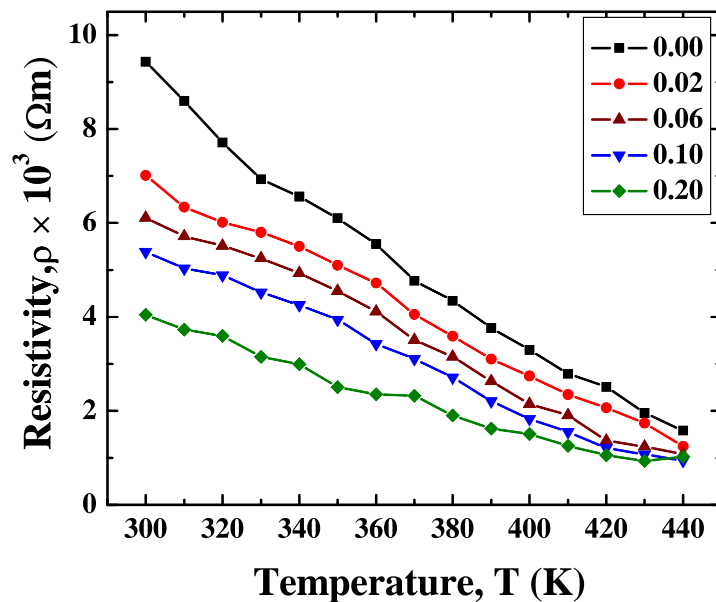

Fig.5.11: Variation of resistivity with temperature of $Zn_{1-x}Mn_xO$ films for different concentrations.

From the Fig.5.11, it is clear that resistivity decreases with increase of temperature in all cases. Which shows that the semiconducting behaviour of the sample having negative temperature coefficient of resistance**.** Which are due to the substitutional doping of Mn at the ZnO sites creates extra free carrier in the process. As the doping level is increased, more dopant atoms occupy lattice sites of zinc atoms resulting in more charge carriers.

5.6.2 Variation of conductivity with temperature

Conductivity of the $Zn_{1-x}Mn_xO$ thin films with x = 0.00, 0.02, 0.06, 0.10 and 0.20 were calculated from the resistivity measurements. Conductivity increases with the increase of temperature as shown in Fig. 5.12.

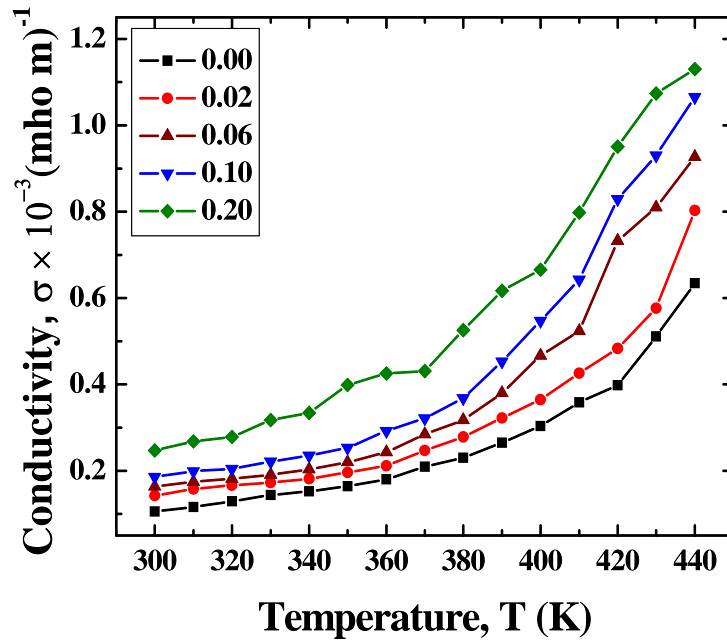

Fig.5.12: Variation of conductivity with temperature of $Zn_{1-x}Mn_xO$ films for different concentrations.

It is observed from the curve that the minimum conductivity is found for undoped ZnO thin films and the conductivity rise with doping concentration and temperature. Form the Fig.5.12, also observe that there is a non-linear variation of conductivity indicating that may be more than one kind of conduction mechanism is involved in this material in the temperature region we have used. Variation of the lnσ versus $1/T$ plot for five films with different doping concentration of Mn is shown in Fig.5.13.

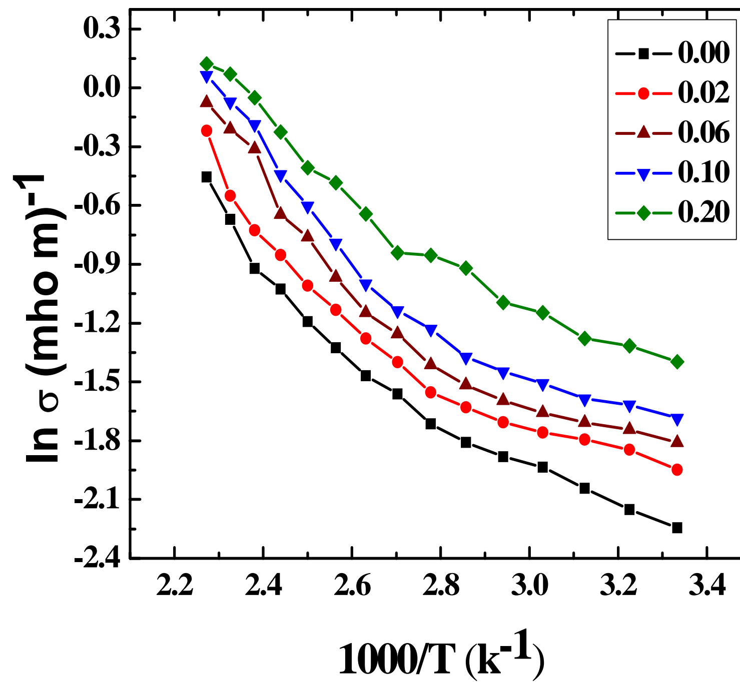

Fig.5.13: Variation of ln σ with 1/T of $Zn_{1-x}Mn_xO$ films for different concentrations.

5.6.3 Estimation of activation energy

The energy requisite to transfer charge from one neutral island to another is known as activation energy. Activation energy was calculated by using the relation

$$\sigma = \sigma_0 \exp\left(-\frac{\Delta E}{2k_B T}\right) \qquad (5.3)$$

where, ΔE is the activation energy, k_B is the Boltzmann constant and σ_o is the pre-exponential factor. Following this relation, the activation energy, ΔE of the $Zn_{1-x}Mn_xO$ thin films were calculated from the slope of the lnσ versus $1/T$ plot shown in Fig.5.14. The calculated values of ΔE are given in Table-5.4.

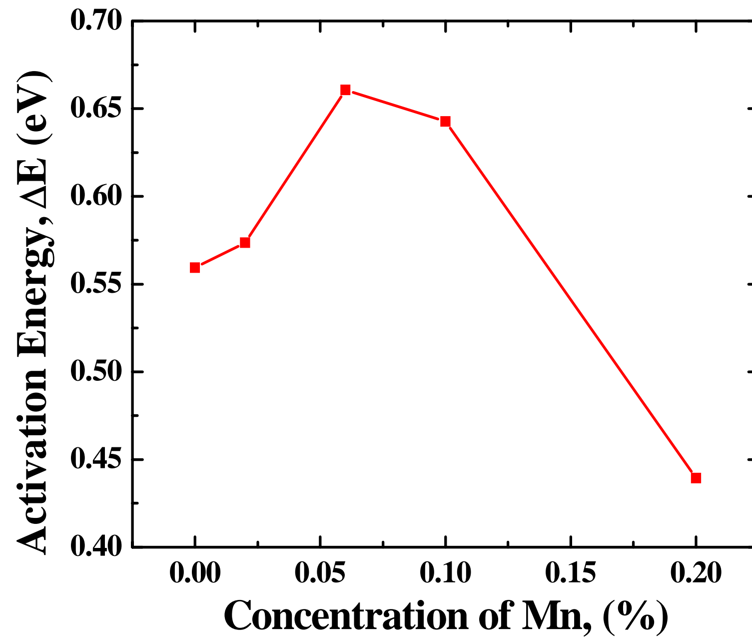

Fig.5.14: Variation of activation energy of $Zn_{1-x}Mn_xO$ films for different Mn concentrations.

Table-5.4: Variation of activation energy for $Zn_{1-x}Mn_xO$ thin films.

Sample	Values of x	Activation energy, ΔE (eV)
$Zn_{1-x}Mn_xO$	0.00	0.55
	0.02	0.57
	0.06	0.66
	0.10	0.64
	0.20	0.44

From the table 5.4 it is clear that activation energy is increasing up to 6% and then its decreases with the higher percentage of the Mn concentration. These values of activation energy are lower compared to the band gap energy (shown in Table-5.3). Hence the activation energy Value may indicate the position of localized gap states below the conduction band edge in the film.

5.7 Measurement of Hall Effect

Hall effect measurements were made on ZnO and Mn-doped ZnO thin films using Van-der Pauw's method. Measurements were made at room temperature and in a constant field of 9.815 KG. Hall co-efficient R_H, carrier concentration n have been calculated from Hall effect measurements. The variation of Hall co-efficient R_H, carrier concentration n with doping concentration of Mn are shown in figures 5.15,5.16 respectively and there values are presented in table -5.5.

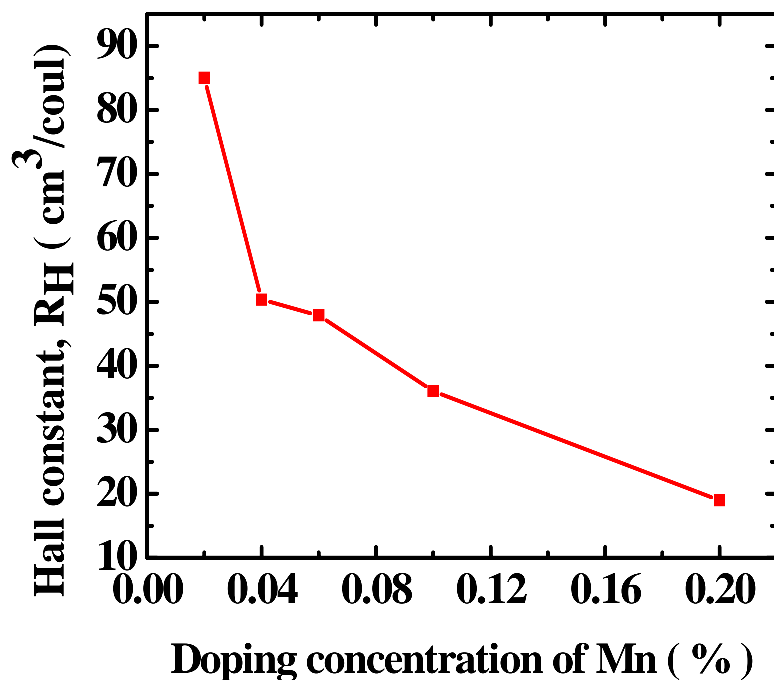

Fig. 5.15: Variation of Hall constant R_H with Mn concentration for Mn-doped ZnO thin films at room temperature.

From the Hall effect measurement it is seen that Mn-doped ZnO thin films have negative Hall co-efficient, R_H and this indicates the n-type behavior of ZnO:Mn at room temperature.

Figure 5.15 shows the variation of Hall co-efficient, R_H with doping concentration. From this graph it is seen that Hall co-efficient sharply decreases with doping concentration up to 4% and then gradually decreases with high percentage of Mn concentration. Figure 5.15 show that variation of carrier concentration with doping concentration. In this figure we have seen that carrier concentration increase at 4%

Mn concentration and then show a slightly decrease at 6% . Finally carrier concentration increases up to higher percentage of Mn concentration. The carrier concentration of the film is of the order of 10^{18} cm^{-3} .

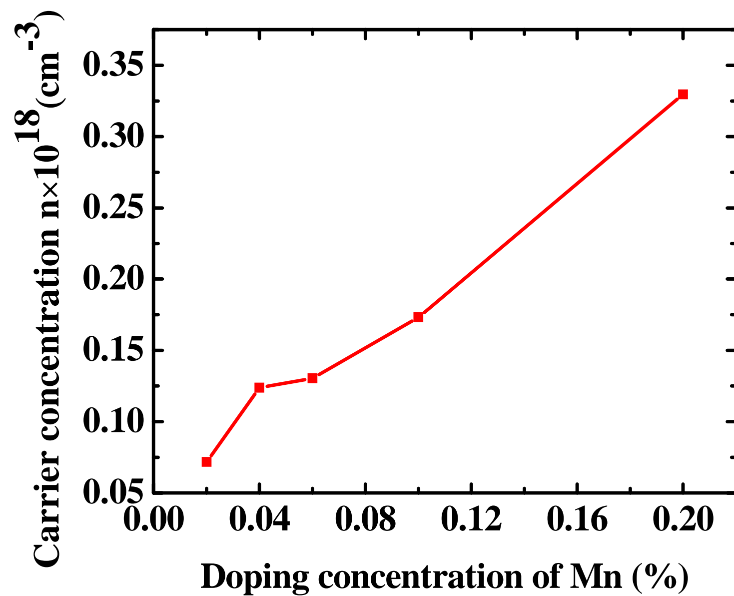

Fig. 5.15: Variation of carrier concentration n with Mn concentration for Mn-doped ZnO thin films at room temperature.

Table-5.5: Values of Hall co-efficient, R_H and carrier concentration n for different Mn concentration at room temperature.

Doping concentration of Mn	Hall co-efficient R_H in cm^3/coul	carrier concentration $n \times 10^{18}$ in cm
X=0.02	85.0575	0.07347
X=0.04	50.3744	0.12390
X=0.06	47.8687	0.13051
X=0.10	36.0241	0.17320
X=0.20	18.9602	0.32961

References

[1] Wang,W., Xiog, J., Zhu, C. F., Jing, G. S., “Preparation of CIGS Thin Films by Electrodeposition Method”, Chinese Journal of Chemical Physics, 23(4), 467 (2010) .

[2] Oja, M., Nanu, Katerski, A., Krunks, M., Mere, A., Raudoja, J., Goossens, A., “Crystal quality studies of CuInS2 films prepared by spray pyrolysis”, Thin Solid Film, 480-481, 82- 86 (2005).

[3] Cullity, B. D., “Elements of X-ray diffraction”, Addision- Wesley Publishing Co. Inc. (1967) 262.

[4] Gao, Li., and Zhang Jian-Min., “Effects of doping concentration on properties of Mn-doped ZnO thin films”, IPO Science, Vol 18 No 10, 1674-1056 (October 2009).

[5] Subramanian, M., Selvaraj1, V., Ilanchezhiyan, P., Kumar, G., M.,, Jayavel, R., and Soga, T., “Band Gap Variation of Mn Doped ZnO Films Prepared by Spray Pyrolysis Technique”, Japanese Journal of Applied Physics, 48, 06FF07 (2009).

[6] Abd Rashid, A. R., Menon, P. S., “Effect of Mn Doping on the Structural and Optical Properties of ZnO Films” ICSE2010 Proc. (2010).

[7] Thakur, P., Gautam, S., and Chae, K. H., X-ray Absorption and Emission Studies of Mn-doped ZnO Thin Films, Journal of the Korean Physical Society, Vol. 55, No. 1, pp. 177-182 (July 2009).

CHAPTER-VI
CONCLUSIONS AND SUGGESTIONS FOR FUTURE WORK

CHAPTER-VI
CONCLUSIONS AND SUGGESTIONS FOR FUTURE WORK

6.1 Conclusion

In the present work, ZnO and Mn-doped ZnO thin films were prepared by spray pyrolysis method. In the light of the experimental investigations and analysis on the structural, optical and electrical studies of $Zn_{1-x}Mn_xO$ thin films fabricated on glass substrate at 300 °C, the following conclusions may be drawn:

$Zn_{1-x}Mn_xO$ thin films have been successfully fabricated on glass substrates at 300°C with good in terms of their uniformity of thickness and colour. It is found that the deposition of $Zn_{1-x}Mn_xO$ films depends on various parameters like substrate temperature, concentration of solution used, spray rate and deposition time.

From the SEM image we have seen that more or less smooth surface and a large variety of crystal growth, such as circular disk, nano-ropes, structure were randomly distributed around the nucleation centre.

The EDX analysis corresponds to Zn and O peaks of the spectrum, which confirms the ZnO thin films. For different concentration of Mn in the film, there is also Mn peak in the spectrum. Finally EDX result reveals that the as-deposited $Zn_{1-x}Mn_xO$ films are very nearly-stoichiometric.

The structural properties were investigated by XRD analysis. It is found that the as-deposited $Zn_{1-x}Mn_xO$ thin films are crystalline in nature. Five different peaks are identified for the samples, which were compared with the standard JCPDS files. Diffraction peaks revealed the presence of hexagonal wurtzite structure without any secondary phase. Lattice constant is calculated a=3.23 Å and c=5.17Å. The observed grain sizes are found in the range of 9 nm to 18 nm.

From the optical studies it is observed that the $Zn_{1-x}Mn_xO$ thin films are direct band gap semiconductor. The transmittance of the $Zn_{1-x}Mn_xO$ films shows that highly transparent near about 80% in VIS region. Optical band gap was calculated from the

optical measurement. Band gap tuning were found with different Mn concentration. The bandgap energy is observed to vary from 3.10 eV to 3.24 eV at different doping concentrations. The optical band gap decreases when the Mn concentration increases from 0 to 4% and then increases upto 10%. For 15% Mn doped ZnO film, the band gap then shows a decrease upto 20%. The refractive index (1.25-2.65) depending on the doping concentration and thickness of the films and does not change sensibly with wavelength. The optical conductivities have been studied. The optical conductivities are increases with photon energy, this means that photons having lower energy are absorbed while photon having higher energy can transmit through the thin films.

The electrical measurements of the $Zn_{1-x}Mn_xO$ films have been investigated from room temperature to 440 K. Resistivity decreases with increase of temperature in all cases of the samples. Which confirms that the semiconducting behaviour of the sample having negative temperature coefficient of resistance**.** The activation energy was measured from the slopes of $\ln\sigma$ verses $1/T$ graph and its value is found 0.44 eV to 0.66 eV.

Hall effect measurements wear made on a number of films having different concentrations at room temperature. From Hall effect measurement it is found that Mn-doped ZnO thin film is an n-type material having carrier concentration is of the order of 10^{18} cm^{-3}. It is also found that the carrier concentration increases with increasing doping concentration of Mn.

6.2 Suggestions for Future Work

This is the first time that Mn doped ZnO thin flims have been prepared in our laboratory. May be some magnetic properties are present there because of Mn doped into the sample. To prepare high quality films and their characterization more works are necessary, such as :

1) Study of the magnetic properties.
2) Study of temperature dependence Hall effect.
3) Study of the AFM.

APENDIX

Optical Data

Table 1: Absorbance data for $Zn_{1-x}Mn_xO$ thin films

W.L.	X=0.00	X=0.02	X=0.04	X=0.06	X=0.10	X=0.15	X=0.20
1100	0.0549	0.0702	0.0624	0.0513	0.0433	0.0242	0.0256
1080	0.0568	0.0721	0.0656	0.0538	0.0455	0.0262	0.028
1060	0.0593	0.0747	0.0691	0.057	0.0483	0.0291	0.0308
1040	0.0619	0.0771	0.0729	0.0602	0.0509	0.0317	0.0334
1020	0.0629	0.0776	0.0742	0.0613	0.0518	0.0331	0.0347
1000	0.0646	0.0796	0.0774	0.0642	0.0544	0.0363	0.0378
980	0.066	0.0817	0.0803	0.0669	0.0568	0.0392	0.0408
960	0.0677	0.0837	0.0836	0.0699	0.0594	0.0426	0.0442
940	0.0695	0.0857	0.0868	0.073	0.062	0.0464	0.048
920	0.0712	0.0875	0.0898	0.0759	0.0648	0.0502	0.0516
900	0.073	0.0895	0.0934	0.0793	0.0679	0.0546	0.0559
880	0.075	0.0918	0.0977	0.0833	0.0715	0.0599	0.0612
860	0.0768	0.0941	0.1019	0.0876	0.0753	0.0656	0.0668
840	0.0787	0.0963	0.1062	0.092	0.0792	0.0717	0.073
820	0.0806	0.0989	0.112	0.097	0.0836	0.0784	0.0796
800	0.0831	0.1016	0.1163	0.1021	0.0881	0.0854	0.0867
780	0.0856	0.1044	0.1219	0.1073	0.0928	0.0929	0.0942
760	0.088	0.1073	0.1277	0.1129	0.0977	0.1008	0.1022
740	0.0911	0.1105	0.134	0.1185	0.1028	0.1088	0.1105
720	0.094	0.114	0.1409	0.1243	0.1079	0.1167	0.1187
700	0.097	0.1177	0.1478	0.13	0.113	0.1241	0.1261
680	0.1007	0.1216	0.1552	0.1356	0.1182	0.1311	0.1332
660	0.1042	0.1261	0.1635	0.142	0.1239	0.1392	0.1417
640	0.1084	0.1309	0.1727	0.1497	0.131	0.1495	0.1534
620	0.1127	0.1359	0.1826	0.1578	0.1388	0.1613	0.167
600	0.1173	0.1416	0.1942	0.1683	0.1484	0.175	0.1819
580	0.1228	0.1482	0.208	0.1804	0.1597	0.1908	0.1981
560	0.1285	0.1558	0.2242	0.1948	0.173	0.2083	0.2164
540	0.1348	0.165	0.2451	0.2141	0.1918	0.2336	0.2415
520	0.1416	0.1761	0.2719	0.2382	0.2164	0.266	0.2699
500	0.1487	0.1902	0.3069	0.2666	0.2461	0.3029	0.2985
480	0.157	0.2084	0.3529	0.3019	0.2831	0.3466	0.3309
460	0.1677	0.2329	0.4141	0.3486	0.3315	0.4061	0.3785
440	0.1808	0.2631	0.4868	0.4054	0.3899	0.4806	0.4452
420	0.2056	0.3064	0.5732	0.4746	0.46	0.5736	0.5398
400	0.2759	0.389	0.6973	0.5647	0.5488	0.6932	0.6683
380	0.5927	0.6379	1.0071	0.7443	0.7087	0.8748	0.8391

Table 2: Transmittance data for $Zn_{1-x}Mn_xO$ thin films

W.L.	X=0.00	X=0.02	X=0.04	X=0.06	X=0.10	X=0.15	X=0.20
1100	0.8792	0.8492	0.8644	0.8872	0.9037	0.9446	0.9409
1080	0.8759	0.8459	0.859	0.8824	0.8998	0.9407	0.937
1060	0.8708	0.8409	0.8517	0.8761	0.8939	0.9346	0.931
1040	0.866	0.8364	0.8447	0.8698	0.8885	0.9287	0.925
1020	0.8643	0.8353	0.842	0.8676	0.8868	0.9258	0.9225
1000	0.8608	0.8315	0.8359	0.8617	0.8816	0.9193	0.9159
980	0.8578	0.8279	0.8302	0.8563	0.8767	0.9128	0.9095
960	0.8545	0.8239	0.824	0.8505	0.8713	0.9055	0.9022
940	0.8512	0.8202	0.818	0.8445	0.8658	0.8978	0.8948
920	0.8479	0.8168	0.8121	0.8389	0.8606	0.89	0.887
900	0.8445	0.813	0.8055	0.8323	0.8546	0.8809	0.8782
880	0.8406	0.8087	0.798	0.8246	0.8473	0.8701	0.8677
860	0.8368	0.8043	0.7902	0.8164	0.84	0.8588	0.8564
840	0.8333	0.8003	0.7823	0.8081	0.8324	0.847	0.8446
820	0.8297	0.7958	0.7738	0.7992	0.8241	0.8339	0.8318
800	0.825	0.7909	0.7645	0.79	0.8157	0.8206	0.8184
780	0.8202	0.7858	0.755	0.7808	0.807	0.8066	0.8044
760	0.8156	0.7805	0.745	0.7708	0.798	0.7922	0.7898
740	0.8101	0.7748	0.7344	0.7607	0.7886	0.7778	0.775
720	0.8046	0.7687	0.7231	0.7509	0.7793	0.764	0.7607
700	0.7988	0.7623	0.7114	0.7431	0.7704	0.7512	0.7478
680	0.7924	0.7555	0.6995	0.7318	0.7615	0.7391	0.736
660	0.7858	0.7478	0.6864	0.7212	0.7516	0.7257	0.7214
640	0.7784	0.7395	0.6721	0.7087	0.7396	0.7089	0.7023
620	0.7711	0.7314	0.6571	0.6951	0.7266	0.6898	0.681
600	0.7627	0.7216	0.6396	0.679	0.7107	0.6683	0.6581
580	0.7534	0.7108	0.6201	0.6604	0.6924	0.645	0.6342
560	0.7438	0.6985	0.5973	0.639	0.6718	0.6196	0.6083
540	0.7332	0.684	0.5695	0.6116	0.6437	0.5846	0.5742
520	0.722	0.6667	0.535	0.5786	0.6083	0.5425	0.5377
500	0.7102	0.6456	0.4933	0.5417	0.568	0.4979	0.5031
480	0.6968	0.6194	0.4432	0.4989	0.5214	0.4497	0.4664
460	0.6799	0.5856	0.3851	0.4476	0.4658	0.3923	0.4178
440	0.6599	0.5461	0.3262	0.3931	0.4071	0.3307	0.3588
420	0.6237	0.4939	0.2672	0.3353	0.3469	0.2671	0.2888
400	0.53	0.408	0.2006	0.2726	0.2828	0.2024	0.2144
380	0.2557	0.23	0.0983	0.1801	0.1956	0.1334	0.145

Table 3: Electrical data for temperature dependant resistivity of $Zn_{1-x}Mn_xO$ thin film. Doping concentration of Mn = 0 %

Temperature in K	T^{-1} in $K^{-1} \times 10^{-3}$	Resistivity ρ in Ohm-m $\times 10^{-3}$	Conductivity σ in $Ohm\text{-}m^{-1} \times 10^{-3}$
300	3.33333	9.43212	0.10602
310	3.22581	8.59847	0.1163
320	3.125	7.71334	0.12965
330	3.0303	6.92901	0.14432
340	2.94118	6.56618	0.1523
350	2.85714	6.10057	0.16392
360	2.77778	5.55171	0.18012
370	2.7027	4.7689	0.20969
380	2.63158	4.34285	0.23026
390	2.5641	3.76765	0.26542
400	2.5	3.29599	0.3034
410	2.43902	2.79116	0.35827
420	2.38095	2.51237	0.39803
430	2.32558	1.95692	0.51101
440	2.27273	1.57663	0.63427

Table 4: Electrical data for temperature dependant resistivity of $Zn_{1-x}Mn_xO$ thin film. Doping concentration of Mn = 2 %

Temperature in K	T^{-1} in $K^{-1} \times 10^{-3}$	Resistivity ρ in Ohm-m $\times 10^{-3}$	Conductivity σ in $Ohm\text{-}m^{-1} \times 10^{-3}$
300	3.33333	7.01214	0.14261
310	3.22581	6.3377	0.15779
320	3.125	6.01579	0.16623
330	3.0303	5.80251	0.17234
340	2.94118	5.50321	0.18171
350	2.85714	5.10145	0.19602
360	2.77778	4.72445	0.21166
370	2.7027	4.05241	0.24677
380	2.63158	3.5898	0.27857
390	2.5641	3.10176	0.3224
400	2.5	2.74061	0.36488
410	2.43902	2.34634	0.4262
420	2.38095	2.06819	0.48351
430	2.32558	1.73513	0.57632
440	2.27273	1.24589	0.80264

Table 5: Electrical data for temperature dependant resistivity of $Zn_{1-x}Mn_xO$ thin film. Doping concentration of Mn = 6 %

Temperature in K	T^{-1} in $K^{-1} \times 10^{-3}$	Resistivity ρ in Ohm-m × 10^{-3}	Conductivity σ in $Ohm\text{-}m^{-1} \times 10^{-3}$
300	3.33333	6.11226	0.16361
310	3.22581	5.71427	0.175
320	3.125	5.51364	0.18137
330	3.0303	5.24917	0.19051
340	2.94118	4.92812	0.20292
350	2.85714	4.55241	0.21966
360	2.77778	4.11245	0.24316
370	2.7027	3.51269	0.28468
380	2.63158	3.14988	0.31747
390	2.5641	2.63105	0.38008
400	2.5	2.14301	0.46663
410	2.43902	1.90986	0.5236
420	2.38095	1.36526	0.73246
430	2.32558	1.23464	0.80995
440	2.27273	1.07919	0.92662

Table 6: Electrical data for temperature dependant resistivity of $Zn_{1-x}Mn_xO$ thin film. Doping concentration of Mn = 10 %

Temperature in K	T^{-1} in $K^{-1} \times 10^{-3}$	Resistivity ρ in Ohm-m × 10^{-3}	Conductivity σ in $Ohm\text{-}m^{-1} \times 10^{-3}$
300	3.33333	5.38993	0.18553
310	3.22581	5.03254	0.19871
320	3.125	4.88519	0.2047
330	3.0303	4.51912	0.22128
340	2.94118	4.25441	0.23505
350	2.85714	3.94421	0.25354
360	2.77778	3.42334	0.29211
370	2.7027	3.11088	0.32145
380	2.63158	2.71475	0.36836
390	2.5641	2.20547	0.45342
400	2.5	1.82623	0.54758
410	2.43902	1.55546	0.6429
420	2.38095	1.20548	0.82955
430	2.32558	1.07457	0.9306
440	2.27273	0.93886	1.06513

Table 7: Electrical data for temperature dependant resistivity of $Zn_{1-x}Mn_xO$ thin film. Doping concentration of Mn = 20 %

Temperature in K	T^{-1} in $K^{-1} \times 10^{-3}$	Resistivity ρ in Ohm-m × 10^{-3}	Conductivity σ in $Ohm\text{-}m^{-1} \times 10^{-3}$
300	3.33333	4.04483	0.24723
310	3.22581	3.72807	0.26823
320	3.125	3.59467	0.27819
330	3.0303	3.15128	0.31733
340	2.94118	2.99043	0.3344
350	2.85714	2.50643	0.39897
360	2.77778	2.35213	0.42515
370	2.7027	2.3212	0.43081
380	2.63158	1.90321	0.52543
390	2.5641	1.62134	0.61677
400	2.5	1.50231	0.66564
410	2.43902	1.25364	0.79768
420	2.38095	1.05213	0.95045
430	2.32558	0.93156	1.07347
440	2.27273	1.02145	1.13021

Table 8 : Values of Hall co-efficient, R_H and carrier concentration n for $Zn_{1-x}Mn_xO$ thin film.

Doping concentration of Mn	Hall resistance $R_{ABCD} \times 10^5$ Ohm	Hall co-efficient R_H in cm^3/coul	carrier concentration $n \times 10^{18}$ in cm
X=0.02	2.0000	85.0575	0.07347
X=0.04	1.1538	50.3744	0.12390
X=0.06	1.0714	47.8687	0.13051
X=0.10	0.8000	36.0241	0.17320
X=0.20	0.4285	18.9602	0.32961